ABSTRACT

Title of Document: PROGNOSTICS DEMONSTRATION OF ELECTRONIC COMPONENTS SUBJECTED TO VIBRATION ENVIRONMENT OF A LIGHT MILITARY TACTICAL VEHICLE

Alan Yu, Master of Science (M.S.), 2007

Directed By: Professor, Donald B. Barker, Department of Mechanical Engineering

A demonstration of the Prognostics and Health Management (PHM) method in a military vehicle environment was performed. The purpose of the demonstration is to show rapid and cost effective means to increase reliability and effectiveness of in-cabin equipment through PHM implementation. The PHM method allows for prediction of damage accumulation in a system while in its operating environment. Prediction is achieved by monitoring and assessing appropriate product parameters.

An experimental setup to perform in-cabin accelerated testing on printed circuit boards (PCB) was developed. Strain, acceleration, continuity, and GPS data were recorded during testing. Using recorded data, life prediction with cycle counting and PSD load blocking techniques was demonstrated for BGA components. A limited set of terrain and loading conditions was characterized using Root Mean Square (RMS) and Power Spectral Density (PSD).

PROGNOSTICS DEMONSTRATION OF ELECTRONIC COMPONENTS SUBJECTED TO VIBRATION ENVIRONMENT OF A LIGHT MILITARY TACTICAL VEHICLE

By

Alan T. Yu

Thesis submitted to the Faculty of the Graduate School of the
University of Maryland, College Park, in partial fulfillment
of the requirements for the degree of
Master of Science
2007

Advisory Committee:
Professor Donald B. Barker, Chair
Professor Abhijit Dasgupta
Associate Professor Peter Sandborn

Dedication

To my family and friends.

Acknowledgements

I would like thank my advisor, Professor Donald Barker for all his support, guidance and encouragement. Also, I would like to thank Professors Abhijit Dasgupta and Peter Sandborn for their helpful suggestions and insight. In addition, special thanks to Gilad Sharon, Patrice Gregory, Saifa Hasin, and Jamie Watkins for all the assistance and support they provided me over the course of this project.

I want to express my sincerest thanks to Jonathan Lococo, Mary Calomeris, and Greg Dogum. Without their assistance, testing at Aberdeen Proving Grounds would not have been possible. I would also like to thank Craig Hershey, Mark Bounds, and Chi Wang for their assistance.

I am extremely thankful for the support provided by my friends at Maryland including Forbod Askari, Jirapat Supamusdisukul, Eakalak Intarakosit, Jie Gu, Brian Tuchband, Abdou Diallo, Pedro Quintero, Tim Seeley, and Shaughn Roettele. I am also thankful for the help provided by the CALCE staff and students, including Anshul Shrivastava, Howard Williams, David Eisner, Lei Nie, Lyudmyla Panashchenko and the Spring 2007 German students.

Table of Contents

List of Tables

List of Figures

Abbreviations

AMSAA: US Army Materiel Systems Analysis Activity

APG: Aberdeen Proving Ground located in Aberdeen, Maryland

BGA: Ball grid array package

BIT: Built in test

CALCE: Center for Advanced Life Cycle Engineering

CalcePWA: CALCE software for simulation based failure assessment of printed wiring assemblies

E-SEM: Environmental Scanning Electron Microscope

LCM: Life Consumption Monitoring

LMTV: Light Medium Tactical Vehicles

PCB: Printed circuit board

PHM: Prognostics and Health Management

PoF: Physics of Failure

PSD: Power Spectral Density

RMS: Root mean square

SOIC: Small outline integrated circuit

SOT: Small outline transistor

Chapter 1: Introduction

1.0 Project Introduction

The primary motivation behind this thesis is to improve the reliability of electronic equipment operating in military vehicle environments. Improvements in reliability come from implementing the Prognostics and Health Management (PHM) method. PHM is a method of evaluating the reliability of a system in its actual life cycle conditions [1]. PHM method involves using the life consumption monitoring process (LCM) to assess or predict a product's remaining life by measuring physical parameters of the product's environment [2]. Use of a PHM system can improve safety margins, minimize life cycle costs, maintain equipment effectiveness through timely maintenance actions, and many other benefits as detailed in [1][2][3]. While the LCM process is conceptually clear and straightforward, there are several different implementation methods to choose from depending on system requirements.

1.1 PHM Implementation Background

Vichare [6] provides extensive background on the four main categories of PHM implementation methods. These are built-in-test (BIT), canaries, precursors to failure, and modeling accumulated damage based on life cycle loads. BIT involves on-board hardware and software to identify and locate faults in a system. Studies of BIT show that it is prone to false alarms [6], thus it primarily serves as a diagnostic tool rather than a prognostic tool. Canaries, otherwise known as fuses, provide early

warning of failure and can be pre-calibrated to fail within a defined time period or 'prognostic distance' before failure of actual component. Monitoring precursors to failure is the third PHM category. Precursors are any performance or operating parameters that can be indicative of impending failure. An example of a failure precursor is the number of observed voltage spikes beyond normal operational range that typically occur before a component fails. By monitoring for these voltage spikes, failure can be predicted for a pre-calibrated prognostic distance. The last category, which is the approach of this project, involves testing prognostic algorithms that utilize damage models to compute remaining life. For an extensive survey of PHM technologies and current research see [9]. Note that each one of these PHM implementation approaches has different limitations and prediction uncertainties.

In spite of the variety of PHM approaches available, PHM has not been widely implemented in military vehicle systems. This may be partially attributed to the cost of implementing a PHM system. Until recently, most areas of PHM implementation were for high cost systems with long life spans such as fixed wing aircraft, rotorcraft, power plants, bridges, and other similarly high cost systems [9][10]. Justifying the cost of developing, implementing, and maintaining a PHM system for products without high individual value can be difficult. However, if the proper data is collected, an increase in fleet availability and equipment reliability is possible while decreasing overall maintenance and system cost [10]. In addition, a PHM system can be indirectly valuable by providing operational environment data that otherwise would be unavailable. Accurate characterization of operating

environments is crucial for redesigning equipment, but is often not readily available and maybe expensive to obtain. Another barrier to PHM implementation is the lack of understanding of issues surrounding appropriate data, data collection, data reduction, and data processing before performing any damage assessment. The PHM implementation in this project will demonstrate a variety of easy to implement data collection, processing, and analysis methods that address these barriers.

Due to the potential benefits of PHM, a number of university, government, and industry research centers are actively addressing the barriers to PHM implementation. Center for Advanced Life Cycle Engineering (CALCE) research consortium is one of these places performing research to address these issues. In the past several years, CALCE research center has conducted three research projects that are of particular relevance to this thesis.

Two previous CALCE projects involving vehicles were conducted. The first project involved mounting a printed circuit board (PCB) to the exhaust manifold of a passenger vehicle using two aluminum strips on opposing sides of the board [1]. A data recorder logged thermal and vibration environment for the under-hood of the car. The test lasted four days after which the PCB was thermally cycled in a laboratory environment until failure. Damage accumulation was calculated using CalcePWA software and compared to actual testing. The second project was a similar, but longer (31 days) and included unintended shock loading due to an accident [2].

A key difference between the first and second CALCE project involved how the PCB was mounted. The first project mounted the PCB in a simply supported fashion, while the second project mounted the PCB in a cantilever fashion. Both projects used a board consisting of eight surface mounted leadless inductors. In the second project, damage accumulated mainly through vibration, while in the previous project damage was primarily due to thermal cycling. An obvious conclusion from these two experiments is that the manner in which the board is mounted affects the failure mode.

Another CALCE PHM project of interest involves a prognostics implementation under vibration loading [7]. Testing in this project was performed on a laboratory vibration shaker table. In this project, the bending curvature of the PCB is monitored using strain gauges. Strain time history is transformed for use in a vibration fatigue model. The technique developed to transform measured response to interconnect strain is useful. However, mounting strain gauges on functional PCBs may not be practical or possible. Adding strain gauges to the board near components of interest requires taking up valuable board space and increases wiring on or around the board. Therefore, adding strain gauges to an existing PCB design will require an expensive redesign of the PCB. Due to size restrictions (e.g. PCBs in cell phones), often there simply is not enough space to fit strain gauges on a densely populated PCB while meeting PCB size requirements.

Testing on vibration shaker tables raises another issue about implementing PHM. Vibration based PHM demonstrations have been conducted in the laboratory with representative acceleration Power Spectral Density (PSD) data collected from the field or with artificial PSDs developed through design requirements. However, to obtain accurate experimental results, accurate and representative PSDs from the field is necessary but challenging. Issues such as which sampling rate to use, accelerometers to use (range, sensitivity, etc.), and selecting sample data for calculating PSD need to be considered carefully. Without a high awareness level of specific operating environments, developing "representative" PSD can be a difficult task. In this project, PCBs are tested in the field rather on a vibration shaker table to avoid issues with obtaining representative PSDs.

For this project, the PCB is mounted in a four-point bending fixture. The experimental fixture is placed in equipment bins inside the vehicle. Because temperatures inside the vehicle cabin are significantly lower than the under-hood of a car, thermal loading is unlikely to play a role in damage accumulation rate; especially since PCBs are mounted in a fashion to induce vibration for accelerated testing purposes. Therefore, it is significantly less important to monitor temperature than in the previous two projects where the PCB was mounted in the under-hood of a car. Another difference is the magnitude of vibration expected between a passenger car driving over paved roads and a military vehicle traversing over many different road surfaces including off road conditions. Unlike previously described CALCE vehicle projects, surface mounted leadless inductors will not be tested. Instead, BGA,

capacitor, SOT, and SOIC packaging types will be tested. The last difference is the test fixture cannot be semi-permanently attached to the test vehicle as in the two previous experiments. This is due to the fact that experiments will be run on different military ground vehicles that may have individual requirements for placement of equipment.

1.2 Project Objectives

The main goal of this project is to perform electronic component testing in a "representative" environment for military ground vehicles. To achieve this goal, testing occurred on military ground vehicles over specially designed courses at Aberdeen Proving Ground (APG), Aberdeen, Maryland. Electronic component failures caused by vibration induced fatigue are desired because fatigue is the most common mode of failure in mechanical and structural systems [14]. Multiple electronic component packaging types were tested to determine the effect of vibratory loading on each package type. A successful comparison between test failures and predictions by damage models is the desired result of this project. A secondary goal of this project is to statistically characterize a limited set of terrain and loading conditions available at APG for demonstration purposes.

1.3 Organization of Thesis

The layout of this thesis is as follows. Chapter 2 covers project objectives, experimental setup, and testing in detail. Chapter 3 covers time domain and frequency domain data processing and analysis techniques. Chapter 4 covers the general

behavior of the experimental fixture as determined from data analysis of strain and acceleration time history. Chapter 5 details experimental failures and compares failure predictions with experimental failures. Chapter 6 involves a discussion about the demonstration project and results. Chapter 7 covers the contributions and suggested future work.

Chapter 2: Demonstration Project

2.0 Objectives

The objective behind this project is to increase reliability of electronic components operating in military vehicles. This objective is achieved by implementing a PHM system in one such military vehicle, the Light Medium Tactical Vehicle (LMTV). Further, this project will demonstrate prognostic tools for vibration and shock loading. Now that the general objectives of this project have been covered, more specific goals and methods are detailed below.

The overall goal of testing is to generate failures in the field that can be predicted by data collected from available sensors. To generate failures, test PCBs are subjected to accelerated testing. Accelerated testing involved amplifying the loading on the test PCBs with a forcing vibratory input. The goal is to generate failures within several hours of testing so that testing multiple samples is practical. However, due to the stochastic nature of fatigue, failures can be highly unpredictable.

To help account for scatter in fatigue, PCBs were populated with the same component type. Multiple components allows for calculation of failure statistics. In addition to being populated with the same components, previously characterized PCBs were needed. Otherwise, PCBs would have to be tested to obtain failure data necessary to develop damage accumulation models.

Another important test requirement is low cost. Development and unit costs of a PHM system for military vehicles cannot be a significant portion of the vehicle cost [10]. This requires the use of simple and easily implemented PHM algorithms that can be processed with a low powered on-board computer and with limited set of sensors.

The last test requirement involves that the design of the experimental setup be portable and easy to use. This requirement is necessary since the same vehicle will not always be available for testing and different personnel at Aberdeen Proving Ground (APG) will be setting up the instrumentation on the vehicles. Therefore, moving the instrumentation needs to be as easy as possible and setting up the instrumentation needs to be almost self-explanatory.

2.1 Preliminary Experimental Setup

A preliminary experimental setup meeting some of the previously described objectives was developed to help gain insight into vibration testing in a vehicular environment. This setup consisted of a Somat eDAQ-lite unit made by nCode International and a custom layer stacked on top of the eDAQ unit used to fixture the test PCBs.

During testing, the Somat eDAQ-lite was used to record GPS, continuity, strain, and accelerometer data. It also has the ability to link to the vehicle bus to

record engine and drive train parameters. The DIO layer records data from digital channels (e.g. vehicle bus, GPS) while the bridge layer records data from analog channels (e.g. strain, acceleration). In addition, the eDAQ has a 166 MHz processor, 256MB of DRAM and 2GB memory storage for on-board data processing and storage. While in use, the unit consumes an estimated ~12 watts at ~0.8 amps. For more information see [11] for more detailed specifications. The approximate dimensions of the unit are shown in Figure 1.

Figure 1. Somat eDAQ-lite unit with dimensions

The eDAQ-lite unit was chosen as the data acquisition unit due to its use at Aberdeen Proving Ground (APG). The US Army Materiel Systems Analysis Activity (AMSAA) group, which assisted in testing at APG, has extensive experience in using the eDAQ unit. This experience proved to be invaluable in troubleshooting hardware and software issues on and off the APG test site. In addition, using the eDAQ unit opened up the possibility of piggybacking on AMSAA tests and synching with the AMSAA eDAQ unit during testing. Synching eDAQ units together allows for data collected on different units to be shared and merged together.

The initial design concept (Figure 2 and Figure 3) involved mounting a printed circuit board (PCB) in a cantilever fashion on top of the eDAQ-lite unit. A custom layer that fits over the support posts at the corners of the eDAQ unit was developed. The custom layer clamps the PCB at one end while a weight is attached on the other end of the PCB. The weight functioned as a simple load amplification device for the PCB. In addition, this design allows for the smallest overall footprint since it adds only to the height of the eDAQ unit.

Figure 2. eDAQ-lite with custom layer

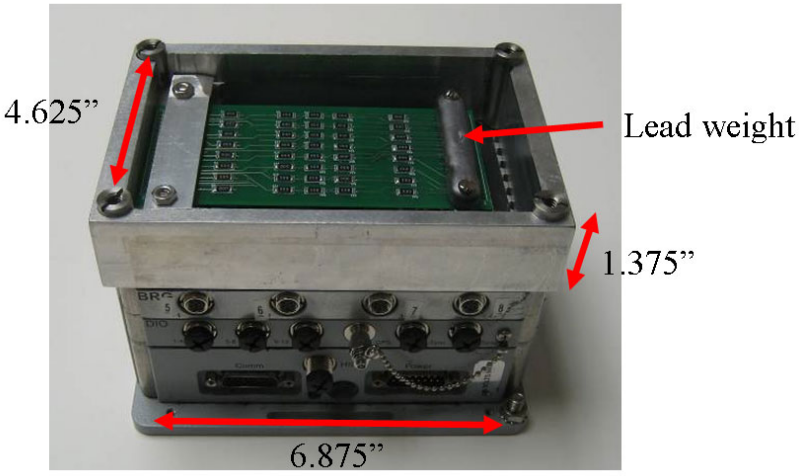

Figure 3. eDAQ-lite with custom layer, PCB exposed

There were several issues with this preliminary design. Given the layer thickness shown in Figure 3, maximum possible deflection of the free end without

striking components on other layers is 0.6 inches. Testing showed that average strain level produced by this setup is ~500 μstrain while maximum strain experienced was ~1800 micro strain. At around 2500 micro strain, free end of the PCB starts to run out of clearance with the layer below. To fail 2512 resistor boards seen in Figure 3 rapidly, higher strain levels are required.

Increasing layer thickness to increase the maximum possible deflection of free end encountered several problems. Large deflections require that a protective layer be added to separate the bridge layer components from potential damage. In addition, the maximum board length that a layer can accommodate is ~ 5.5 inches. To achieve maximum desired deflection, the end weight would have to be increased significantly due to non-linear properties of fiberglass. The volume of this increase in weight needs to be considered because it adds to required layer thickness. Increasing layer thickness to accommodate desired maximum deflection would increase overall height of eDAQ significantly over 7 inches. The resulting height would make the eDAQ unit unwieldy to handle. The size increase requires that the whole unit be fixed inside a case to solve portability problems. In addition, only components near the clamped edge see desired strain levels. Components near the free end experience a small fraction of the desired strain levels. Only a small fraction of total number of components is located near the clamped edge. Therefore, to compile component failure statistics, uniform loading across the components is necessary. In addition, boards larger than 5 inches in length were necessary to test larger packages such as ball grid array (BGA) packages.

The solution to uniform loading across components came in the form of a four-point bending fixture. In addition, an independently mounted bending fixture could accommodate larger PCBs and maximum deflections than possible with the layer design. However, the four-point bending design increases the size, weight, and complexity of the experimental setup.

2.2 Refined Experimental Setup

An experimental setup resolving issues with the preliminary setup and meeting objectives described in Section 2.0 was developed (with exception of measuring continuity for individual components). Experimental setup components consist of a Pelican 1520 case, Endevco 7290A-30 accelerometer, Wall Industries QAW24S12-40 DC to DC converter, Somat eDAQ-lite, Vishay foil type strain gauges (CEA-06-062UW-350), PCBs with various component types, and a four-point bending fixture.

The purpose of the Pelican case is to contain and fixture the various components to prevent movement. In addition, the Pelican case is rugged and can withstand some damage on its own without affecting the components within. Interior dimensions are shown in Figure 4 and Figure 5. Power cord shown in Figure 4 delivers power from vehicle electrical system. The equipment accepts both 12 volt DC power from passenger cars or 24 volts DC from military vehicles. The power switch seen in Figure 4 is the main power switch.

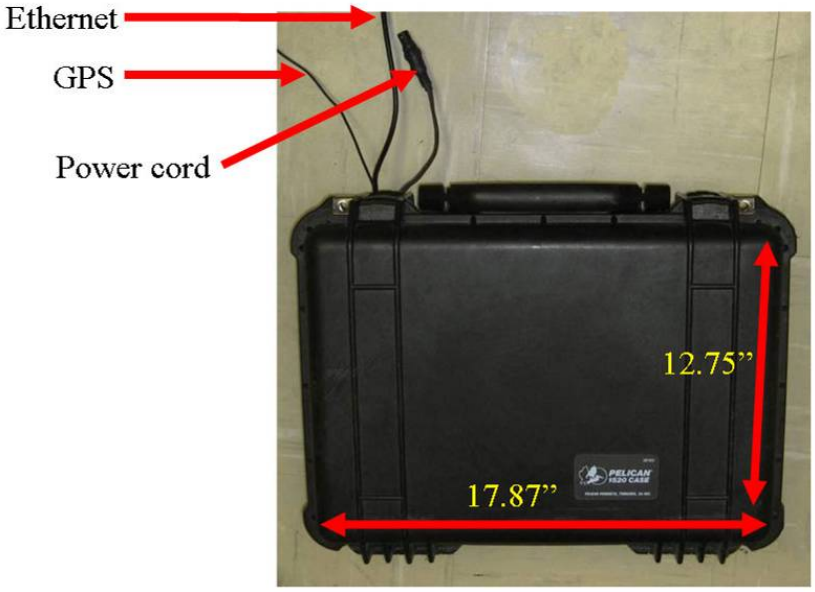

Figure 4. Pelican case, side view

Figure 5. Pelican case, top view

The four point bending fixture allows for amplified loading of the PCBs. Dimensions of the fixture are shown in Figure 6. PCBs are mounted with components facing up. Static strain on PCBs is ~1400 micro strain. The fixture can fit two PCBs at a time side by side. Rods located at the ends of the boards clamp down the boards while the two rods in the middle have some tolerance to allow for movement.

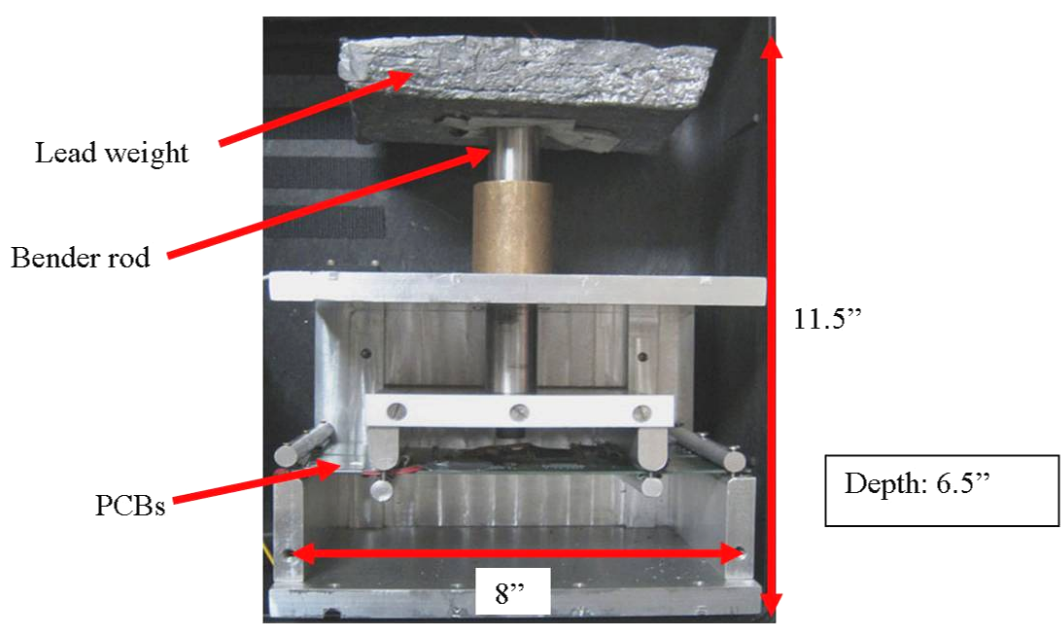

Figure 6. Four-point bending fixture

After the four point bending device was built, severe frictional forces were found in the system. Frictional forces can be attributed to several factors: the width between the blades of the four-point bender to accommodate component location on PCBs, two PCBs located parallel to each other, and clamped condition on both ends of the PCBs. With two PCBs mounted in the device, responses to even severe forcing inputs were found to be minimal. To overcome these frictional forces weight was gradually added to the top of the bender rod to increase response to forcing inputs. The final lead weight sitting on top of the bender rod weighs approximately 11 lbs. One foot drop tests were conducted to determine if desired peak strain levels could be reached with this weight. Results from this testing showed that peak strain values beyond 4000 micro strain in magnitude was possible. At this strain level, the four-point bending device has the ability to accumulate significant damage rapidly in the components. In addition to load amplification, the lead weight lowers the natural frequency of the system. Measured natural frequency of the board-mass system is

approximately between 8 to 10 Hz. A major problem with using such a large mass is that it significantly increases the chance of failures due to overstress rather than fatigue.

PCBs containing components with five different component types were tested. Components were solder reflow mounted onto 4 layer boards with overall thickness of 0.062 inches. Topline manufactured the 256 BGA, SOIC-8, SOT 223-4, SOT-23 components while the 1206 capacitors were manufactured by Kemet. Basic component dimensions are listed in Table 1. More details on PCB construction and component dimensions can be found in the Appendix.

Table 1. Individual Component Dimensions

Component	**Details**
Topline 256 BGA	Balls: 256 Size: 17 mm square Pitch: 1 mm Height: 1.76 mm
Kemet 1206 capacitor	Length: 3.2 mm (0.126 in) Height: 1.6 mm (0.063 in) Width: 1.6 mm (0.063 in)
Topline SOIC-8	Length: 4.9 mm Height: 1.6-1.7 mm Width: 3.9 mm Pitch: 1.27 mm
Topline SOT 23	Length: 2.9 mm Height: 1 mm Width: 1.3 mm
Topline SOT 223-4	Length: 6.5 mm Height: 1.8 mm Width: 3.5 mm

Pin outs near the short edges of the PCBs are used for checking continuity. Unless these pins are daisy-chained together with wires, continuity can be monitored for only one component. This is due to the limited number of bridge channels available on the eDAQ. Therefore, detection of the failure time for each individual component is not possible. First mode natural frequencies of these boards are in the range of 70 Hz according to CalcePWA analysis. Dimensions of the PCBs are shown in Figure 7.

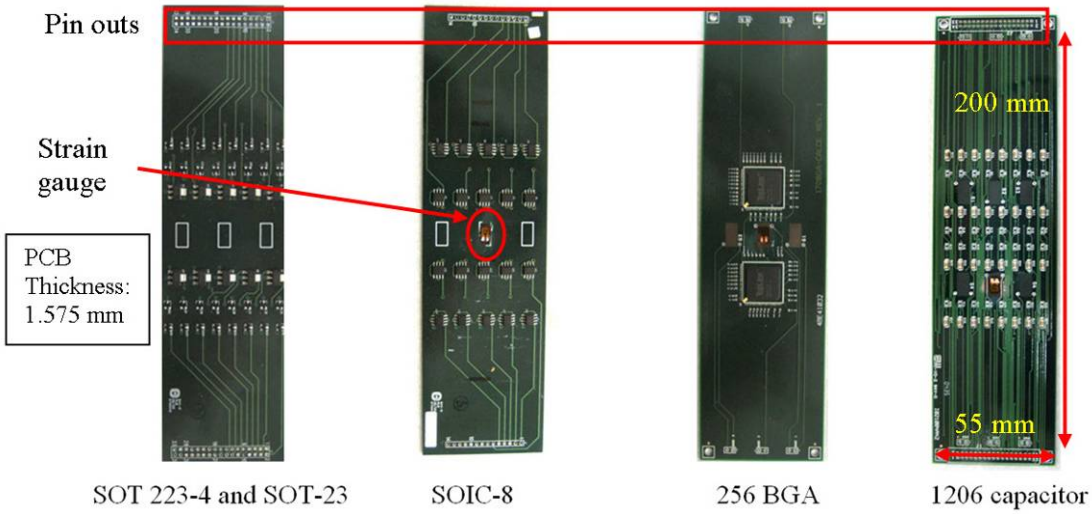

Figure 7. Tested Printed Circuit Boards (PCB)

Strain gauges seen in Figure 7 are located in the center of the PCB. Location of the accelerometer can be seen in Figure 8. Accelerometer is variable capacitance type with a range of +/- 30 g's. Both the strain gauges and accelerometer sample at 100 Hz. One continuity channel records at a sampling rate of 1 Hz. GPS is also sampled at 1 Hz. This is the sampling rate allowed by the GPS antenna. DC to DC converter shown below can accept DC voltages between 9 to 36 volts and transform to 12 volts DC output. Figure 8 shows complete experimental setup inside case.

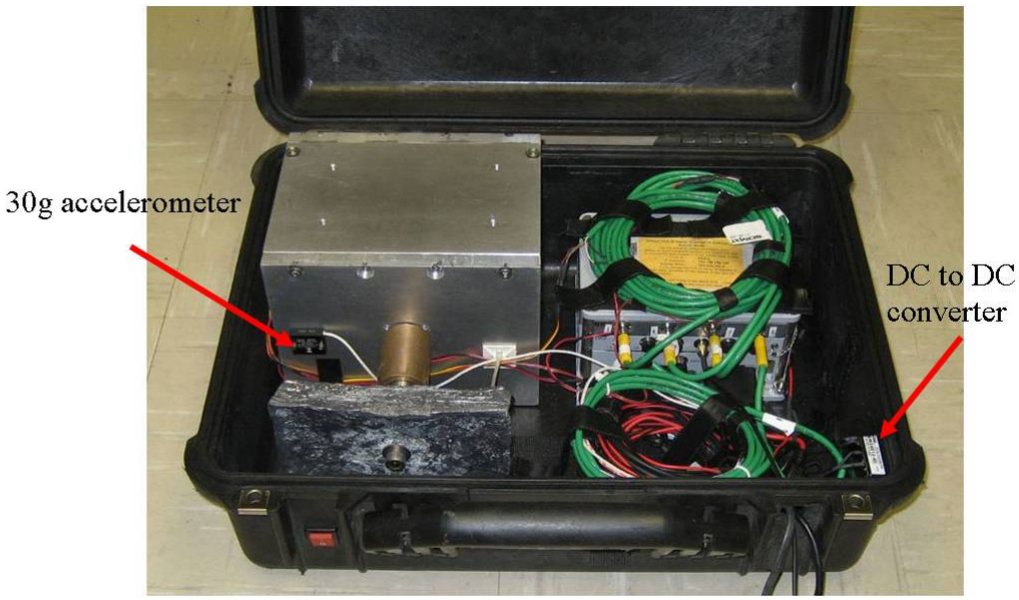

Figure 8. Fully Assembled Experimental Setup

2.3 Experimental Testing

Vehicular testing with the experimental setup shown in Figure 8 was conducted in two phases. In the first phase, testing was performed in a private passenger vehicle to determine if any major issues needed to be resolved before testing began at APG. One of the major concerns addressed by preliminary testing was the durability of the wiring connections. Shock testing in the passenger vehicle showed that strain relief built into the wiring and the soldered connections were strong enough with withstand high loads. Also, the data acquisition unit collected data continuously over a period of several days without encountering data corruption issues. Preliminary testing demonstrated high acceleration and strain levels could be achieved from going over kerbing and speed bumps. However, RMS strain levels for paved roads were close to zero. Testing continued at APG with the assumption that RMS strain levels would be higher given the harsh terrain available. In addition,

strain levels similar to speed bumps were expected to occur with high frequency on test tracks at APG.

In the second phase, testing was conducted at APG on Light Medium Tactical Vehicles (LMTV). Testing piggybacked on existing testing conducted by AMSAA. As a result, the test PCBs experienced a variety of loading conditions possible on the LMTV vehicle over a variety of terrain. RMS strain levels remained unexpectedly low even for the harshest environments tested. Continued testing at Aberdeen encountered various data collection issues resulting in significant or complete data loss.

2.3.1 Preliminary Passenger Vehicle Testing

Testing from January to March 2007 occurred at various locations around Maryland. Most of the testing occurred on a Ford F-350 Super Duty pickup truck. In these tests the instrumentation along with a 12 V marine battery were tied down to the truck bed as shown in Figure 9 and Figure 10.

Figure 9. Ford F350 truck

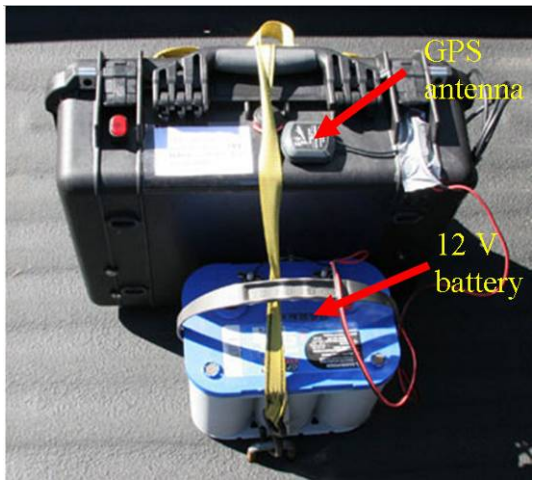

Figure 10. Experimental Setup in truck bed

Two tests were conducted using the Ford truck. A test run from February 1 to February 5, 2007 was used gather data on paved road response from the PCBs. In the course of testing, the instrumentation experienced varying paved road conditions between College Park and Eastern Shore of Maryland. The test also helped determine if there were any intermittent electrical problems with the components when running a long test. In addition, the test did not have any data corruption problems that can occur with large amounts of data collected over long periods of time. Total time of test was 86 hours before the battery ran out of energy. Another test conducted on March 2 consisted of repeatedly running over speed bumps and kerbing around College Park as seen in Figure 11. This test helped to determine if all the components could survive the harsh vibration environment at Aberdeen Proving Ground (APG). In addition, it gave an idea of the of response levels to expect from the PCBs under shock loading.

Figure 11. Shock Testing with Ford truck

Data in Figure 12 comes from the Ford truck running over 20 mph speed bumps at ~35 mph. This level of loading shown in Figure 12 (~2000 μstrain, 2 g's) was expected to be reproduced at high frequency at APG due to the harsh testing terrain available.

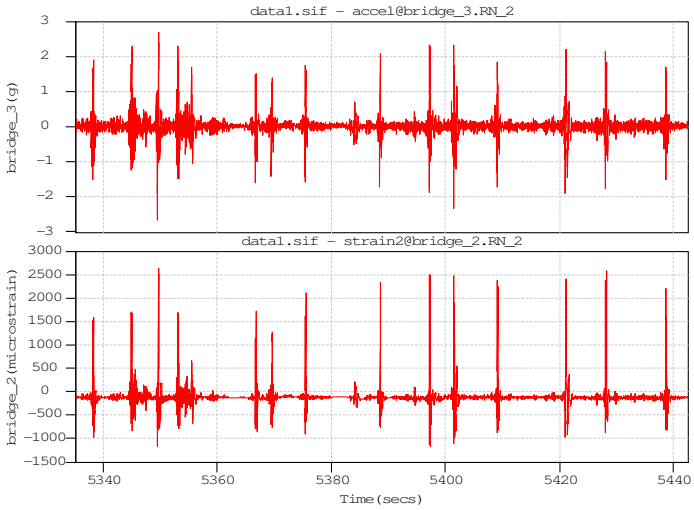

Figure 12. Data from Ford truck going over speed bumps

2.3.2 Testing at Aberdeen Proving Ground

At APG, the experimental setup was placed inside a Light Medium Tactical Vehicle (LMTV) similar to vehicle shown below. The box was placed inside a

storage bin behind the passenger seat directly below the arrowhead in Figure 13. Vehicle electrical system provides 24 V of DC power when vehicle engine is on.

Figure 13. Light Military Tactical Vehicle (LMTV)

Figure 14, Figure 15, and Figure 16 show the route from building 436 to Perryman Test Area, Perryman courses, and Munson courses, respectively. All military vehicle testing were performed at these locations with the exception of Churchville Test Area, which is not displayed. Perryman Test area is divided into Perryman Paved, A, 1, 2, 3, and various other courses not used in this project. Perryman A and 1 are secondary roads consisting of improved surfaces such as gravel. Perryman 2 and 3 are off road surfaces with increasing course numbers indicating increasing terrain severity. Descriptions of the Munson courses are shown in Figure 16.

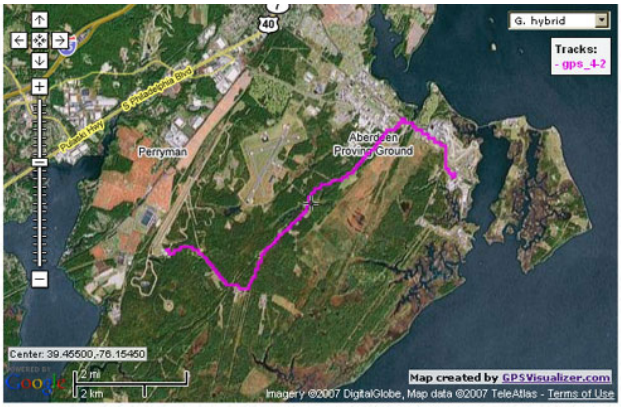

Figure 14. Route from Building 436 to Perryman Test Area

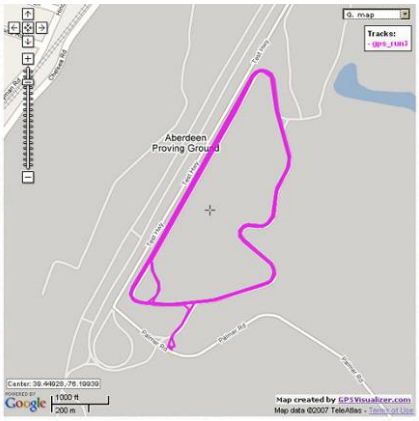

Figure 15. Perryman test courses

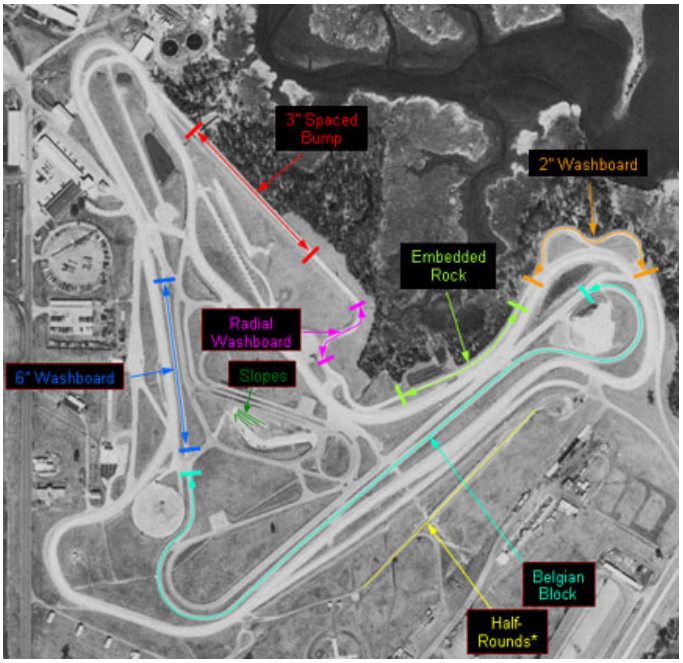

Figure 16. Munson test courses

Test plan used for the 256 BGA and the 1206 capacitor PCBs is detailed in the Table 2.

Table 2. Test plan for 256 BGA and 1206 capacitor

Date	Run number	Course	Notes
4/2/2007	1	Building 436 to Perryman	
4/2/2007	2	Perryman A	Highway, 55 psi tire pressure
4/2/2007	2	Perryman A	Cross Country, 31 psi
4/2/2007	2	Perryman A	Sand, 18 psi
4/2/2007	3	Perryman to Building 436	
4/3/2007	1	Building 436 to Perryman	
4/3/2007	2	Perryman 1	Highway, 55 psi
4/3/2007	2	Perryman 1	Cross Country, 31 psi
4/3/2007	2	Perryman 1	Sand, 19 psi
4/3/2007	3	Perryman to Building 436	
4/4/2007	1	Building 436 to Perryman	
4/4/2007	2	Perryman 2	Highway, 54 psi, Rain/Mud
4/4/2007	2	Perryman 2	Cross Country,31 psi, Rain/Mud
4/4/2007	2	Perryman 2	Sand, 18 psi, Rain/Mud
4/4/2007	2	Perryman 3	Highway, 54 psi, Rain/Mud
4/4/2007	3	Perryman to B436	
4/4/2007	4	B436 to Perryman	
4/4/2007	5	Perryman 3	Cross Country, 31 psi, Rain/Mud
4/4/2007	5	Perryman 3	Sand, 18 psi, Rain/Mud
4/4/2007	5	Perryman to B436	

Only a rough test plan for the SOT and SOIC PCBs are available due to data recording issues encountered. Data available column indicates availability of strain and acceleration data. No GPS data is available for these tests. All available information is in Table 3:

Table 3. Test plan SOT and SOIC

Date	Course	Notes	Data Avail.
4/11/2007	Paved full throttle runs at Perryman. Load vehicle 5000 lbs, weight vehicle.	Highway, cross country	Yes
4/12/2007	Munson gravel, Belgian Block. Perryman Paved.	Highway, Cross Country, Sand. Highway.	No
4/13/2007	Perryman A. Perryman 1. Perryman 2.	Highway, Cross Country, Sand. Sand, Cross Country, Highway, Max Safe Lap. Highway, Cross Country.	Yes
4/14/2007	Perryman 2. Perryman 3.	Sand. Sand 5 mph&10 mph, Cross Country, Highway.	Yes
4/16/2007	Perryman Paved. Churchville B.	Cross Country, Sand. Highway, Cross Country, Sand.	Yes
4/17/2007	Perryman Paved. Churchville B.	Highway. Highway, Cross Country, Sand.	No
4/18/2007	Not Available.	Not Available.	Yes
4/20 to 4/24	Not Available.	Not Available.	No
5/2 to 5/3	Perryman Paved, A, 2, 3.		No
5/3/2007	Munson 2”-4” radial washboard. Munson 3” spaced bump. Munson Belgian Block. Munson Turning Circle.		No
5/4/2007	Churchville B		No

Chapter 3: Data Processing and Analysis Techniques

3.0 Background Information

Random vibration is motion that is not regularly periodic and must be specified with statistical methods [12]. A ground vehicle experiences random vibrations due to irregularities in paved or off-road surfaces. Over the course of its life, a military ground vehicle will experience a wide range of vibration levels caused by numerous types of terrain, loading conditions, and transient events such as ruts, kerb strikes, and pot holes. One way to view the life profile of a military ground vehicle is a mixture of various deterministic and stochastic events [8].

Deterministic signals are when the value of the signal can be determined at anytime using a mathematical expression or rule [13]. Deterministic signals include harmonic excitation, step or ramp input, half-sine pulse, and other signals with defined profiles. While a deterministic signal profile is well defined, the events producing deterministic signals are highly unpredictable. Examples of deterministic events include striking kerbs, potholes, and going over evenly spaced bumps. Deterministic events are represented in the time domain [8].

Stochastic signals cannot be determined at any time using a mathematical expression. The unpredictable nature of stochastic signals requires the use of statistics to analyze their behavior [13]. Examples of stochastic events include driving over

paved roads, wind turbulence, and wave loading on offshore structures [8]. It is usually preferable to represent stochastic signals in the frequency domain in the form of power spectral density (PSD) to improve statistical confidence, data computation, and storage [8]. Stationary random vibrations are more usefully studied in the frequency domain than the time domain [14]. Wirsching, *et al.* [14] extensively discusses methods to analyze random vibrations in both the time and frequency domains. Following sections describe methods used to process data in time and frequency domains.

3.1 Time Domain Analysis

3.1.1 Utilizing GPS data and Load Blocking Technique

GPS is the most important piece of information used to process other test data. GPS fundamentally belongs to the time domain since location is of little use without time information. GPS information is invaluable for breaking up acceleration and strain data to correspond to a particular course of terrain. In addition, speed data calculated from GPS signal is useful for signal-triggered data processing. For example, the data acquisition unit can be set to record data only when vehicle is moving and if a GPS signal is available. Military vehicles often spend a significant amount of time idling. Signal triggering for speed significantly reduces the amount of recorded data and can be used as a data reduction method. In addition, data from idling can be significantly different from when the vehicle is moving. Analyzing stationary data together with moving data can skew results badly. Therefore, knowing what is stationary data and stripping it out be analyzed separately is very important.

GPS was used extensively to perform load blocking as demonstrated in the remainder of this section.

Test data shown in Figure 17 was recorded on 4/2/2007. According to the test plan, three runs on Perryman A were conducted on this day. A map of GPS data in Figure 17 is shown in Figure 15 in Section 2.3.2. GPS data confirms that associated acceleration and strain data are from tests on Perryman A from 4/2/2007. Figure 17 demonstrates that blocking strain and acceleration data according each test condition can be obvious with speed information.

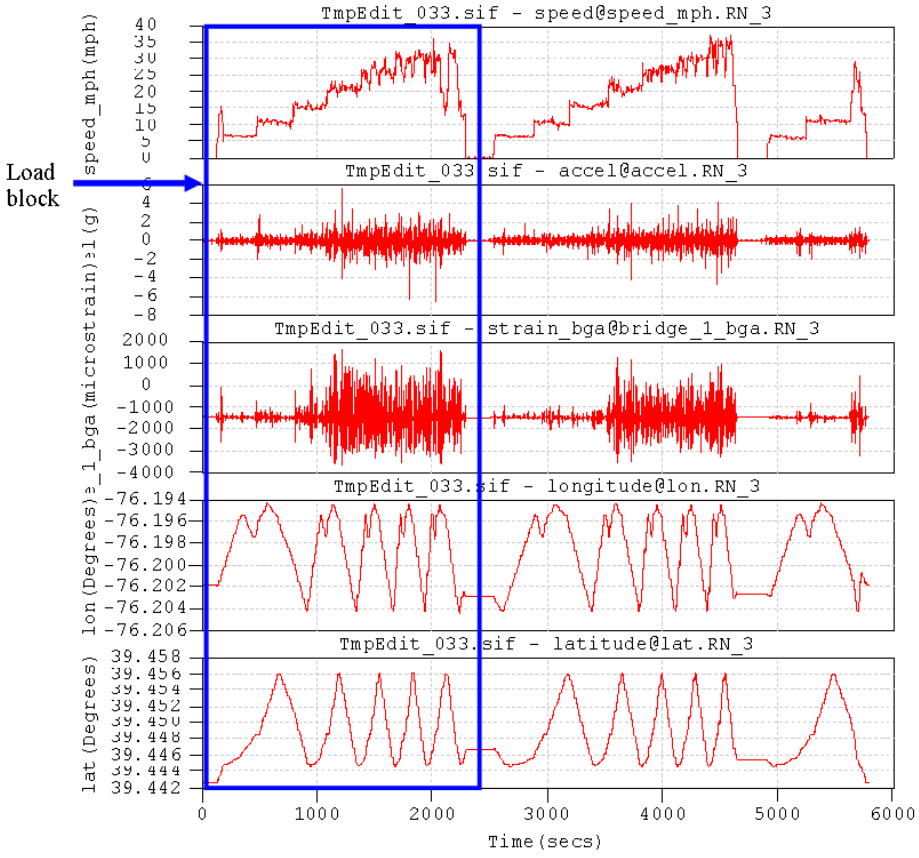

Figure 17. Perryman A Test Data, 4-2-2007

After performing load blocking, data can be analyzed according to each separate condition or terrain as seen in Figure 18. At this point GPS information is

discarded as the location has been determined in previous step prior to load blocking seen in Figure 17.

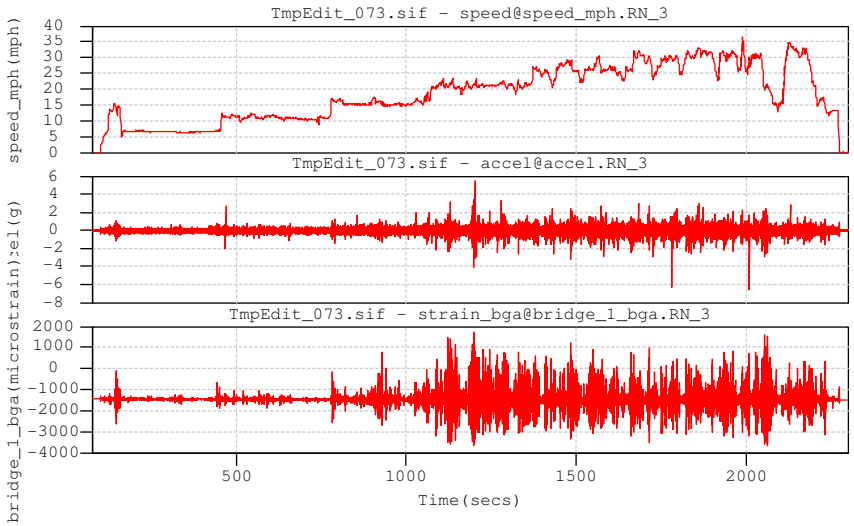

Figure 18. Load Block- Perryman A, 55 psi, 4-2-2007

3.1.2 Calculating RMS

Root mean square (RMS) [15] is a statistical measure of the magnitude of a varying quantity and is especially useful for analyzing waves.

$$x_{\mathrm{rms}} = \sqrt{\frac{1}{n}\sum_{i=1}^{n} x_i^2} = \sqrt{\frac{x_1^2 + x_2^2 + \cdots + x_n^2}{n}} \quad [15]$$

RMS of acceleration levels is one way of obtaining an idea of terrain 'roughness'. RMS strain levels along with natural frequency of system may allow for an approximate estimation of damage accumulation rate. RMS is calculated for each sample or block of data. Therefore, picking an optimal sample window size is very important.

Richard Heine [10] performed a study on sample window size for data obtained from military vehicles operating in primary, secondary, and off-road terrain.

Heine observed that speed changed significantly over sections longer than 20 seconds, while sections less than 0.5 seconds contained too little terrain information to provide good statistical measures. Initial visual inspection of data did not show obvious superiority of a particular sample rate between 0.5 and 20 seconds [10]. However, using a terrain identification scheme, Heine showed that longer sample window sizes increased the accuracy of his terrain identification scheme. For this project, a sample window size of 15 seconds was chosen based on visual inspection of data and Heine's work.

Statistical analysis by terrain rather than set time intervals is shown in the Appendix. Statistics used in analysis include RMS, kurtosis, skewness, and Crest Factor.

3.1.3 Cycle Counting and Binning

Now that data processing methods for the time domain has been covered, time domain analysis of damage accumulation will be covered. Time domain analysis of damage revolves around cycle counting and binning methods. Perhaps the most popular method of cycle counting is the rainflow cycle counting method. Refer to reference [16] for more information on rainflow and other cycle counting methods. The main idea behind cycle counting is to transform a time history consisting of a number of reversals into an equivalent time history [16]. Once reversals are identified and classified as a cycle of quantified amplitude, cycles within each defined range of values are counted. This is data binning. The remainder of this section covers the software program used to perform rainflow cycle counting.

Before data can be cycle counted and binned, it first needs to be filtered. The need to filter data is demonstrated in Figure 19 where the zoomed in strain time history shows multiple data points around peaks and valleys. These multiple data points complicate the task of identifying cycles and need to be filtered out as seen in Figure 20 before cycles can be counted.

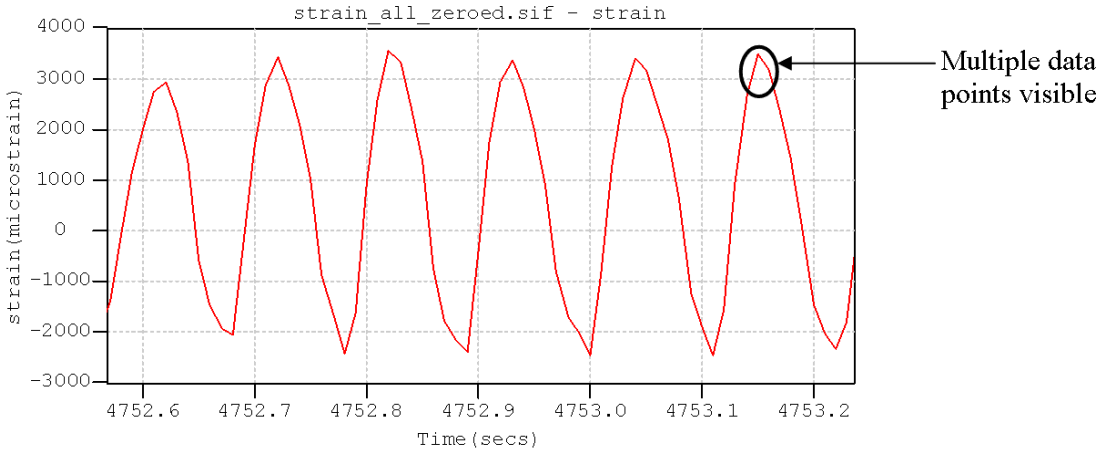

Figure 19. Sample strain time history

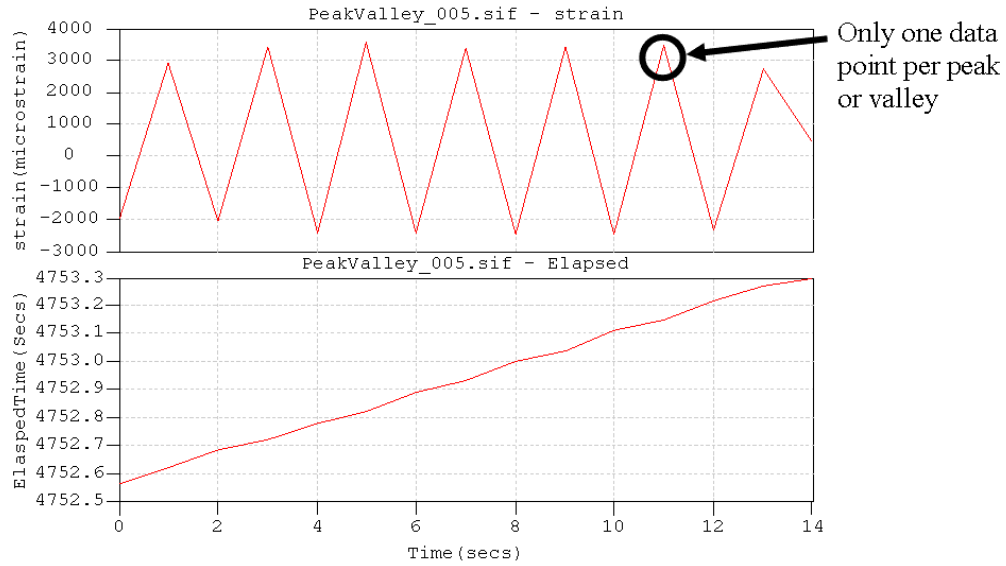

Figure 20. Filtered sample strain time history

For demonstration purposes, the brief strain time history data shown in Figure 21 is cycle counted and binned. Figure 22 shows the InField software settings for the

Rainflow function used to calculate and bin cycles. The hysteresis setting seen in Figure 22 is the setting used to obtain the filtered data seen in Figure 23. The strain bins used to count strain ranges are listed in Table 4.

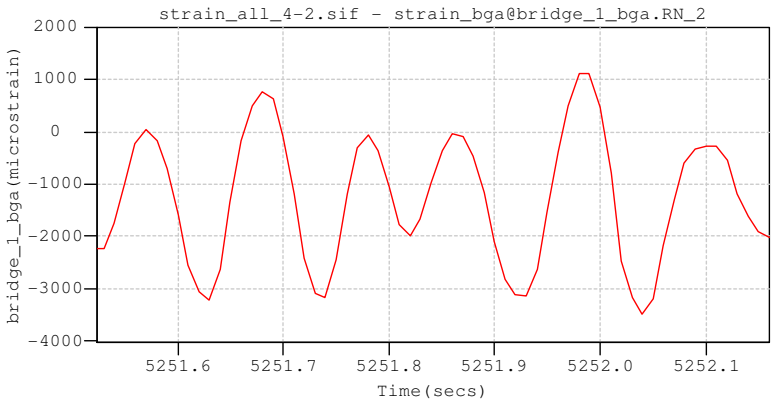

Figure 21. Sample Strain Time History #2

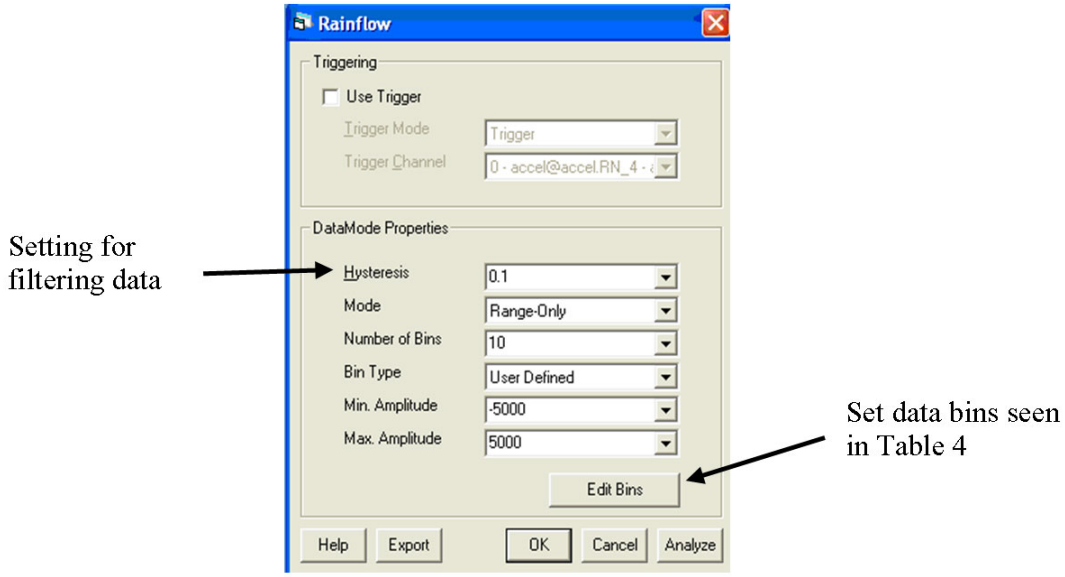

Figure 22. InField Rainflow Settings

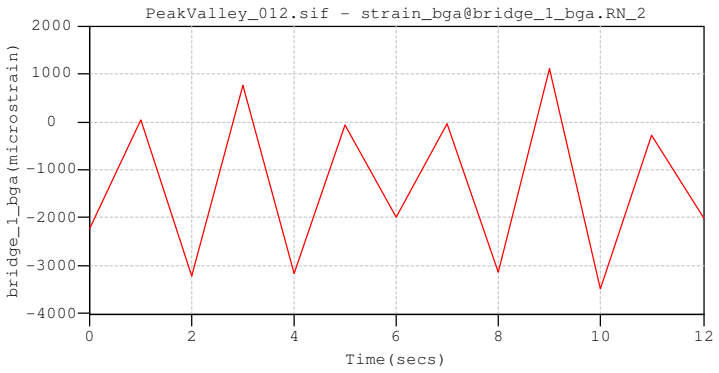

Figure 23. Filtered Strain Time History #2 (see Figure 21)

Table 4. Strain Bins

Strain bin (µstrain)
-4000 to -3000
-3000 to -2000
-2000 to -1000
-1000 to 0
0 to 1000
1000 to 2000

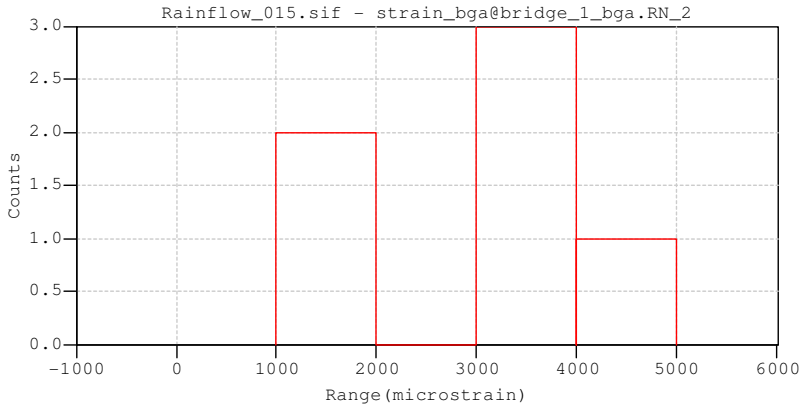

Figure 24. Strain Time History #2 Cycle Counted and Binned

Figure 24 shows the results of cycle counting and binning. The results match with a visual inspection of Figure 23. Six cycles were counted and binned. The second to last cycle in Figure 23 is clearly above 4000 µstrain range. The cycle between ~4.5 seconds and ~6.1 seconds and the last cycle in Figure 23 appear to be

below the 2000 μstrain range. The remaining three cycles appear to be within the 3000 and 4000 range as confirmed by the rainflow counting results.

3.2 *Frequency Domain Analysis*

A common method for analyzing random vibration data in the frequency domain is with the power spectral density (PSD) function. PSD indicates frequency distribution of signal power [18]. A useful assumption is to assume Gaussian amplitude distribution. Making this assumption significantly simplifies damage calculations as the RMS is equal to one standard deviation [17]. Wirsching [14] extensively covers the mathematical background necessary to calculate and use the PSD function.

Before detailing PSD use in this project, several issues regarding analysis of frequency spectrum needs to be noted. Each peak in PSD or FFT plot does not necessarily correspond to a distinct mode, it may be due to higher harmonics or electrical noise [18]. In addition, do not apply FFT or PSD on minimum or maximum principle strain data, as this does not correspond to strain at a fixed location and orientation in the system [18]. This is not the case in this experiment as PSD is calculated for only direct strain measurements. Another issue of note is that continuous static loading on PCBs results in a DC component in strain data that appears as a peak at zero frequency in FFT or PSD plot. The following two sections discuss the need to use proper windowing when calculating PSD and the procedure to obtain PSD for a particular loading condition.

3.2.1 Windowing

To obtain good frequency or amplitude resolution from PSD analysis windowing is often necessary. When PSD or FFT (Fast Fourier Transform) of a non-periodic time trace is computed, the frequency spectrum suffers from leakage, the result of energy smearing out over a wide frequency range when it should be in a narrow frequency range [18]. Windowing reduces leakage by applying what is essentially a weighting function that forces start and end points to equal zero [18]. See Figure 25 for an example of a signal calculated with a window (red) and without (black).

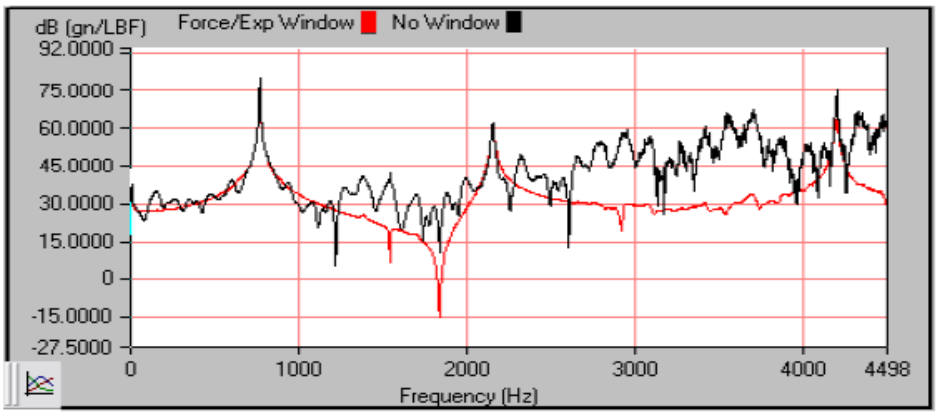

Figure 25. PSD with windowing (red) without (black) [19]

To determine the best windowing function for a signal type, see Table 5. In general, Flat top window is used when the best amplitude accuracy is desired while Hanning window is commonly used when good frequency resolution is required [18]. A disadvantage of windowing functions is the attenuation of the beginning and end of a signal, resulting in a need for overlap processing to recover lost data and reduce measurement time [19].

Table 5. Table of windowing guidelines [19]

Window	Best for these Signal Types	Frequency Resolution	Spectral Leakage	Amplitude Accuracy
Barlett	Random	Good	Fair	Fair
Blackman	Random or mixed	Poor	Best	Good
Flat top	Sinusoids	Poor	Good	Best
Hanning	Random	Good	Good	Fair
Hamming	Random	Good	Fair	Fair
Kaiser-Bessel	Random	Fair	Good	Good
None (boxcar)	Transient & Synchronous Sampling	Best	Poor	Poor
Tukey	Random	Good	Poor	Poor
Welch	Random	Good	Good	Fair

3.2.2 PSD calculation procedure

This section demonstrates the process used to calculate PSD for each load block.

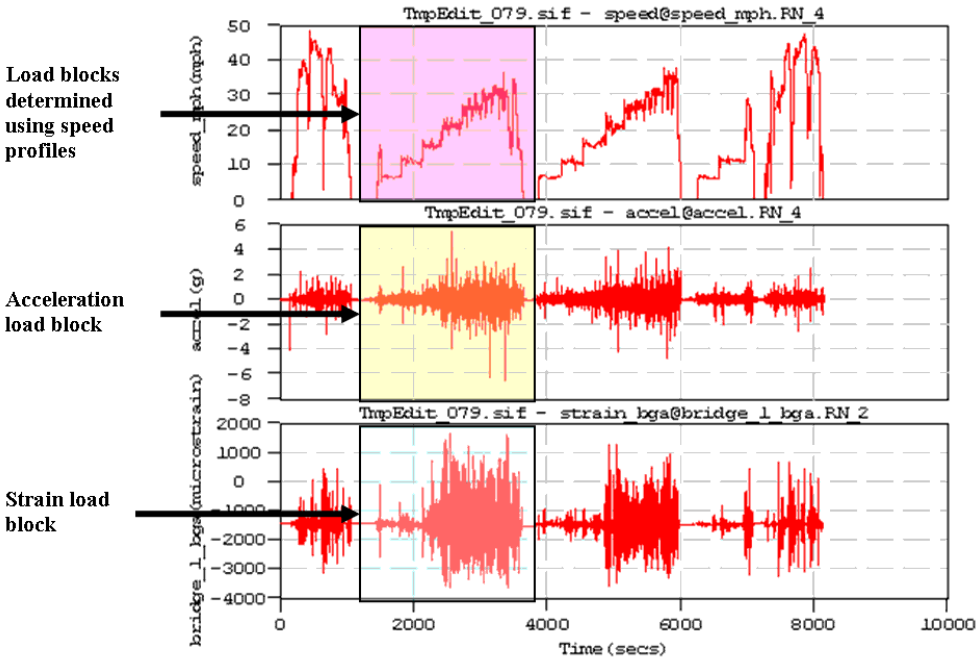

Figure 26. Sample load block used for PSD calculation

Somat InField software calculates PSD for highlighted data shown in Figure 26. Software settings used for PSD calculation are shown in Figure 27.

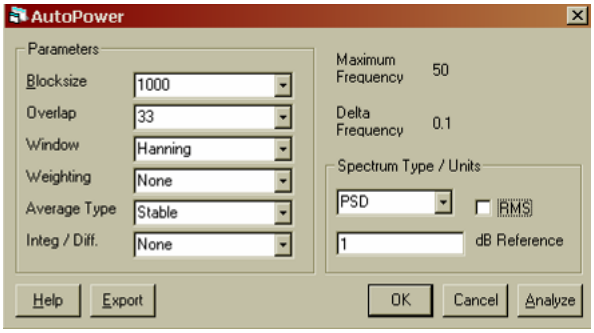

Figure 27. InField software settings for calculating PSD

PSD of sample acceleration load block is shown in Figure 28:

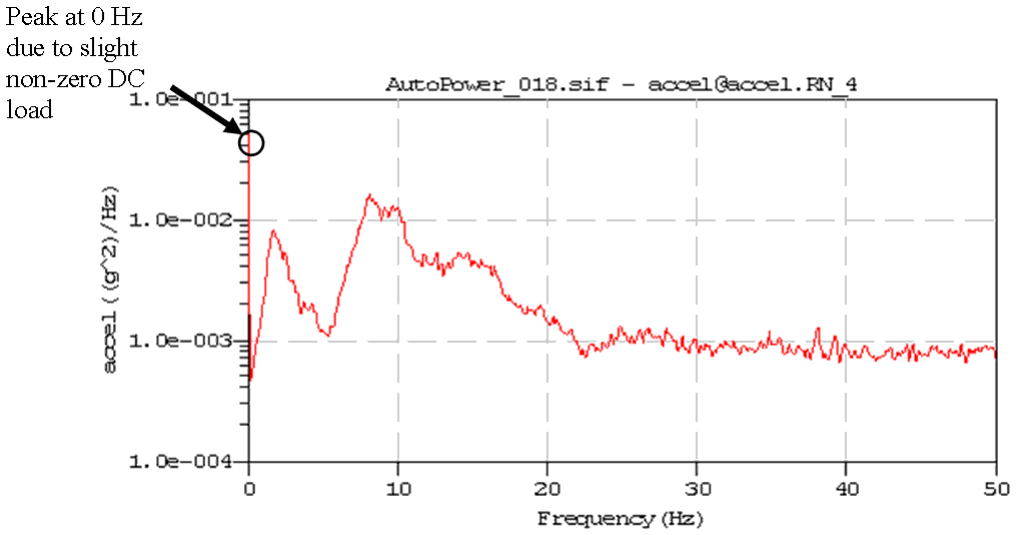

Figure 28. PSD of sample acceleration load block

PSD of sample strain load block is shown in Figure 29:

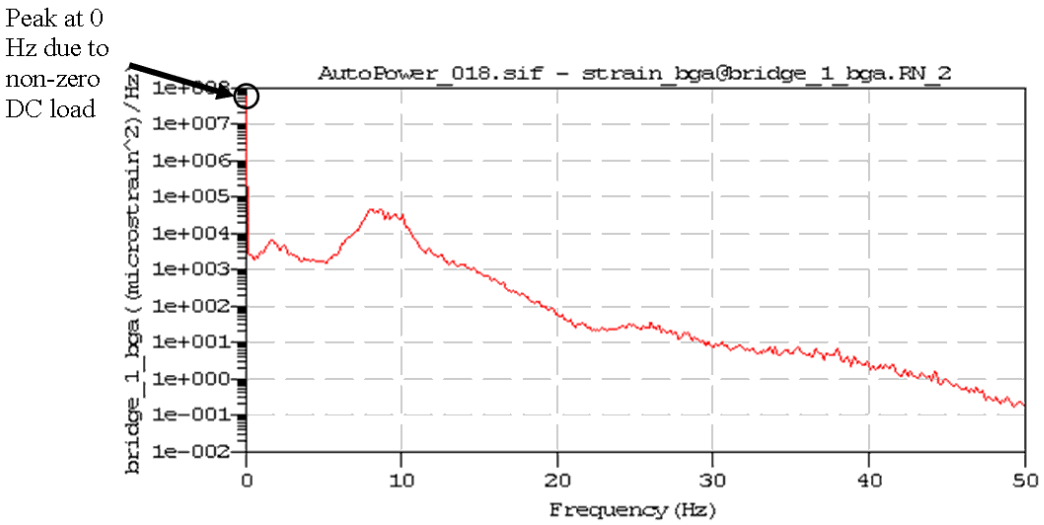

Figure 29. PSD of sample strain load block

3.2.3 Transient Loading PSD

In this section, PSD is demonstrated on short time intervals containing high-level events (Figure 31) instead of load blocks seen in Figure 26. PSD of short time intervals can vary significantly from PSD of longer time intervals. PSD analysis was performed on ~2900 second load block (Figure 30) and a smaller 50 second interval (Figure 31) from the load block.

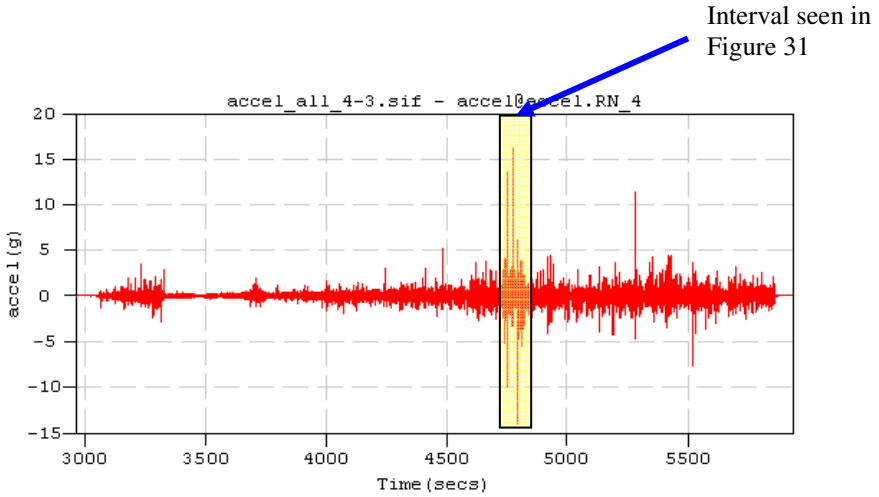

Figure 30. Acceleration Time History of Shock Loads, ~2900s

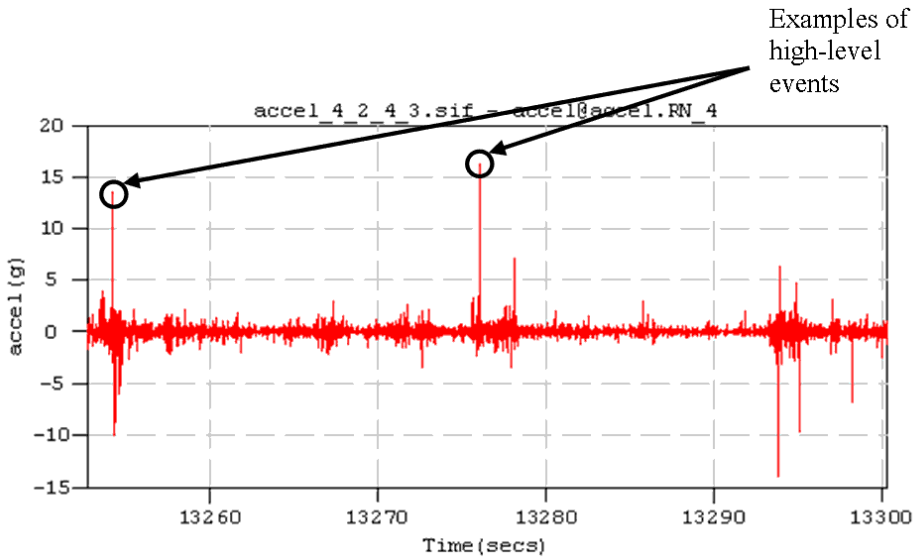

Figure 31. Acceleration Time History of Shock Loads, 50s interval

PSD calculations for acceleration and strain time history data used the same software settings seen in Figure 27. Figure 32 and Figure 33 show the results of PSD calculations.

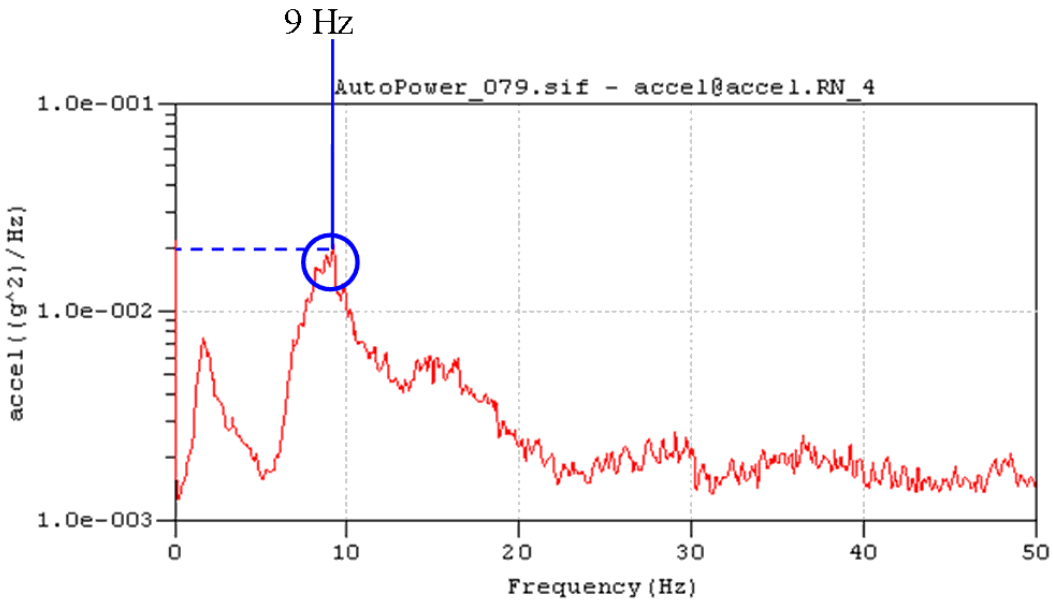

Figure 32. Acceleration PSD of Load Block in Figure 30, 2900s interval

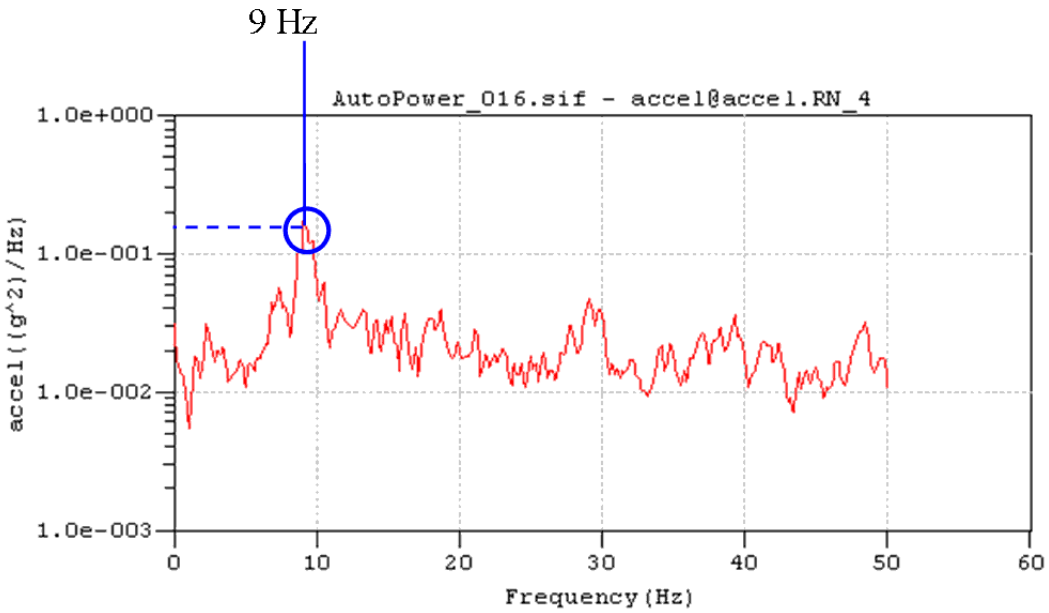

Figure 33. Acceleration PSD of 50s interval in Figure 31

Notice that power at 9 Hz in Figure 33 (~2e-001) is significantly higher than PSD at 9 Hz in Figure 32 (~2e-002). Indeed, PSD in Figure 33 is higher than Figure 32 for all frequencies. This maybe caused by PSD capturing 'ringing' of the PCBs due to shock loads. For a longer time interval, shock events are averaged out into statistical insignificance. This example demonstrates the interval length of a PSD has a significant effect on the results.

Chapter 4: Data Analysis Results

In this chapter, the general behavior of the experimental fixture is presented. First, the behavior of the fixture is evaluated through spectral analysis of the experimental results. Then the recorded parameters are compared against each other along with terrain information. To determine the unique characteristics of the military vehicle environment, comparisons were performed. Comparisons were broken down into two categories, passenger vehicle vs. military vehicle and paved vs. off-road. The passenger vehicle environment was compared to military vehicle environment for paved roads only (the only information available for passenger vehicle). Then paved road data was compared to off-road data for military vehicles only.

4.0 Spectral Analysis of Experimental Setup

Natural frequencies of the experimental setup were determined by calculating PSD for recorded strain and acceleration data. Figure 34 and Figure 35 show the complete strain and acceleration time history of testing between 4-2 and 4-4 at Aberdeen. Figure 27 shows the software settings used to calculate PSDs for the complete strain and acceleration time history. Figure 36 and Figure 37 show the resulting PSDs of strain and acceleration time history between 4-2 and 4-4. PSD spikes around zero hertz are likely due to non-zero system DC response [18].

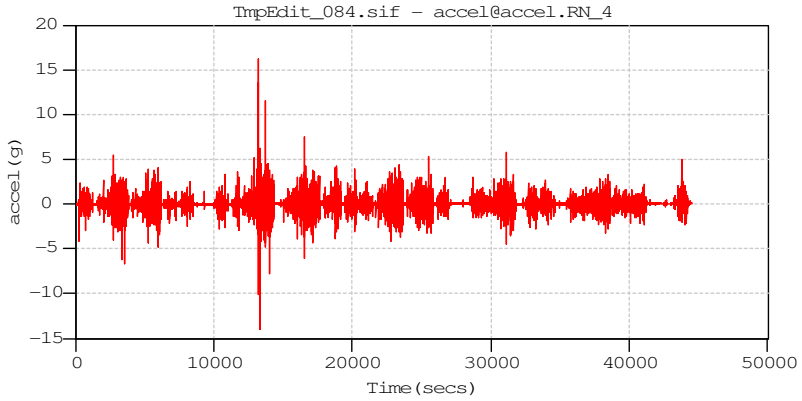

Figure 34. Acceleration Time History, 4-2 to 4-4

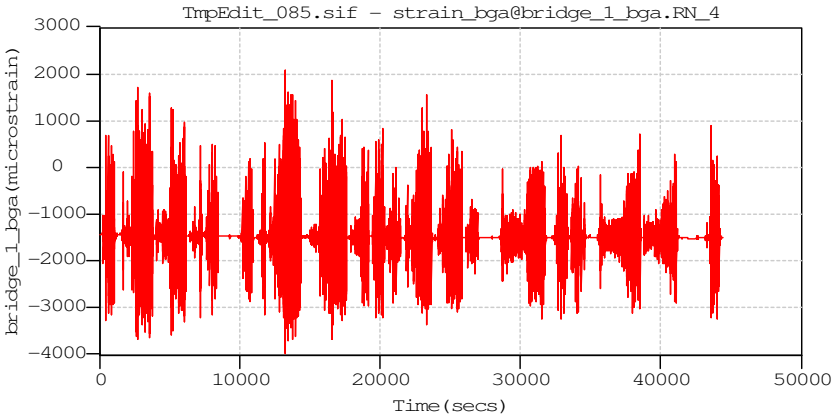

Figure 35. Strain Time History, 4-2 to 4-4

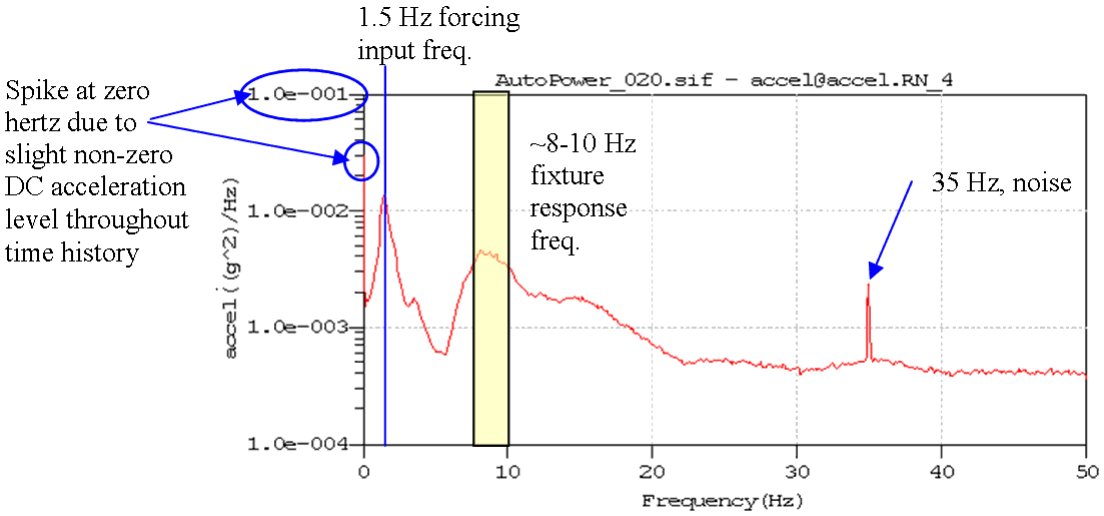

Figure 36. Acceleration PSD, 4-2 to 4-4

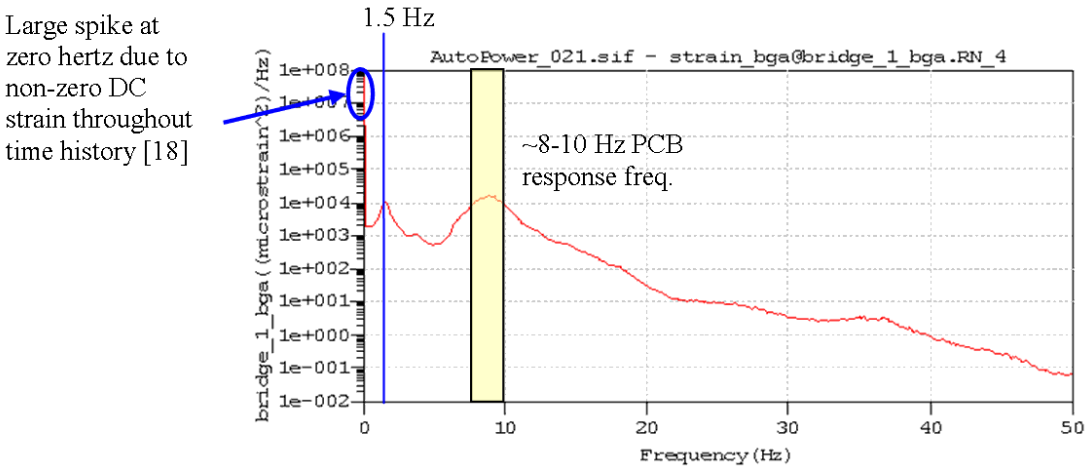

Figure 37. Strain PSD, 4-2 to 4-4

As seen in Figure 36 and Figure 37, amplitudes peak around 1.5 Hz and 8 to 10 Hz. Acceleration PSD is higher at 1.5 Hz than 8-10 Hz. An accelerometer is located on the structure of the four-point bending fixture. Therefore, the accelerometer measures the response of the entire fixture rather than just the response of the PCBs. Due to higher amplitude acceleration PSD at 1.5 Hz than acceleration PSD amplitude at 8-10 Hz, it is suspected that 1.5 Hz is for forcing input frequency of the experimental setup. This frequency is within the well-known expected sprung mass response of many road vehicles (1-2 Hz). Consequently, the measured acceleration response around 8-10 Hz is expected to be the fixture response. Strain PSD amplitude is higher at 8-10 Hz than strain PSD amplitude at 1.5 Hz. Because strain gauges directly measure the response of the PCB, 8-10 Hz is expected to be natural frequency of the lead weight and PCB system. The input forcing frequency of 1.5 Hz also shows up in the PCB response. Only it shows up at lower strain PSD amplitude because it is not at a natural frequency of the system. However, a higher mode of this forcing frequency (1.5 Hz * 6 = 9 Hz) is in the range of measured PCB natural frequency and is able to excite PCBs beyond the input strain PSD level.

4.1 Parameter Correlations

To determine if correlations exist between measured acceleration, strain, and speed, these variables were plotted against one another. The RMS statistic was used because it is useful for quantifying the magnitude of a varying quantity with positive and negative values such as strain and acceleration measurements [15]. RMS of measured variables was calculated in 15-second intervals to preserve general data trends while reducing the appearance of scatter and wild data points. A more detailed description on determining suitable interval length is discussed in Section 3.1.2 and reference [10].

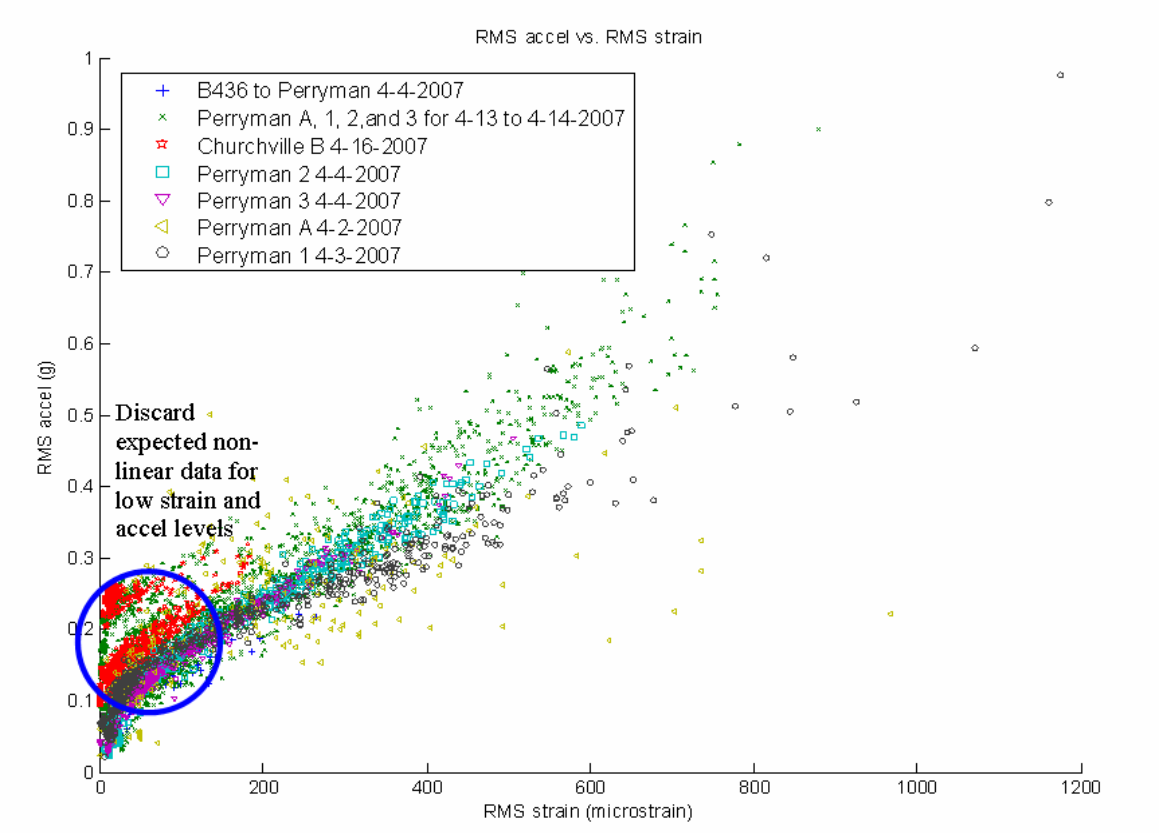

Figure 38. RMS acceleration vs. RMS strain

In Figure 38 and Figure 39, there appears to be a linear correlation between RMS strain and RMS acceleration. This nearly linear correlation appears to have the same approximate slope regardless of terrain. For RMS strain values less than 50, the slope of the correlation appears to higher than for RMS strain values greater than 50. Non-linear behavior is to be expected at low strain and acceleration values. This non-linear behavior is likely caused by frictional damping or material properties of PCBs playing a bigger role at low strain and acceleration levels. Figure 39 shows the linear regression fit between RMS acceleration and RMS strain excluding strain data below 50 μstrain. The correlation coefficient of linear regression fit (R^2= 0.74) demonstrates the loose correlation between acceleration and strain.

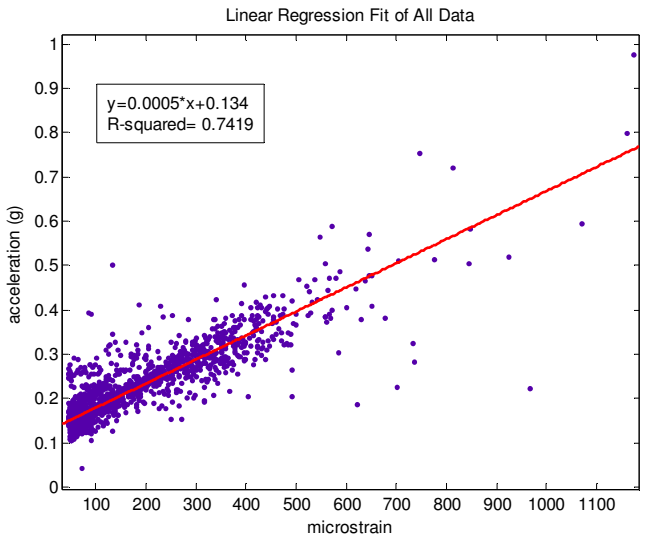

Figure 39. Linear Regression Fit of data in Figure 38, excluding data below 50 μstrain

As seen in Table 6, significant amount of scatter is caused by Perryman A and Churchville B data. The remaining data (paved, Perryman 1, Perryman 2, and Perryman 3) all show moderate to strong correlation between RMS acceleration and RMS strain.

Table 6. Linear Regression Fit by Terrain, excluding data below 50 µstrain

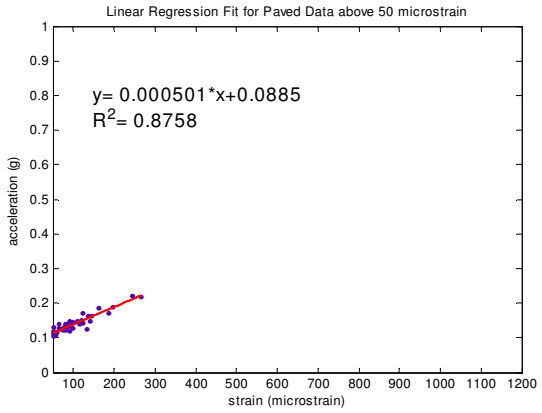

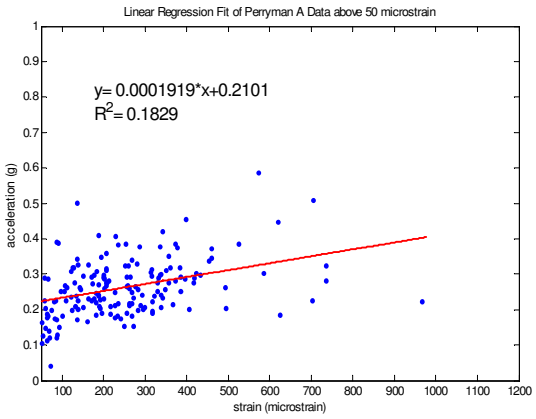

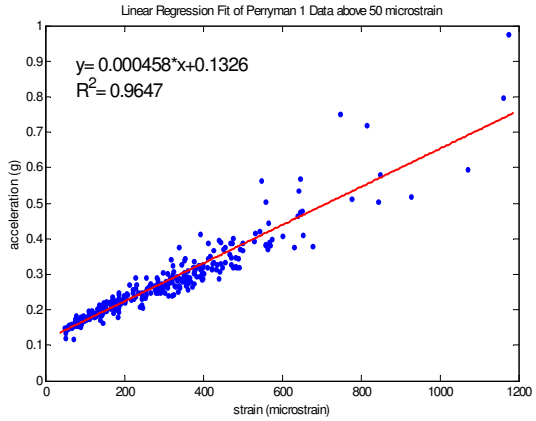

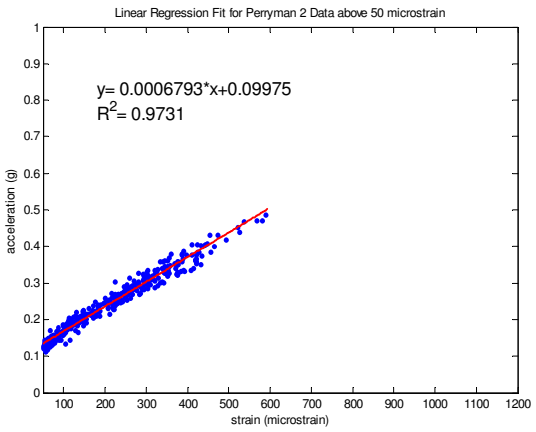

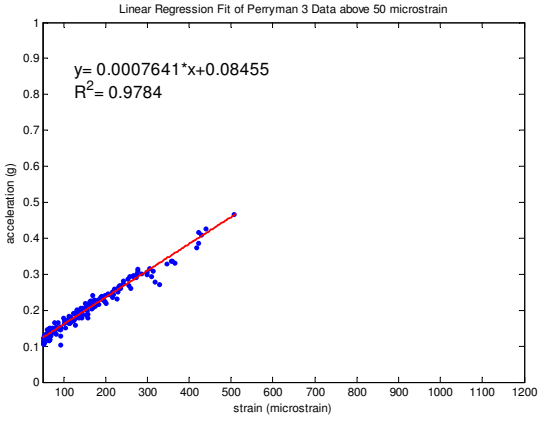

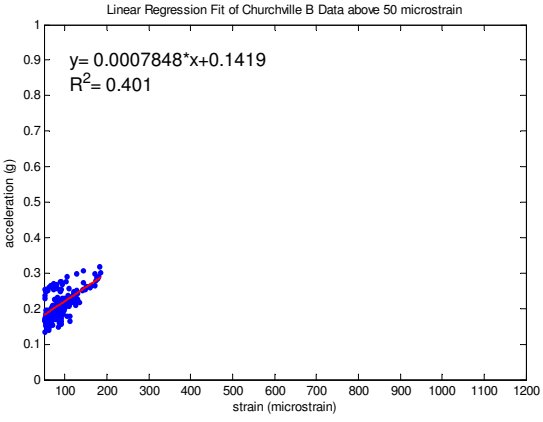

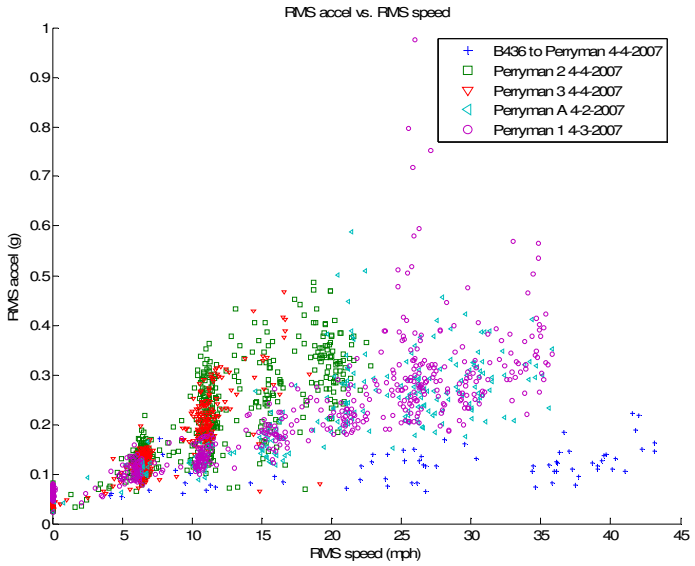

Figure 40. RMS acceleration vs. RMS Speed

In Figure 40, RMS acceleration appears linearly correlated to speed, although with increasing scatter with increasing RMS speed. The clustering of data points according to terrain is apparent in Figure 40. Therefore, a terrain identification scheme using RMS acceleration and RMS speed may be possible.

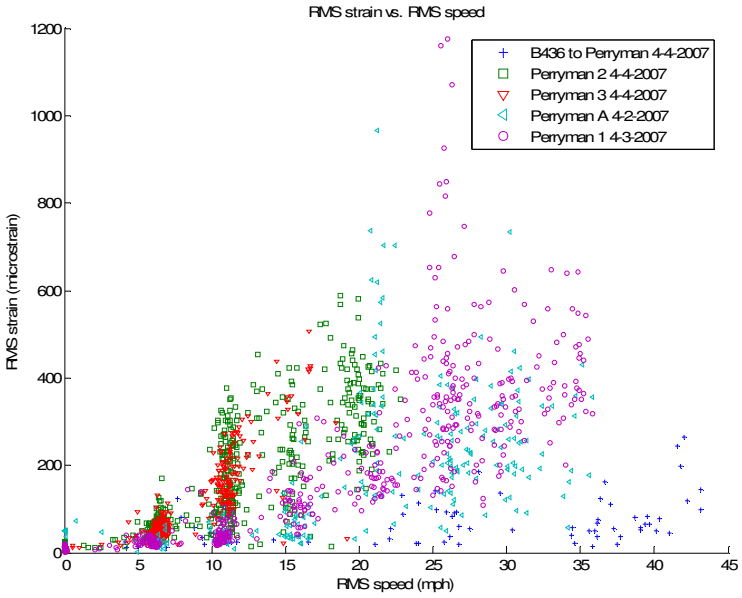

Figure 41. RMS strain vs. RMS speed

Figure 41 shows a loose correlation between RMS strain and RMS speed. This correlation appears to be similar to the correlation between RMS acceleration and RMS speed in Figure 40. The most apparent similarity is the clustering of data points for different terrain types, with increasing scatter for increasing RMS speed. Therefore, a terrain identification scheme using RMS strain and RMS speed may be possible. However, strain data is not usually practical due to space and wiring requirements on PCBs. For a more detailed discussion on issues with using strain gauges see Section 1.1. An accelerometer located near components of interest is much easier and more practical to implement.

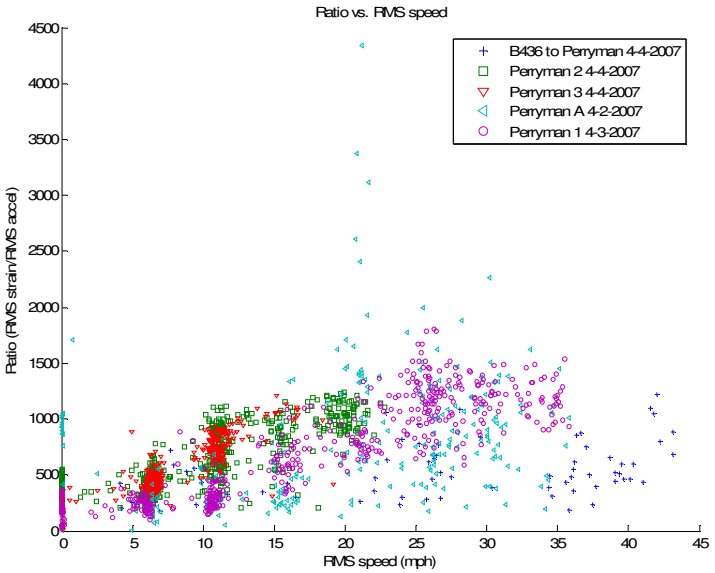

Figure 42. Ratio (strain/acceleration) vs. RMS speed

Ratio is strain divided by acceleration. The primary purpose of the Ratio variable is to determine the relationship between strain, acceleration and speed on the same graph. Figure 42 shows a loose relationship between Ratio and speed. In general, as speed increases, Ratio increases linearly with some scatter. Both of these observations are also apparent in plots of RMS acceleration vs. RMS speed and RMS

strain vs. RMS speed. Therefore, use of the Ratio variable does not appear to give any new insights into the relationship between strain, acceleration, and speed. However, if the relationship between strain and acceleration can be established through experimental testing, then strain maybe estimated using acceleration level without need for strain gauges. Strain or displacement information can then be used for damage calculations that do not utilize acceleration information.

4.2 Passenger vs. Military Vehicles over Paved Roads

In this section, the load environment of a military vehicle environment is compared to the load environment of a passenger vehicle. A comparison between RMS acceleration, RMS strain, Ratio (strain to acceleration), and PSD is performed. However, only a comparison for paved surfaces is possible because off road testing of passenger vehicles was not performed.

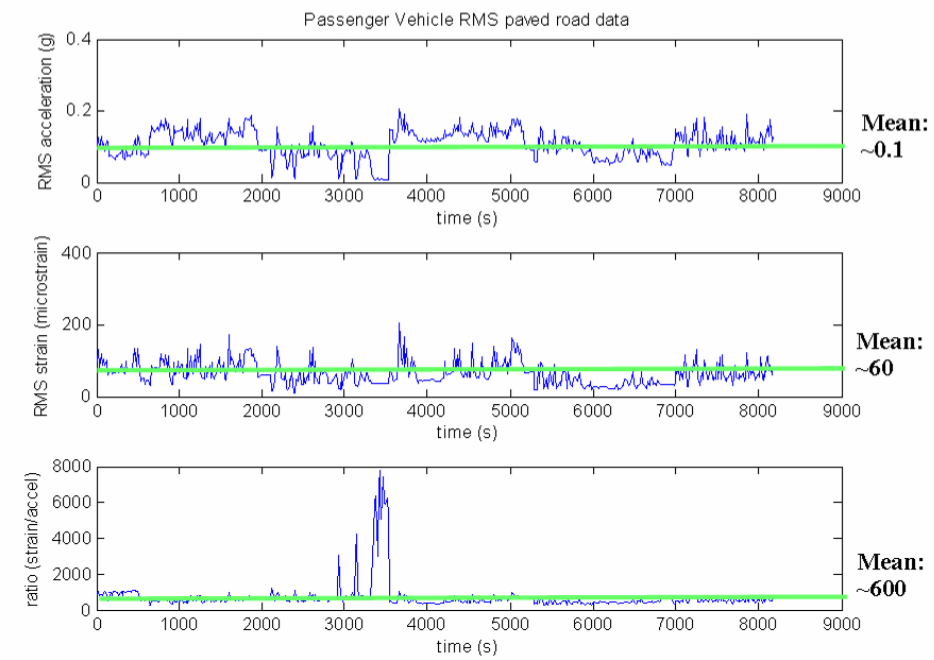

Figure 43. RMS acceleration, RMS strain, and Ratio of Passenger Vehicle over Paved Roads

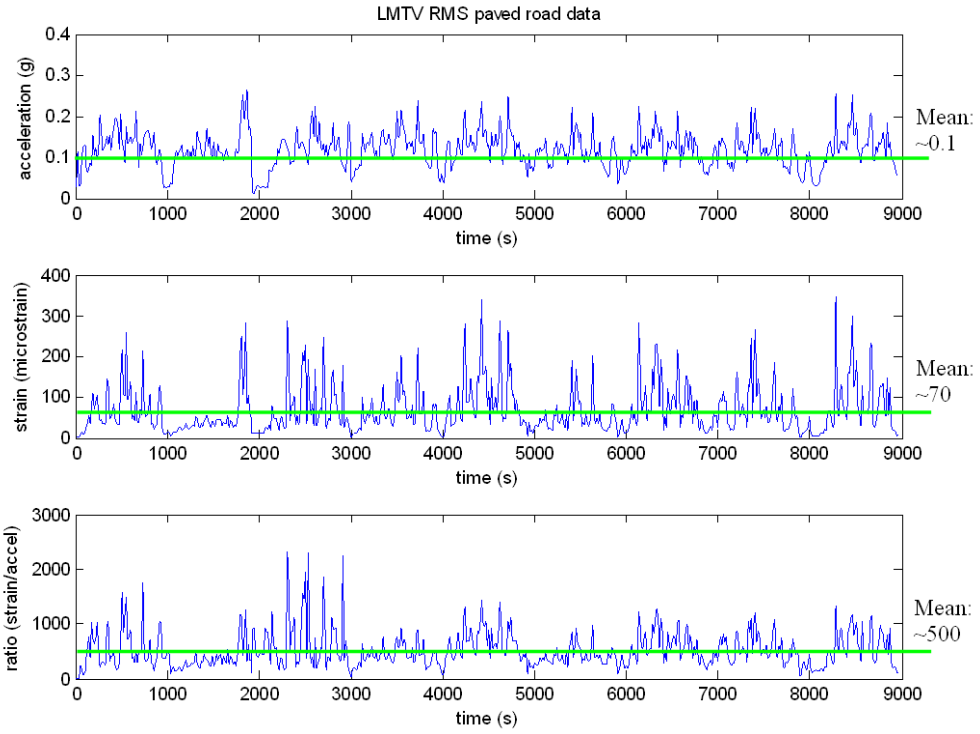

Figure 44. RMS acceleration, RMS strain, and Ratio of LMTV over Paved Roads

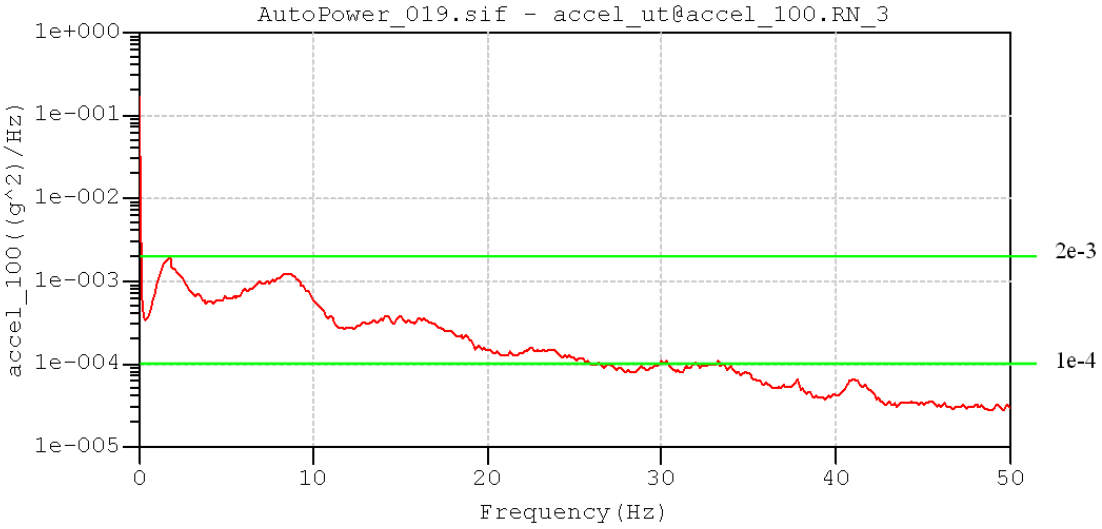

Figure 45. PSD of Passenger Vehicle Accelerometer Data over Highway Roads

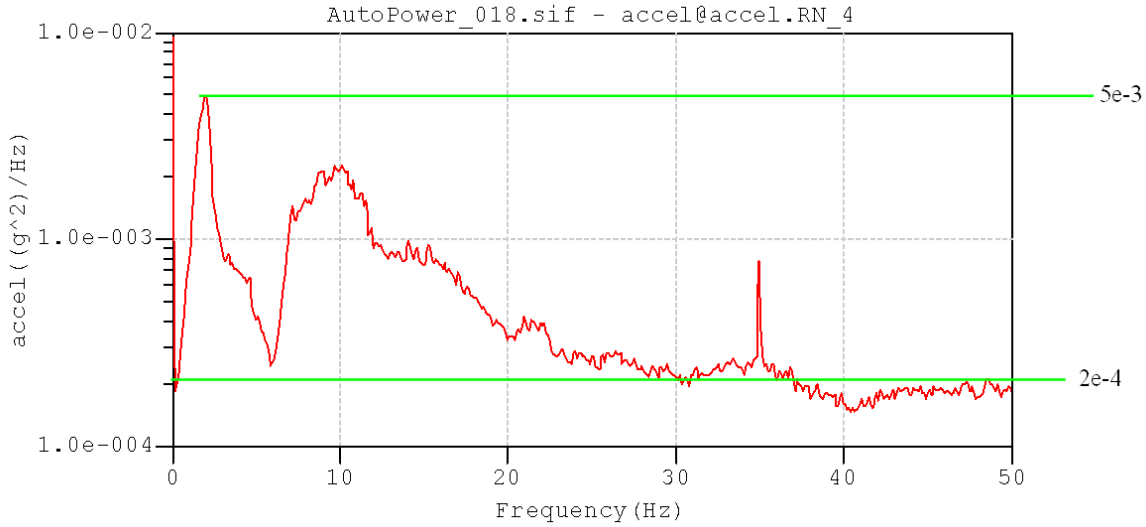

Figure 46. PSD of LMTV Accelerometer Data over Highway Roads

Mean RMS values shown in Figure 43 and Figure 44 are rounded off to the nearest first significant digit. As demonstrated by these figures, the passenger vehicle environment appears to be very similar to military vehicle environment according to RMS strain and RMS acceleration levels. However, a comparison of PSD plots in Figure 45 and Figure 46 demonstrates a different reality. The military vehicle environment PSD is approximately twice that of passenger vehicle environment PSD. Therefore, military vehicle environment is significantly more damaging than passenger vehicle environment for paved roads. This example helps illustrate that RMS levels can be deceptive and hide the existence of a harsher environment than expected when considering only RMS levels.

4.3 Paved Road vs. Off-road for Military Vehicles

As seen in Figure 47, Figure 48, and Figure 49, most off road conditions display higher PSD levels than paved roads (B436 to Perryman). However, for 18 psi

condition, off-road PSD levels appear to be relatively close to paved road PSD levels. This maybe attributed to the low speeds run at this condition (5-10 mph), resulting in similar excitation levels despite differences in terrain. In addition, PSD levels for Perryman 3 are generally similar to PSD levels for paved road. Low speeds on Perryman 3 may also be the reason behind the low PSD levels. PSD levels for Perryman A, 1, and 2 appear to be surprisingly similar. The exception is the input excitation at 1.5 Hz for Perryman 2. PSD levels are significantly higher for Perryman 2 and Perryman 3 at 1.5 Hz than other terrain. This suggests that the Perryman 2 and Perryman 3 contain terrain features that excite at 1.5 Hz, the natural frequency of the LMTV suspension. Potentially, PSD level at 1.5 Hz can be used to identify off-road terrain more severe than Perryman 1.

There are distinct differences in PSD levels around 7-11 Hz between different tire pressures. The exception is for paved surfaces and Perryman 3. Paved surfaces are smooth and cause minimal excitation regardless of tire pressure. Also, driving speeds on Perryman 3 are low (usually 5-10 mph) and keeps most excitation centered around 1.5 Hz, the natural frequency of the LMTV. Figure 47, Figure 48, and Figure 49 show noticeable decreases in PSD levels around 7-11 Hz as tire pressure decreases. However, differences in PSD levels for paved and Perryman 3 for different tire pressures is much smaller. PSD levels around 7-11 Hz could potentially identify changes in tire pressure for conditions similar to Perryman A, 1, and 2.

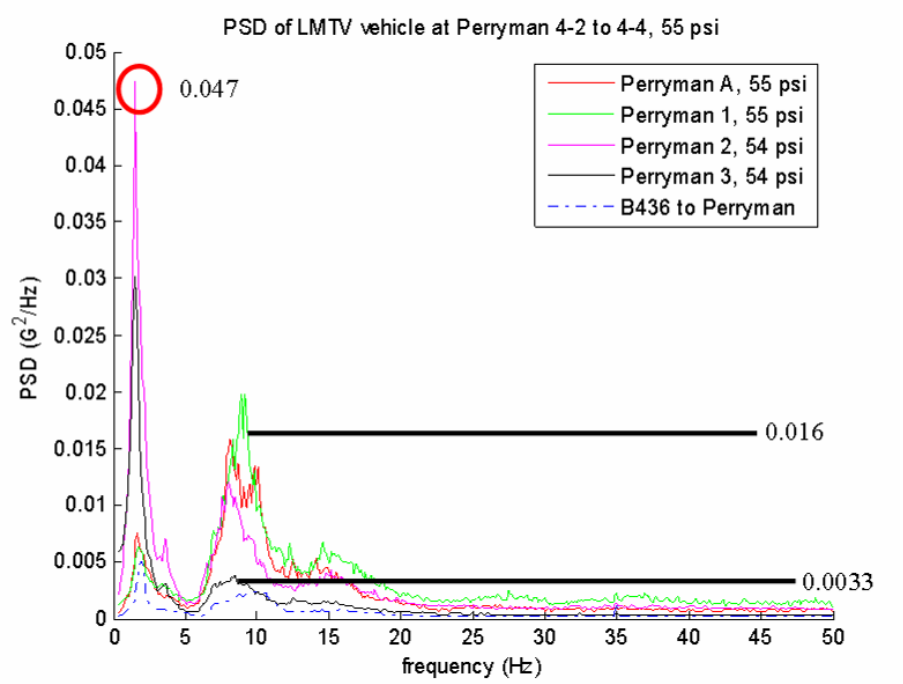

Figure 47. PSD of LMTV, 55psi, 4-2 to 4-4

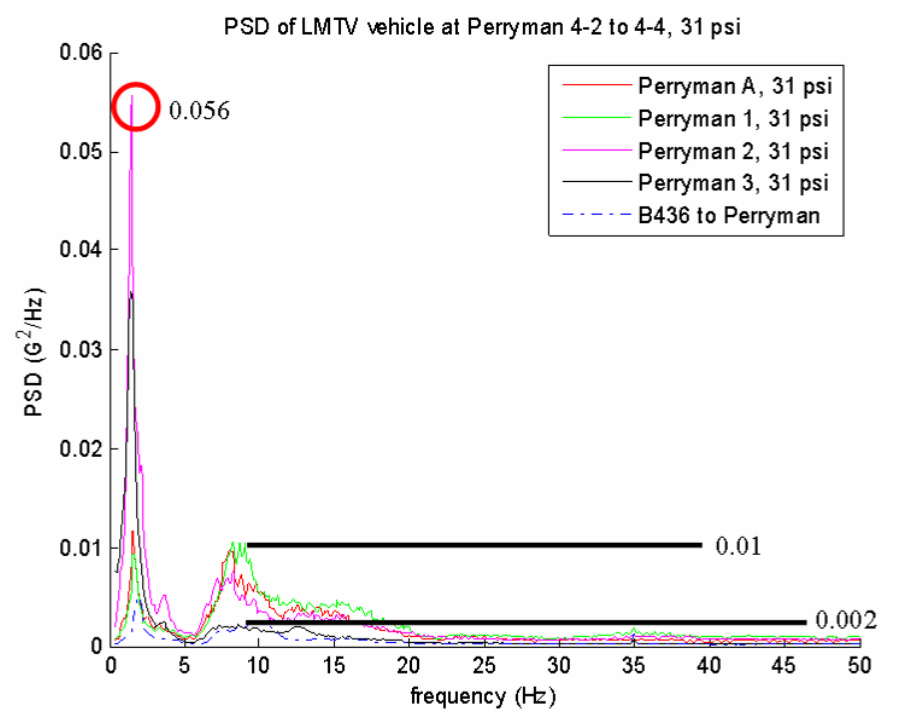

Figure 48. PSD of LMTV, 31psi, 4-2 to 4-4

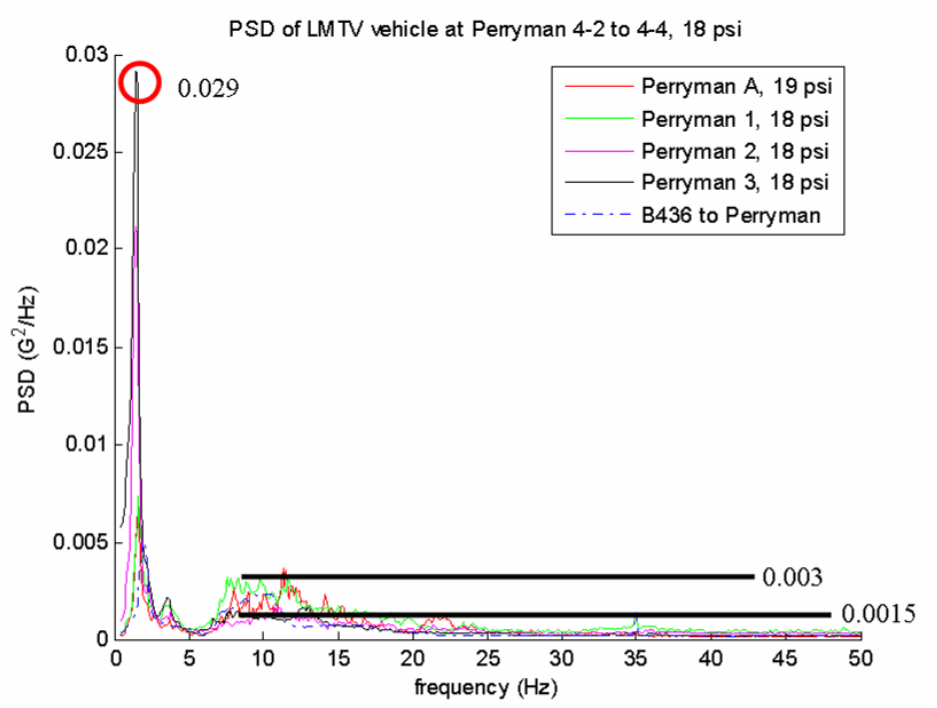

Figure 49. PSD of LMTV, 18psi, 4-2 to 4-4

Potential terrain identification schemes were seen in correlation graphs between measured parameters seen in Section 4.1. The most promising and practical of these correlation graphs is the RMS acceleration vs. RMS speed graph. Both acceleration and speed information is readily available with minimal wiring and instrumentation requirements. As seen in Figure 50, RMS acceleration has a loose linear correlation with RMS speed. RMS acceleration increases approximately linearly with RMS speed. The slope of this correlation between acceleration and speed increases with increasing terrain 'roughness'. This result confirms the terrain identification scheme developed by Heine [10].

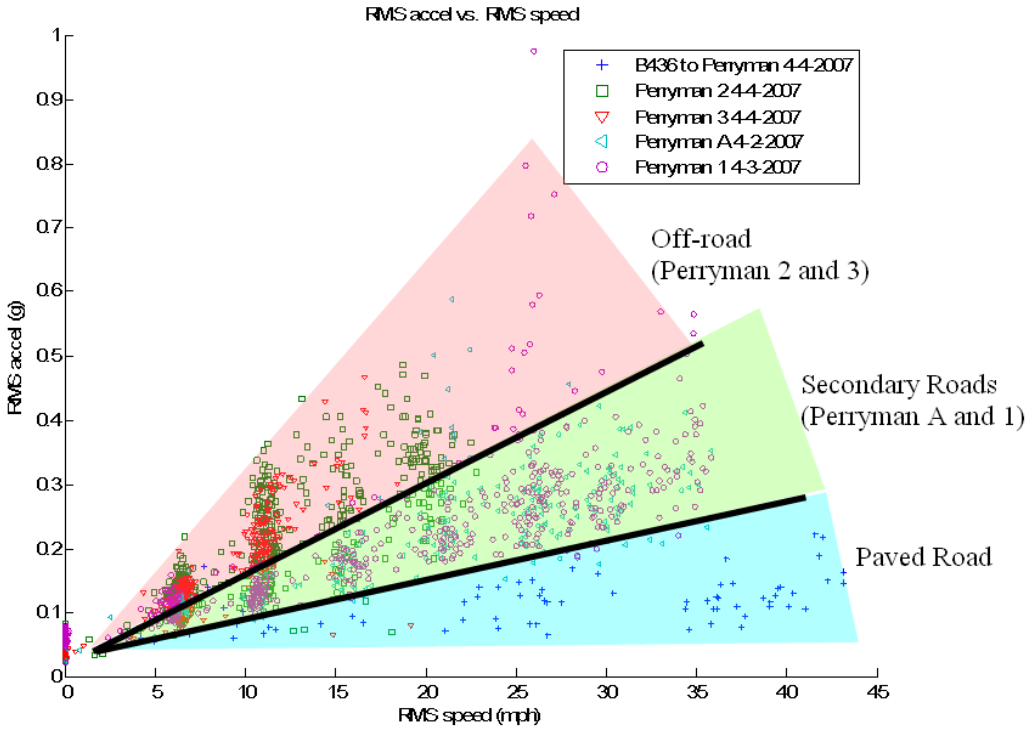

Figure 50. Terrain Identification using RMS acceleration vs. RMS speed

Chapter 5: Failures and Failure Prediction

5.0 Component Failures from Experimental Testing

5.0.1 BGA Failures

BGA components seen in Figure 51 were tested at APG from 4-2-2007 to 4-4-2007. After testing, the BGA pins were checked for continuity. Twelve pin out failures were detected in BGA 1 while BGA 2 had eleven pin out failures. These failures are indicated with red arrows. The failed BGA components were then cross sectioned. E-SEM photos of BGA failures are shown in Figure 52 and Figure 53.

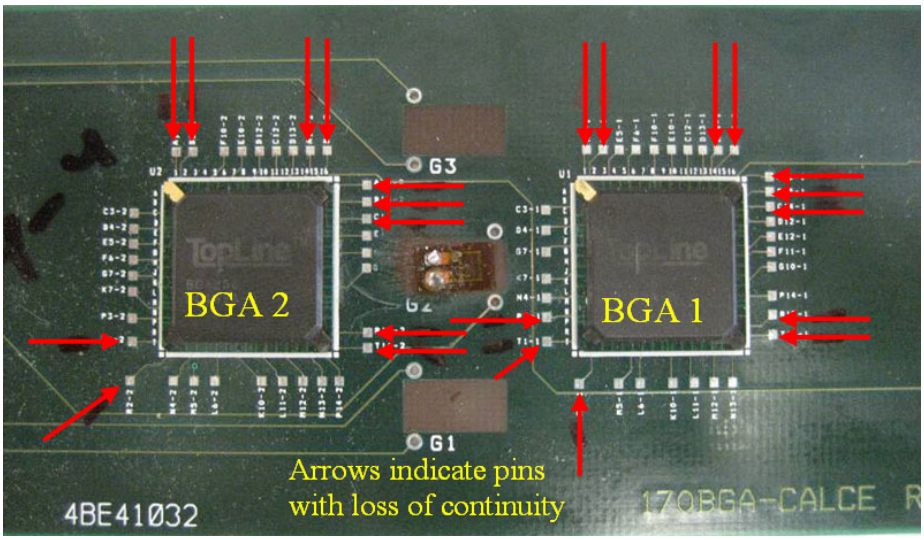

Figure 51. 256 BGA components, tested 4-2 to 4-4

Figure 52 shows some of the cracks found in BGA balls from BGA 1. Figure 52 shows that the cracks extend completely across each BGA ball. Continuity testing of BGA pins showed that these BGA balls had loss of continuity.

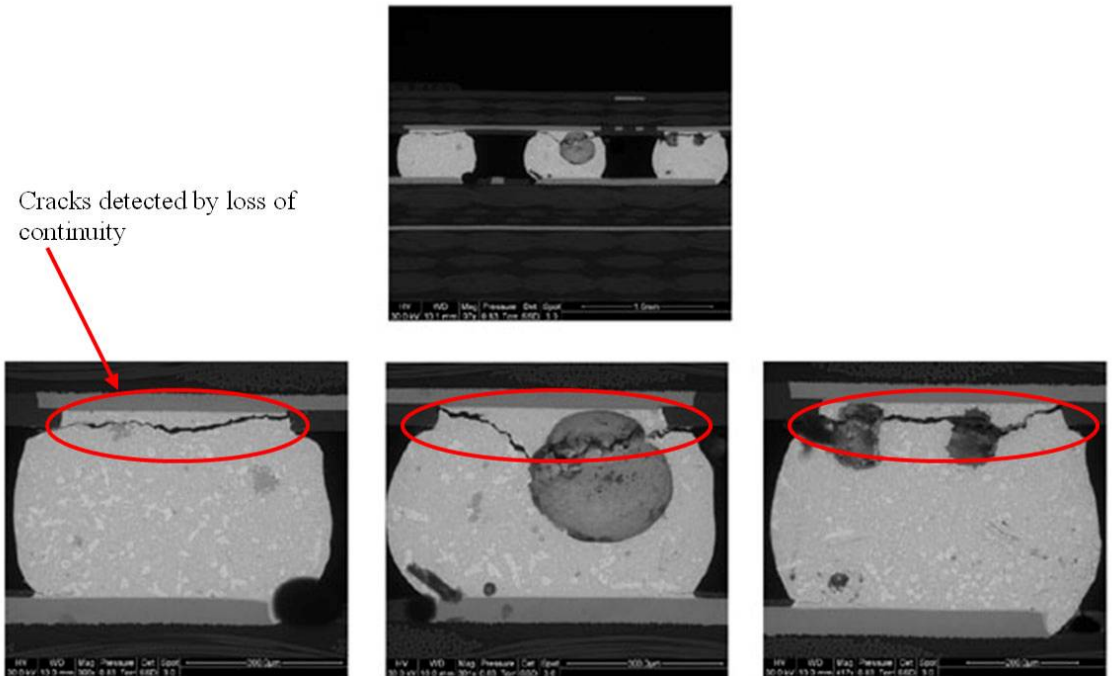

Figure 52. BGA failures, BGA 1

Figure 53 shows some of the cracks found in BGA balls from BGA 2. In addition, each crack shown extends completely across the BGA ball. Before cross sectioning, these BGA balls were detected to have loss continuity.

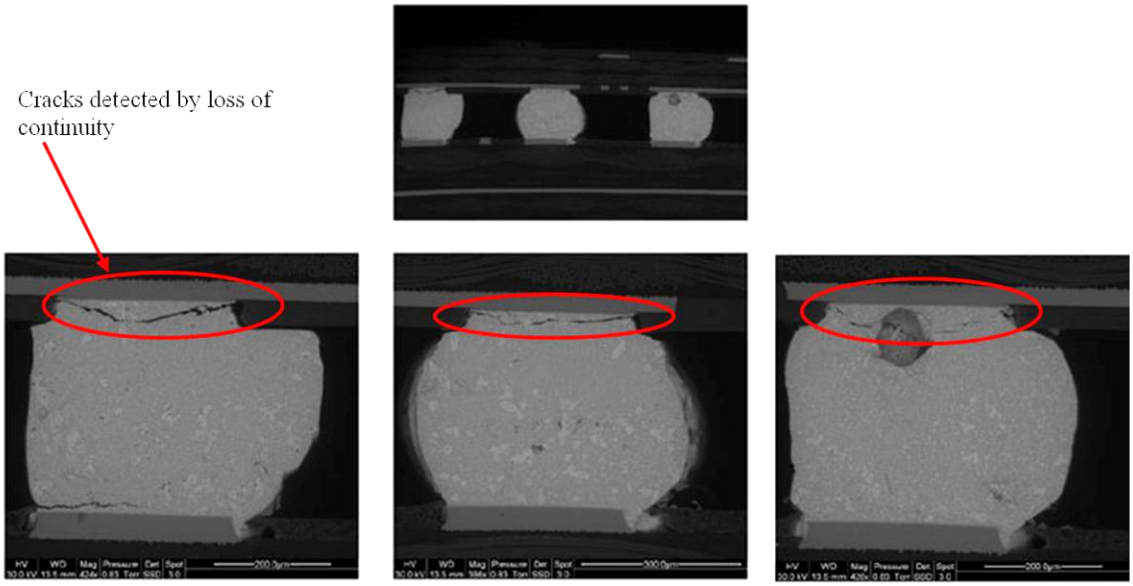

Figure 53. BGA failures, BGA 2

5.0.2 Capacitor Failures

Capacitor components in Figure 54 were tested at APG from 4-02 to 4-04-2007. After testing, the capacitance of each capacitor was checked and recorded. When the measured capacitance deviated by more than 10% from nominal capacitance value of 2.2 µfarads, the capacitor was deemed to have failed. The capacitors indicated with red arrows in Figure 54 are capacitors that failed. Figure 55 and Figure 56 are E-SEM photographs of cracks found in these two failed capacitors.

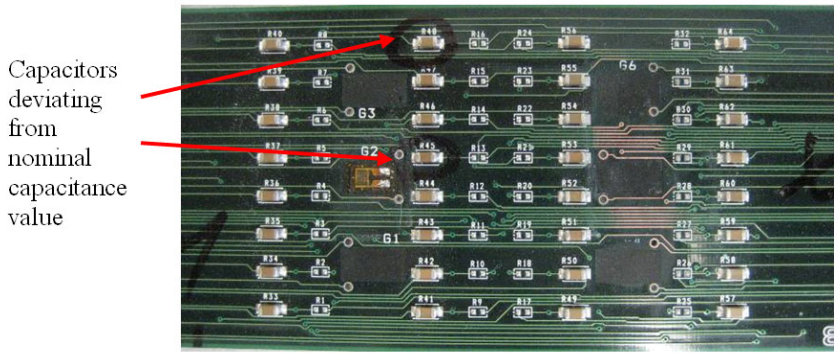

Figure 54. 1206 Capacitor components, tested 4-2 to 4-4

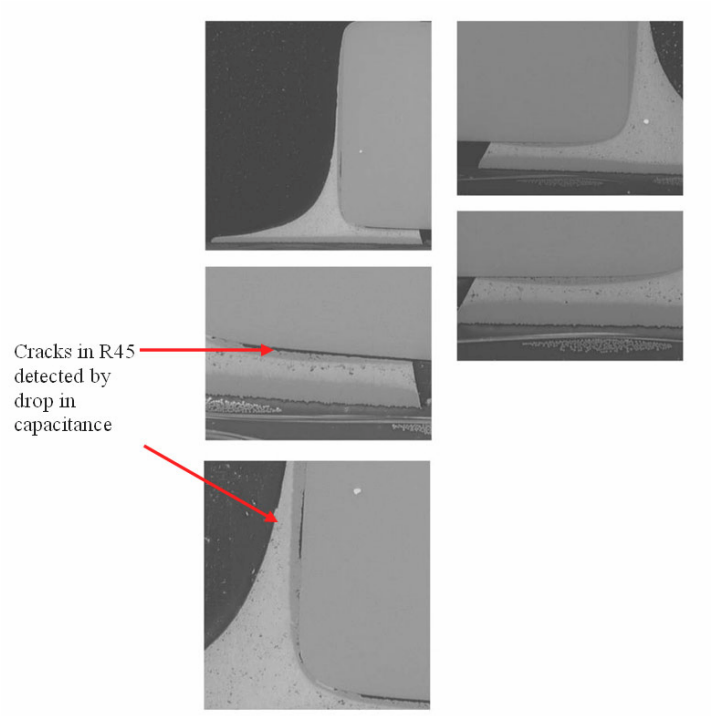

Figure 55. Capacitor Failure R45, 4-2 to 4-4

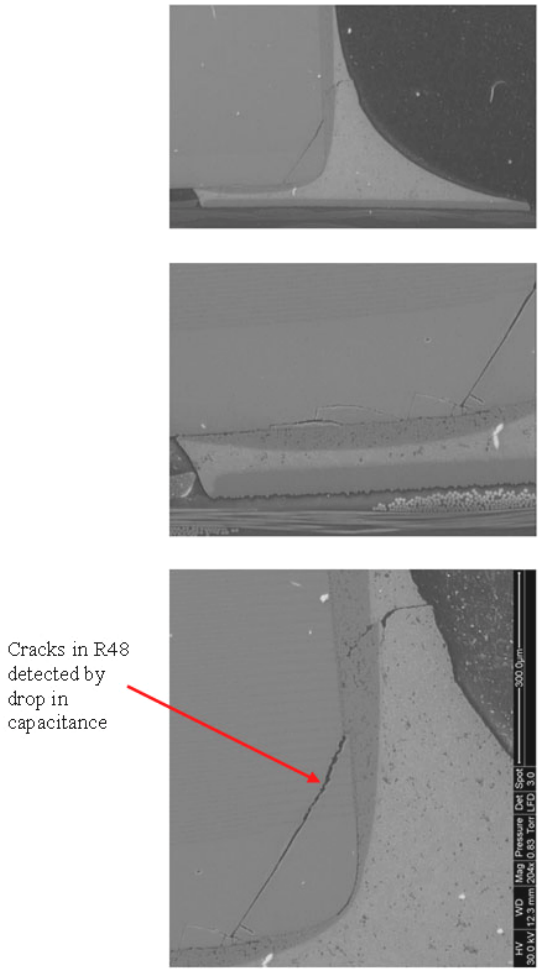

Figure 56. Capacitor Failure R48, 4-2 to 4-4

5.0.3 SOIC Failures

SOIC-8 components seen in Figure 57 were tested from 4-11 to 5-4-2007 at APG. After testing, each component lead was tested for continuity. Only one failure was detected in continuity testing, U19 indicated by red arrow in Figure 57. E-SEM photographs of U19 component seen in Figure 58 and Figure 59 found only small cracks in the gull wing leads.

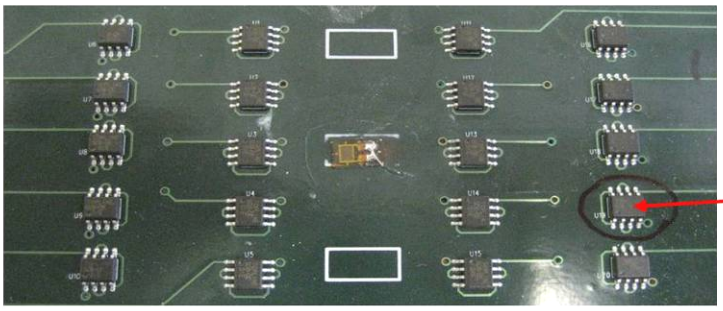

Figure 57. SOIC-8 components, tested 4-11 to 5-4

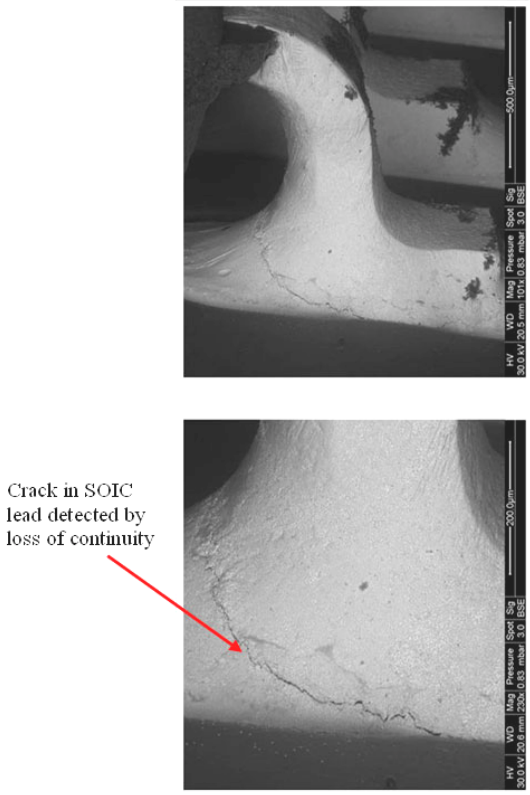

Figure 58. Cracks in SOIC-8 gull wing lead

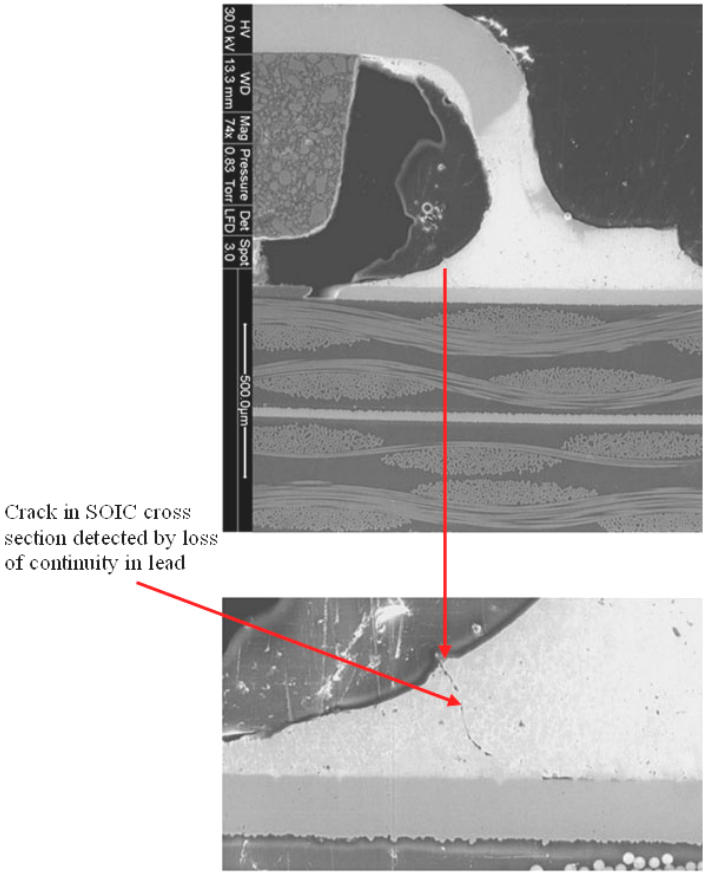

Figure 59. Cross section of crack in SOIC gull wing lead

5.0.4 SOT Failures

SOT 23 and SOT 223-4 components seen in Figure 60 were tested from 4-11 to 5-4-2007 at APG. After testing, each component lead was tested for continuity. Continuity testing showed that three components failed from testing: U1, U35, and U37. These failures are indicated the by red arrows in Figure 60. No cracks were found in SOT 223-4 leads (U1). Cracks were found in the SOT 23 leads (U35 and U37). E-SEM photographs of cracks in SOT 23 leads are show in Figure 61, Figure 62, and Figure 63.

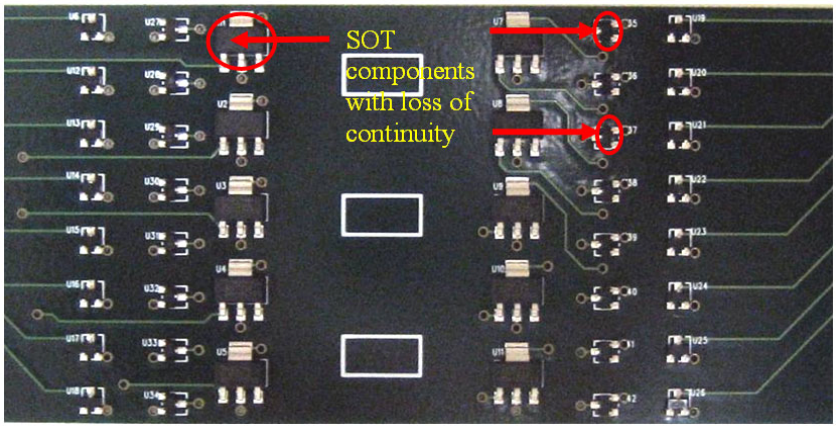

Figure 60. SOT 23 and SOT 223-4 components, tested 4-11 to 5-4

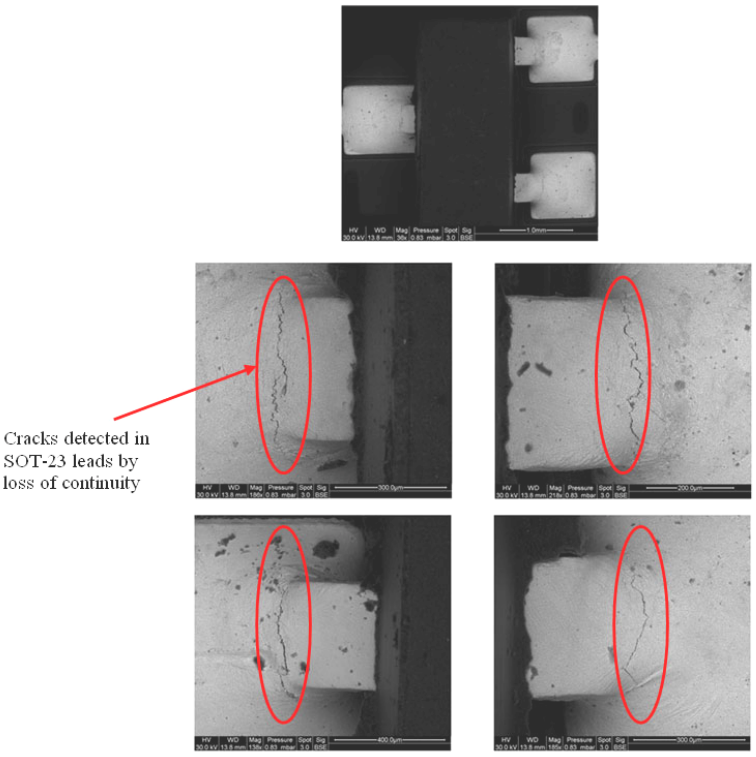

Figure 61. Cracks in SOT-23 leads

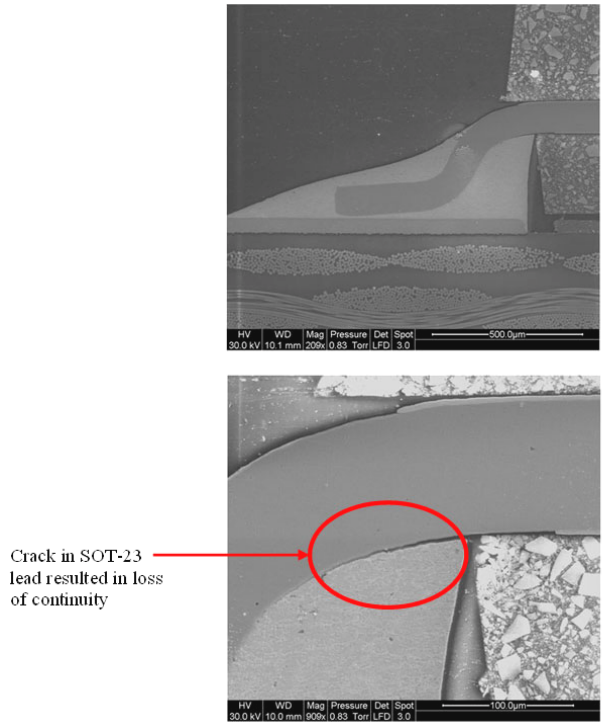

Figure 62. Cross-section #1 SOT-23 lead

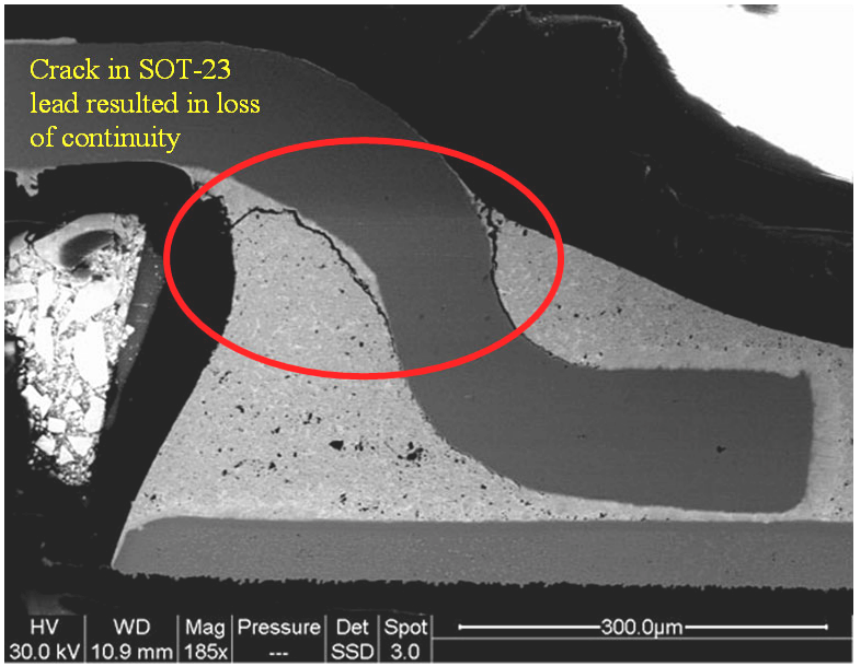

Figure 63. Cross-section #2, SOT-23 lead

5.1 Failure Predictions

5.1.1 Prediction with Cycle Counting

In this section, BGA failures are compared to available BGA low cycle fatigue data. Available fatigue data for PBGA packages under cyclic loading is shown in Figure 64. Data points are from laboratory testing for various CALCE projects [20]. Cycles for data points in Figure 64 are not reversed.

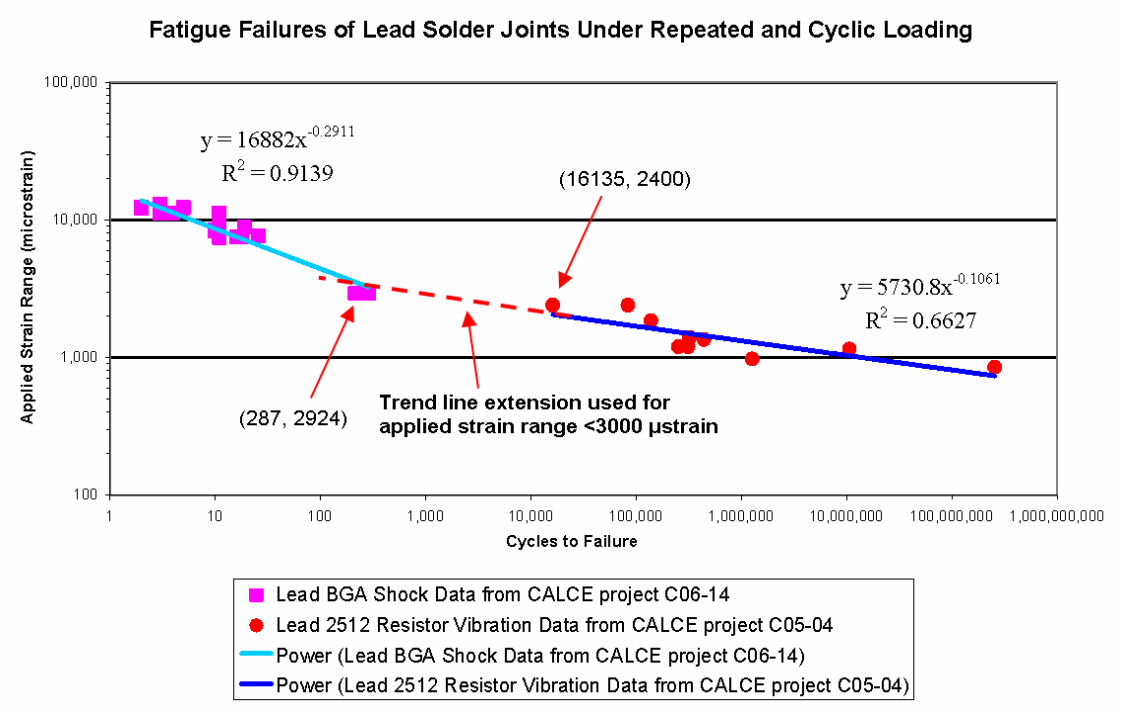

Figure 64. S-N curve of Lead Solder Joints Under Cyclic Loading [20]

Strain time history from before BGA failure occurred (Figure 65) is used in the following failure analysis. Cycle counting procedure illustrated in Section 3.1.3 is used in processing strain time history. This procedure first involved filtering data with Somat's InField software program. Then filtered data was rainflow cycle counted by InField software into user defined data bins. Each data bin has a defined bin width with an upper and lower acceptance limit on strain values for bin (see Figure 24 for

data bin example). Strain range midpoint is defined as the average of the upper and lower acceptance limit for a particular data bin.

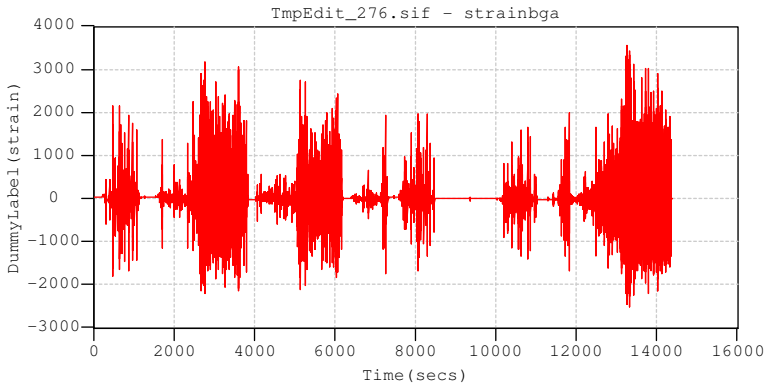

Figure 65. Strain time history before BGA failure, 4-2 to 4-3

Table 7 lists the results of rainflow cycle counting according to the strain range midpoint. Using the equations from S-N curves in Figure 64, cycles to failure given strain range midpoint was calculated and shown in column 3 of Table 7. Damage accumulation of strain range bin was calculated from dividing actual cycles by calculated cycles to failure from S-N curve slopes in Figure 64. Results from Table 7 show damage is accumulated primarily from low cycle, high strain range events. Total damage accumulation is less than an order of magnitude higher than actual failure. Also, BGA failures corresponded well to low cycle fatigue data as seen in Figure 66. In low cycle fatigue, an order of magnitude difference between expected and actual results is reasonable.

Table 7. Damage Accumulation by Strain Range for Strain Data Before Failure

Strain Range (µstrain)	Rainflow Counted Cycles (N)	Calculated Cycles to failure at strain range (N_f) *(Calc. cycles to fail for <= 2750 µstrain) = (strain range/5730.8)^(-1/.1061)* *(Calc. Cycles to fail for >=3100 µstrain) = (strain range/16882)^(-1/.2911)*	Damage accumulation ($D=N/N_f$) *Counted Cycles/ Calc. Cycles to Fail*
250	234,887	6,620,000,000,000	3.55E-08
750	8,300	211,000,000	3.94E-05
1250	3,801	1,710,000	0.002
1750	2,027	71,700	0.028
2250	1,116	6,710	0.166
2750	673	1,010	0.665
3100	182	338	0.539
3500	326	223	1.465
4000	113	141	0.803
4500	109	94	1.161
4900	19	70	0.271
5250	28	55	0.507
5750	11	40	0.272
6250	1	30	0.033
Total cycles:	252,000	Total Damage Accumulation:	5.91

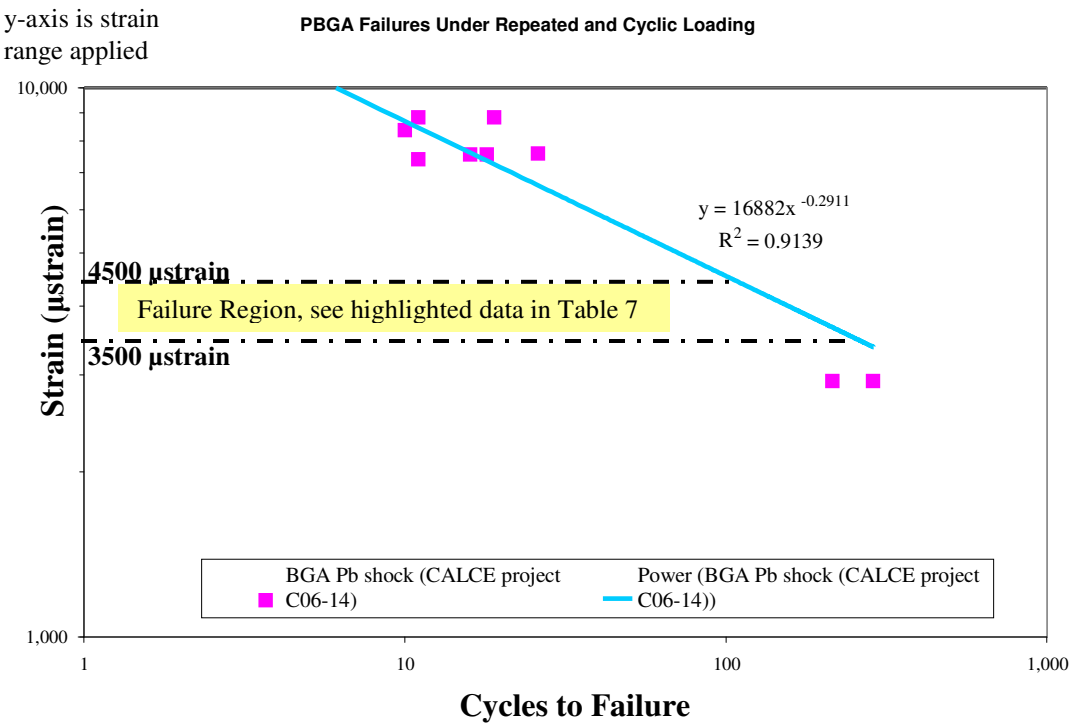

Figure 66. Low cycle S-N curve of PBGA under cyclic loading [20]

Cycle counting and binning is further broken down according to terrain (Table 8) to determine the damage accumulation caused by each terrain before failure. The total number of counted cycles in Table 8 is lower than total cycles in Table 7 due to the exclusion of some stationary or nearly stationary data between different test conditions. The total damage accumulation results (compare Table 9 to Table 7) are almost the same; leading to the conclusion that the excluded data does not affect accumulated damage.

Table 8. Binned Strain Time History by Terrain Seen Before Failure

	Load Block Sequence						
	1	2	3	4	5	6	7
Strain Range (µstrain)	Counted Cycles B436 to Perryman, 4-2 (N_1)	Counted Cycles Perryman A, 55psi, 4-2 (N_2)	Counted Cycles Perryman A, 31psi, 4-2 (N_3)	Counted Cycles Perryman A, 18psi, 4-2 (N_4)	Counted Cycles Perryman to B436, 4-2 (N_5)	Counted Cycles B436 to Perryman, 4-3 (N_5)	Counted Cycles Perryman 1, 55psi, 4-3 (N_6)
250	15,075	27,625	28,127	16,435	14,102	18,210	34,191
750	140	1,907	1,422	90	93	136	4,511
1250	46	790	563	34	41	42	2,286
1750	20	441	271	18	31	15	1,232
2250	11	266	133	7	17	7	672
2750	5	156	72	1	14	4	421
3100	1	50	13	1	2	1	116
3500	2	112	21	1	5	0	186
4000	0	25	8	0	3	0	76
4500	0	24	9	0	0	0	75
4900	0	4	1	0	0	0	15
5250	0	6	0	0	0	0	22
5750	0	0	0	0	0	0	11
6250	0	0	0	0	0	0	1
Rounded cycles:	15,300	31,400	30,600	16,600	14,300	18,400	43,800
Total cycles:	170,000						

Table 9. Damage Accumulation by Terrain Seen Before Failure

		Load Block Sequence						
Strain Range (μstrain)	Calc. Cycles to failure at strain range (N_f)	1 Damage Accumulation B436 to Perryman, 4-2 (N_1/N_f)	2 Damage Accumulation Perryman A, 55psi, 4-2 (N_2/N_f)	3 Damage Accumulation Perryman A, 31psi, 4-2 (N_3/N_f)	4 Damage Accumulation Perryman A, 18psi, 4-2 (N_4/N_f)	5 Damage Accumulation Perryman to B436, 4-2 (N_5/N_f)	6 Damage Accumulation B436 to Perryman, 4-3 (N_6/N_f)	7 Damage Accumulation Perryman 1, 55psi, 4-3 (N_6/N_f)
250	6.62E12	2.28E-09	4.17E-09	4.25E-09	2.48E-09	2.13E-09	2.75E-09	5.17E-09
750	210,000,000	6.64E-07	9.05E-06	6.75E-06	4.27E-07	4.41E-07	6.45E-07	2.14E-05
1250	1,710,000	2.69E-05	4.62E-04	3.29E-04	1.99E-05	2.40E-05	2.46E-05	1.34E-03
1750	71,700	2.79E-04	6.15E-03	3.78E-03	2.51E-04	4.32E-04	2.10E-04	0.017
2250	6,710	1.64E-03	0.040	0.020	1.04E-03	2.53E-03	1.04E-03	0.100
2750	1,010	4.94E-03	0.154	0.071	9.87E-04	0.014	3.95E-03	0.416
3100	338	2.96E-03	0.148	0.038	2.96E-03	5.92E-03	2.96E-03	0.343
3500	223	8.99E-03	0.503	0.094	4.49E-03	0.022	0	0.836
4000	141	0	0.178	0.057	0	0.021	0	0.540
4500	94	0	0.256	0.096	0	0	0	0.799
4900	70	0	0.057	0.014	0	0	0	0.214
5250	55	0	0.109	0	0	0	0	0.398
5750	40	0	0	0	0	0	0	0.272
6250	30	0	0	0	0	0	0	0.033
	damage accumulation:	0.019	1.45	0.395	0.010	0.067	0.008	3.97
	total damage accumulation:	5.92						

Damage accumulation results indicate that by far Perryman 1 at 55 psi contributed most to failure. This corresponds well to actual data, as the BGA components failed rapidly after starting testing on Perryman 1 at 55psi. However, damage accumulation results indicate that the BGA components should have failed earlier on Perryman A at 55 psi. While small spikes in continuity were seen after testing on this terrain, no failures were observed. More testing is required to determine appropriate failure threshold.

5.1.2 Prediction with PSD Load Blocking

The PSD calculation procedure outlined in Section 3.2.2 was used to calculate PSD for each load block seen by the BGA PCB before failure. These PSD load blocks were loaded into CalcePWA and applied in the load sequence seen in Segment Number column of Figure 67. Each load block is applied for 30 minutes (see Table 10) approximately reflecting actual testing time at each load condition.

Segment Number	Segment Name	Stress Type
1.0	B436_Perryman	Random_Vibration
2.0	PerrymanA_55_4-2	Random_Vibration
3.0	PerrymanA_31_4-2	Random_Vibration
4.0	PerrymanA_18_4-2	Random_Vibration
5.0	Perryman_B436_4-2	Random_Vibration
6.0	B436_Perryman_4-3	Random_Vibration
7.0	Perryman1_55_4-3	Random_Vibration
8.0	Perryman1_31_4-3	Random_Vibration
9.0	Perryman1_19_4-3	Random_Vibration
10.0	Perryman_B436_4-3	Random_Vibration

Figure 67. PSD Load Blocks in CalcePWA

The highlighted results listed in Table 10 show that Perryman A at 55 psi and Perryman 1 at 55 psi are the most damaging load blocks. Actual BGA failure detected by loss of continuity occurred on Perryman 1, 55psi which is highlighted in red. The PSD load blocking results are similar to the cycle counting results in Section 5.1.1.

This similarity of results demonstrates that acceleration data could potentially be used in place of strain data to predict failure if no strain data is available.

Table 10. CalcePWA results for PSD Load Blocking

Load Block Sequence	Load Condition	hours to failure (T_{fi})	Damage by Load Condition (D_i= 0.5 hr/ T_{fi})	Cumulative Damage ($\sum D_i$)
1	B426 to Perryman, 4-2	66.8	0.007	0.007
2	Perryman A, 55 psi, 4-2	0.216	2.31	2.32
3	Perryman A, 31 psi, 4-2	1.21	0.412	2.73
4	Perryman A, 18 psi, 4-2	66.8	0.007	2.74
5	Perryman to B436, 4-2	66.8	0.007	2.75
6	B426 to Perryman, 4-3	66.8	0.007	2.76
7 (failure)	Perryman 1, 55 psi, 4-3	0.106	4.73	7.48
8	Perryman 1, 31 psi, 4-3	0.387	1.29	8.78
9	Perryman 1, 19 psi, 4-3	32.7	0.015	8.79
10	Perryman to B436, 4-3	18.25	0.027	8.82

5.1.3 Shock Prediction with CalcePWA

Given the rapid failure of BGA components soon after a 16.1 g shock load on 4-3-2007 (see Figure 68); it was first assumed that the BGA components failed due to this shock load. CalcePWA software was used to verify this assumption. In verifying this assumption, several high acceleration events of varying magnitude were considered (Figure 68). As seen in Figure 68, the first sign of intermittent failure shows up ~40 seconds after shock event of 16.1 g's.

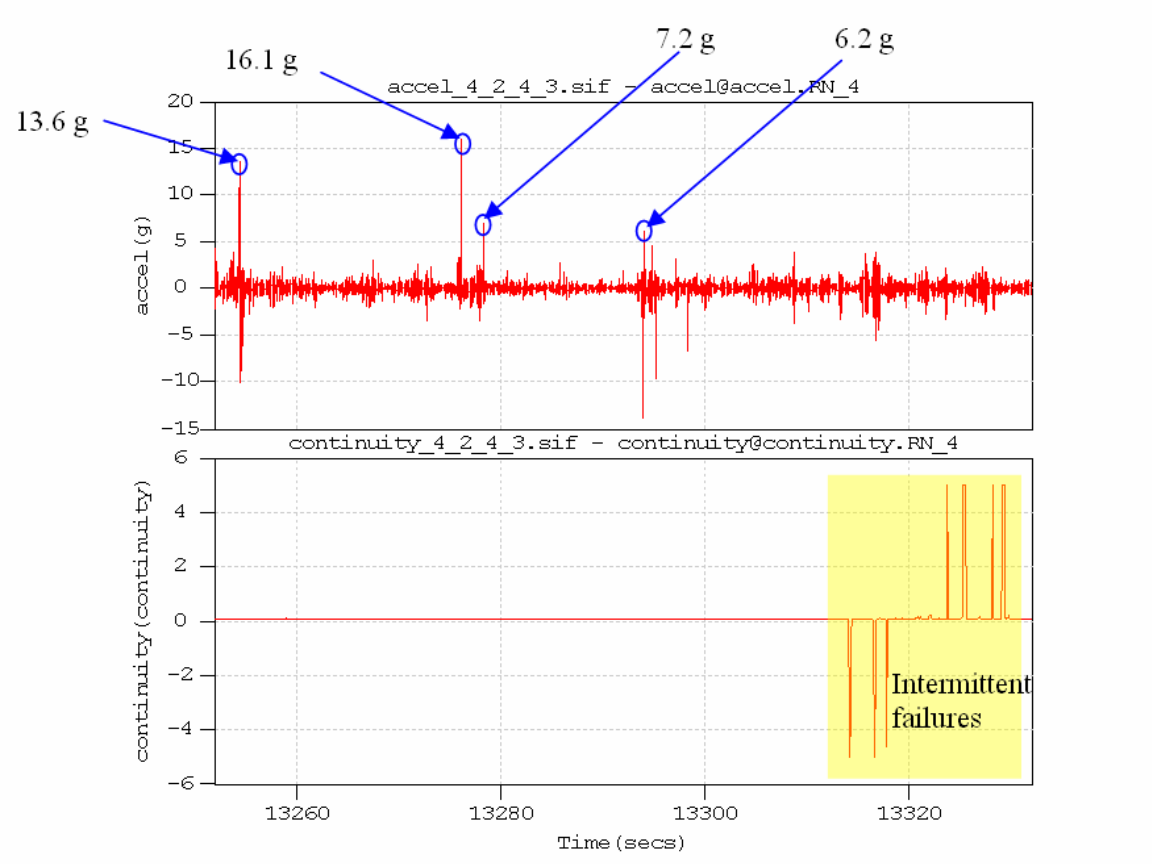

Figure 68. Acceleration time history and BGA continuity, ~100s interval

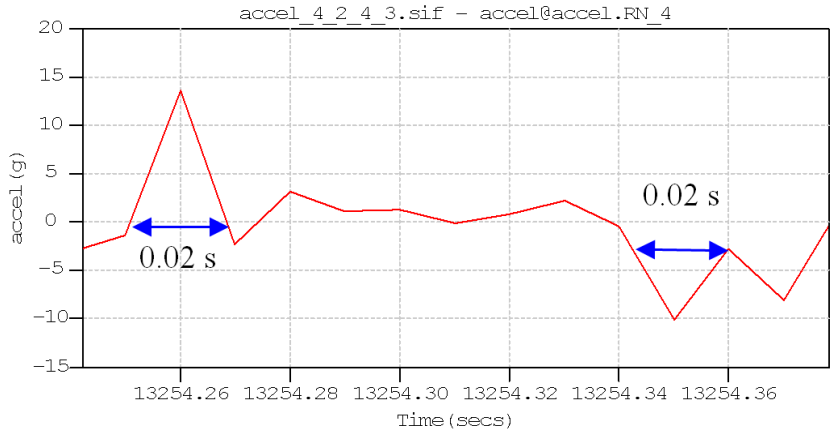

Figure 69. Acceleration time history, 0.14s interval

To use the CalcePWA shock module, the acceleration level and pulse width are required. Since acceleration level is readily available only determining shock pulse width is required. As seen in Figure 69, sample rate of 100 Hz appears too low. The single data points at peaks and valleys appear to demonstrate that pulse width is

less than 0.02 seconds, which is resolution limit of accelerometer. Instead, CalcePWA software will be used to determine sampling rate necessary to capture shock loads that could cause failure.

CalcePWA software simulated half-sine pulse shock loads on the BGA PCBs. The failure criterion used by CalcePWA can be found in the shock models for PCBs in reference [23]. The standard CalcePWA failure model was compared to the new CALCE simple Shock Response Spectrum (SRS) model described in CALCE project C07-15 [24]. The simple SRS model provides less conservative predictions of failures for shock loading. CalcePWA simulation results with individually applied shock loads are presented in Table 11.

Table 11. CalcePWA Shock Results, Individual Loads

Accelerometer sample rate (100 Hz) too low to reach conclusion about cause of failure

		Pulse width (seconds)	0.02 s	0.01 s	0.005 s	0.002 s	0.001 s	0.0005 s
Acceleration level (g)	16.1 g	Old CalcePWA shock results	Failed	Failed	Failed	Failed	Failed	Survives
		New CalcePWA shock results (simple SRS)	Failed	Failed	Failed	Failed	Survives	Survives
	13.6 g	Old CalcePWA shock results	Failed	Failed	Failed	Failed	Failed	Survives
		New CalcePWA shock results (simple SRS)	Failed	Failed	Failed	Failed	Survives	Survives
	7.2 g	Old CalcePWA shock results	Failed	Failed	Failed	Failed	Failed	Survives
		New CalcePWA shock results (simple SRS)	Failed	Failed	Failed	Survives	Survives	Survives
	6.2 g	Old CalcePWA shock results	Failed	Failed	Failed	Failed	Survives	Survives
		New CalcePWA shock results (simple SRS)	Failed	Failed	Failed	Survives	Survives	Survives

Simple SRS CalcePWA results in Table 11 show that pulse width of 0.002 seconds in length can cause failure in BGA components. Actual sampling rate of 100 Hz (0.02 s pulse width) is too low to accurately capture pulse width of shock input. Therefore, it is not possible to conclude if BGA components failed due to shock loads from current accelerometer data.

On the other hand, the PCB response to shock pulses appears to be muted according to Figure 70 and Figure 71. This suggests that the shock pulses observed in testing were too short to increase the vibratory response of the system. Strain response in Figure 71 seems to reflect vehicle suspension response to the terrain rather than from shock pulse. From the strain time history below, it appears that highly damaging strain cycles were not caused by the shock pulses.

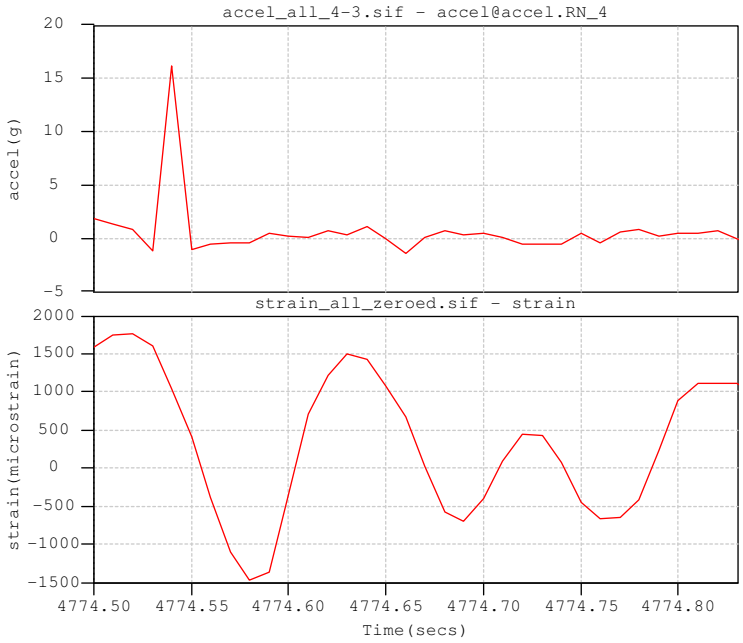

Figure 70. PCB Shock Response #1

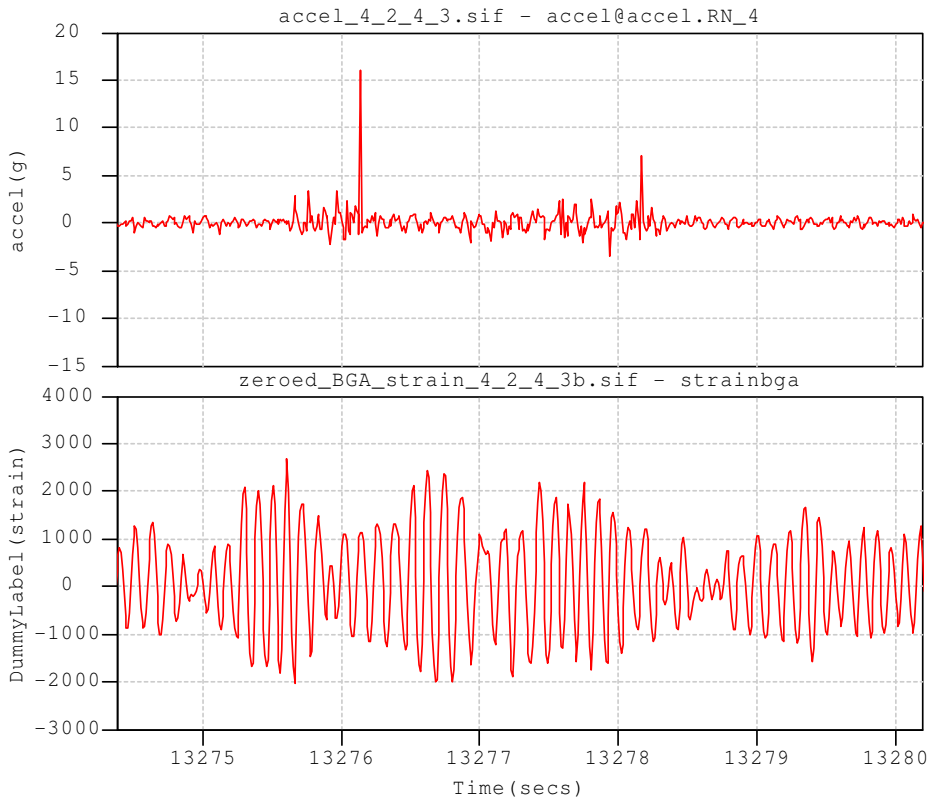

Figure 71. PCB Shock Response #2

In future testing where shock loads are expected, higher sampling rates are required. CalcePWA analysis in Table 11 demonstrates that sampling rate needs to be at least 2000 Hz to capture pulse width of shock load of 16 g and determine if it will cause failure. The 0.001 second column is smallest pulse width column in Table 11 differentiating failure and survival for the revised simple SRS model. At sampling rate of 2000 Hz, pulse widths of 0.001 seconds or greater in length can be captured according to the Nyquist sampling theorem. According to the older, more conservative CalcePWA model, minimum sampling rate of 4000 Hz is required.

Chapter 6: Conclusions and Discussion

This chapter presents a summary of the results and findings for this project. However, before reviewing the conclusions, it is important that the conclusions be viewed in the proper context. All the tested printed circuit boards (PCBs) were of the same thickness, 1.58mm. This was the same thickness as the test BGA PCBs that were used in a different project to generate the master S-N or damage curve that was used for the life calculations. Consequently, strain data measured directly off the board in this project required no transformation to solder joint strain and could be directly compared to the PCB strain observed in the master S-N curve. It must be recognized that in this project the PCBs were loaded with a four point bending fixture driven by the sprung mass excitation of a military vehicle cabin. Thus, the response of the PCBs was driven by the natural frequency of the test fixture and the 4-point loading of the test fixture defined the curvature response of the PCBs. Similarly, it was noted that the Power Spectral Density (PSD) of the fixture base acceleration did not change in shape as a function of frequency throughout the testing. With changes in terrain, the PSD basically changed in magnitude but not shape. To reiterate, with the 4 point bending fixture, there was only one possible deformation mode for the test PCB Therefore, the following conclusions based on PSD analysis must be viewed in this context.

6.0 Life Prediction

A successful comparison between test failures and predictions was achieved. BGA failures caused by low cycle fatigue were compared to failure predictions in the time domain with rainflow cycle counting and in the frequency domain with PSD load blocking techniques. Prediction using the cycle counting method determined that damage ratio was 5.91 at failure. Using PSD load blocking method the damage ratio was 7.48 at failure. Both these damage ratios are within an order of magnitude of actual failure. Due to the stochastic nature of fatigue, an order of magnitude difference between expected and actual failure is reasonable.

Damage accumulation prediction from time domain based shock analysis is unavailable. Analysis determined that accelerometer sampling rate was far too low to capture necessary shock pulse width for a prediction. Therefore, the amount of damage caused by shock loads could not be determined. However, there was no observable strain response to shock pulses. This indicates the system was not responsive to shock pulses, possibly because the pulses were too short. Consequently, it is likely that observed shock pulses did not contribute damage observed in the components. To accurately capture the maximum acceleration level seen during testing (16.1 g), a minimum sampling rate of 2000 Hz is recommended.

6.1 Time Domain or Frequency Domain?

In this project, life prediction was demonstrated in the time domain with cycle counting. However, if strain time history is not available, a hybrid time and frequency

domain approach to processing acceleration time history may be applicable. This hybrid approach, referred to as PSD load blocking, breaks up acceleration time history according to observed loading conditions. Then acceleration PSD is calculated for each block of data. The PSD load blocking technique worked particularly well in this demonstration project because well defined test plans were used. These test plans broke up testing according to specific terrain and tire pressure, making it obvious how to break up time histories into load blocks. However, in actual operating environments there are no defined courses (e.g. Perryman, Munson), and tire pressure and payload information may not be recorded. Therefore, PSD load blocking real mission data is much more challenging than on test courses.

In mission environments, data maybe offloaded and checked every couple of weeks. With two strain channels (100 Hz), one accelerometer channel (100 Hz), and one GPS channel (1 Hz), a 2 GB memory card would be filled in 30 days if data were recorded continuously. On missions, it is likely more data channels and higher sample rates will be used. However, data is not likely to be recorded continuously but only when vehicle engine is on. Therefore, 2 GB is a good base memory capacity requirement for a data acquisition system. Regardless, recording full time histories during missions provides for the most flexibility and should be retained when possible. Always use memory capacities exceeding storage requirements for typical mission durations and data channels to be used.

Consider the cases where limited memory is available. What are some options for compressing time histories? In time domain, strain time history can be cycle counted periodically and cumulative or periodic data bins could be stored while time histories are discarded. Alternatively, using terrain identification scheme developed by Heine [10], RMS speed and RMS acceleration levels could be calculated continuously to determine whether terrain is paved, secondary, or off-road. Then using predefined damage rates for each terrain and duration on each terrain, real-time total damage accumulation can be calculated. Furthermore, low level data recorded while vehicle is idling or driving over paved surfaces can be discarded, as these conditions do not contribute to damage accumulation.

In the frequency domain, when memory is reaching capacity, time history can be converted to PSD. However, unless all driving is over paved and secondary roads or the same mission profile is repeated all the time, PSD will miss changes in mission profile that could significantly alter accumulated damage. Short, highly damaging missions would not be reflected in a PSD of a time history where less damaging missions are more common. A solution would be to take PSD at regular time intervals. This is a form of load blocking but without knowing the loading conditions. In addition, the data acquisition unit could be signal triggered to capture short time histories of transient events such as shock pulses for later analysis. Life prediction can be calculated by combining damage accumulation from all recorded PSD load blocks and time histories. Another solution is to use a terrain identification scheme to determine terrain in real-time and take a PSD of recorded data every time the terrain

changes and discard the time history data. This method works best in conditions where terrain changes infrequently and slowly. Otherwise, numerous PSDs would be collected in a short period of time and memory use would be very high.

6.2 Characterization of Terrain and Loading Conditions

Characterization of a limited set terrain and loading conditions was performed. Time domain analysis of paved road data for the passenger vehicle environment demonstrates average RMS strain and average RMS acceleration levels are similar to levels seen in the military vehicle environment. However, frequency domain analysis show acceleration PSD levels are approximately two times higher in military vehicle than passenger vehicle over captured frequencies. This result indicates the military vehicle environment is harsher than passenger vehicle over paved roads. The conclusion reached by PSD analysis was expected and confirmed by subjective physical experience in both of these environments. In addition, this demonstrates that average RMS levels can be deceptive when comparing different environments. Also, it demonstrates why random vibration environments, such as paved roads, are often analyzed in the frequency domain.

Results from frequency domain analysis for different loading conditions and terrain showed that Perryman 2 and Perryman 3 contain features that excite at frequency of 1.5 Hz. Given the unusually high PSD levels at 1.5 Hz, it was presumed that 1.5 Hz is the natural frequency of the military vehicle suspension. From these results, it appears that PSD level at 1.5 Hz could be used to differentiate severe off-

road terrain (Perryman 2 and Perryman 3) from smoother terrain (paved, Perryman A and Perryman 1). In addition, PSD levels between 7 to 11 Hz decrease with decreasing in tire pressure. This decrease was particularly noticeable in Perryman A, Perryman 1, and Perryman 2 data. Potentially, changes in LMTV tire pressure can be detected by monitoring PSD levels at predetermined frequencies. However, this observation may be limited to the experimental fixture used for testing.

Data analysis showed that a loose positive correlation exists between measured RMS acceleration and RMS strain. The correlation between RMS acceleration and RMS strain was especially strong on Perryman 1, 2, and 3 courses. Correlation was non-existent for Perryman A and Churchville B data. It is important to note that this correlation maybe related to the experimental fixture used and should not be generalized without more rigorous testing. In addition, any correlation factor will change based on whether the acceleration is measured on sprung or un-sprung mass. With such a correlation available, it would be possible to calculate strain time history from an acceleration time history. This correlation would be useful because strain gauges take up valuable board space, have potentially more wiring requirements, and may be more difficult to replace. Because of these challenges, using strain gauges is not always possible.

Furthermore, there appears to be loose positive correlation between RMS acceleration/RMS speed and RMS strain/RMS speed. While either correlation appears suitable for terrain identification, RMS acceleration and RMS speed appears

to more ideal due to issues with strain gauges mentioned previously. Heine [10] has previously demonstrated using RMS acceleration with RMS speed for terrain identification purposes with successful results.

6.3 Lessons Learned

In order to identify and characterize blocks of time history data according to load condition or terrain, speed information is necessary. For example, without speed time history, load blocking in this project would be nearly impossible. In addition, as demonstrated in the Appendix, statistical analysis of load blocks alone without speed information yielded no visible trends. However, in the context of decreasing speeds, the path of RMS strain/acceleration levels over increasing terrain roughness appears reasonable.

Shock events are best analyzed in the time domain. Unfortunately, the accelerometer in this project sampled at 100 Hz. To capture shock events a much higher sample rate is required.

Random vibrations are best analyzed in the frequency domain. Time history data of any length can be compressed into a small amount of data by performing a PSD analysis. Yet all the general characteristics of a random vibration environment are still preserved in the PSD data. Another benefit is transient events (that need to be analyzed separately in the time domain) do not significantly affect PSD results of lengthy time histories.

Load amplification needs to be implemented carefully to ensure loads are not scaled excessively and accelerated testing is performed as desired. In this project, load amplification resulted in failures in the low cycle fatigue regime. In addition, loading caused the experimental fixture to be susceptible to shock loads. If failures from shock loading are not desirable, load amplification amount needs to be determined carefully, with the assistance of virtual qualification testing. Lastly, load amplification by adding mass in an environment where loading frequency is not controlled, reduces natural frequency of the system. If virtual qualification or preliminary testing is not conducted to determine natural frequency of the new system, test time can actually increase. This is possible if the decrease in damage accumulation rate caused by reduction in system natural frequency exceeds the increase in damage per cycle from load amplification.

Chapter 7: Contributions and Future Work

7.0 Contributions

1) The PHM method was used to develop a system for collecting data and predicting failures due to vibration and shock loads in military vehicles. Rainflow cycle counting and PSD load blocking techniques for life prediction were successfully demonstrated.

2) Available data showed a linear relationship between RMS stain and RMS acceleration. While the relationship between strain and acceleration is often assumed, in this project it was demonstrated. However, more tests need to be performed to show that this correlation is not dependent on experimental fixture used. In addition, this correlation will change based on whether acceleration is measured on sprung or un-sprung mass.

3) Acceleration PSD observations described below:

a) Acceleration PSD levels demonstrated that the military vehicle environment is 'harsher' than passenger vehicle environment even over paved roads.

b) Demonstrated that decreases in LMTV tire pressure result in decreases in acceleration PSD level for frequencies around 7-11 Hz. Decrease is much

more noticeable for Perryman A, 1, and 2 than paved road and Perryman 3 conditions. It is important to note that this observation is very likely dependent on the fixture design used. Further testing with the LMTV is required to determine if changes in tire pressure can be reliably detected by the PSD level at some predetermined frequency.

c) Acceleration PSD level at 1.5 Hz demonstrated to be significantly higher for Perryman 2 and Perryman 3 than paved road, Perryman A, and Perryman 1 at the same frequency. Observation is for LMTV vehicle only.

4) Significant amounts of acceleration and strain data were collected at Aberdeen Proving Grounds (APG). This data was used to characterize terrain at APG. Terrain was characterized using RMS, kurtosis, skewness, and Crest Factor (see Appendix). Data analysis showed that terrain could not be characterized by acceleration or strain data alone. Speed data is essential to characterizing terrain and recognizing data trends.

7.1 Future Work

Future work should involve prognostic demonstrations for fatigue failures in the transition and high cycle regime. For this to occur, experimental fixture needs to be redesigned and improved. The main aspect that needs to be redesigned is the amount of weight used for load amplification. Currently, the function of the eleven pound added weight is to overcome the enormous amount of frictional damping

present in the four-point bending fixture. By redesigning fixture to reduce amount of damping in the system, less weight will be needed for load amplification. Less weight also means less susceptibility to shock loads, higher natural frequency, and more cycles to failure.

Reducing frictional damping in the current experimental design can be achieved by redesigning the clamped ends of the PCBs to act more similarly to pinned-pinned ends that have greater freedom to move in the horizontal direction as the PCB flexes. Additionally, the test region on PCBs can be made smaller by placing fewer components on the boards. This will allow the blades on the four-point fixture be placed closer together and apply larger bending moments due to increased distance from the ends of the PCB. In addition, testing only one PCB at a time will reduce the stiffness of the system and resistance to vibration. Suggested changes to the test fixture are also indicated in Figure 72.

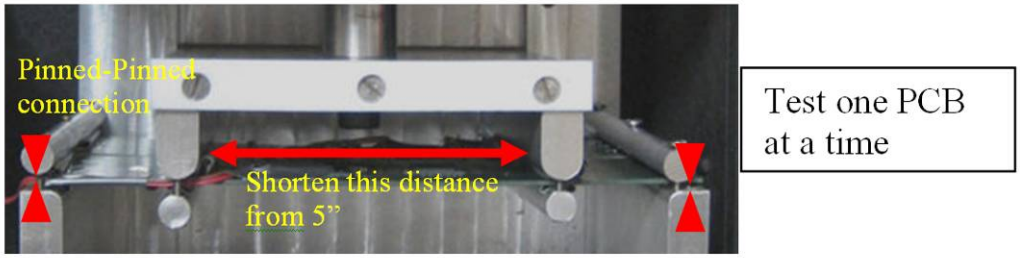

Figure 72. Suggested Changes to Four-Point Bending Fixture

In future experiments, test PCBs should be daisy chained for continuity in a way that works easily with bridge channels on the eDAQ-lite. Most of the boards tested were wired to monitor components individually, with the exception of BGA boards. Rewiring components in daisy chained manner to be monitored using one bridge channel proved cumbersome and unreliable. Alternatively, another option is to

add bridge layers to the eDAQ unit to increase number of bridge channels available for collecting continuity information.

To determine repeatability of failure results, multiple tests for each component packaging type are required. Currently, only one board of each component packaging type has been tested. Future tests need an appropriate sample size of BGA, capacitor, SOT, and SOIC boards tested until failure. Multiple tests in low, transition, and high cycle failure regimes would also be desirable. In addition, future testing can include other component packaging types or component sizes.

Damage accumulation predictions broken down by terrain predicted that BGA components failed earlier on the Perryman A course. Cycle counting predicted that damage ratio was 1.47 after the Perryman A course while PSD load blocking predicted a damage ratio of 2.32. While small spikes in continuity were seen after testing on Perryman A, no clear indications of imminent failure appeared until later. This suggests that more research can be performed to determine a more accurate failure threshold. Further research in this area may be able to determine how well prognostics can account for scatter in fatigue.

Future work could demonstrate using only terrain, loading information, and duration to predict remaining life. Prediction would use a database of prior damage accumulation data with a large variety of conditions. Chapter 5 demonstrated methods used to determine damage the accumulation due to a particular terrain. Damage

accumulation results similar to Table 10 could be expanded into a database of damage accumulation rates according to terrain, tire pressure, component type, etc. In addition, Heine [10] and this project demonstrated terrain identification may be possible with RMS acceleration and RMS speed data. Therefore, in future demonstrations, simply identifying the terrain could result in acceptable life predictions provided the scatter in failure data is manageable.

More rigorous experiments are required to demonstrate that life predictions using acceleration time history can be interchangeable with strain time history. In order for life prediction using acceleration time history to be effective, suitable load blocking techniques need to be developed. In theatre operating environments are not as cleanly partitioned as testing on courses at Aberdeen Proving Ground.

In order to characterize shock loads better, an accelerometer capable of sampling at 2000 Hz or higher needs to be used in future tests. Shock events can be captured at high sampling rates with signal triggering while random vibration data is captured at lower sampling rates. High fidelity shock data can then be input into CalcePWA for damage accumulation predictions.

Appendices

Statistical Analysis by Terrain

Statistics identified in Table 12 were calculated for blocks of acceleration and strain data according to tire pressure and terrain. Results are illustrated in Figure 73 through Figure 80.

Table 12. Potential Statistics for Terrain/Load Characterization

Statistic	**Formula**	**Significance**
RMS [15]	$x_{\mathrm{rms}} = \sqrt{\frac{1}{n}\sum_{i=1}^{n} x_i^2} = \sqrt{\frac{x_1^2 + x_2^2 + \cdots + x_n^2}{n}}$	Statistical measure of the magnitude of varying quantity
Kurtosis [26]	$\gamma_2 = \frac{\kappa_4}{\kappa_2^2} = \frac{\mu_4}{\sigma^4}$ fourth cumulant divided by the square of the variance of the probability distribution	Statistic based on variance of a distribution. Quantifies non-Gaussian nature of a distribution. Kurtosis=3 for Gaussian.
Skewness [27]	$\gamma_1 = \frac{\mu_3}{\sigma^3},$ Third moment about mean divided by standard deviation cubed	Measure of asymmetry in a distribution.
Crest Factor [28]	$C = \frac{\lvert x\rvert_{\mathrm{peak}}}{x_{\mathrm{rms}}}$	Also known as peak to average ratio. Peak amplitude of sample divided by sample RMS.

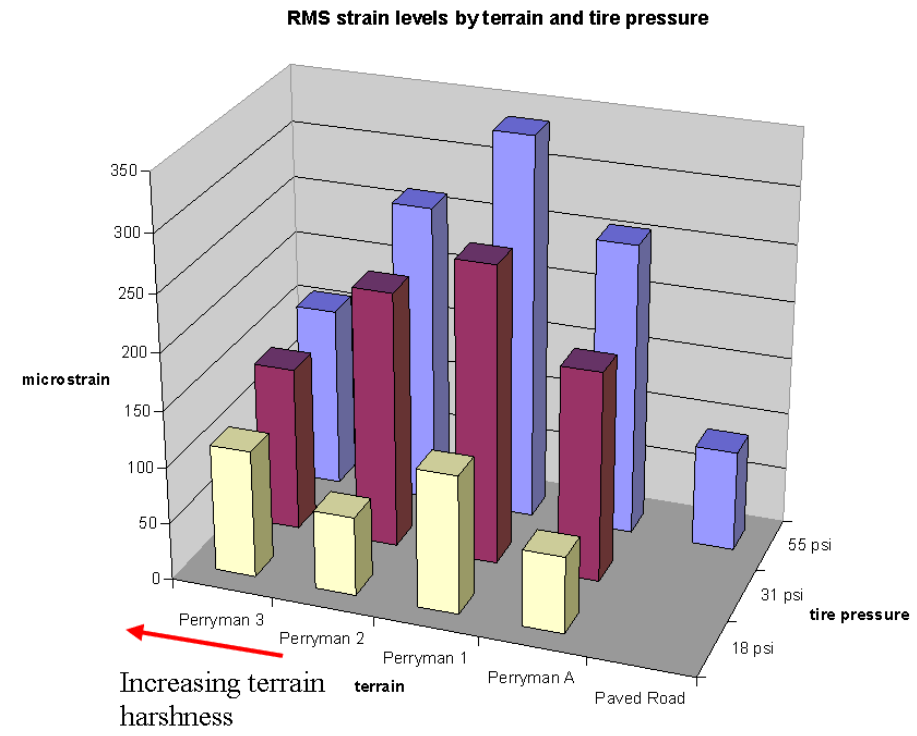

Figure 73. RMS strain vs. Terrain vs. Tire Pressure

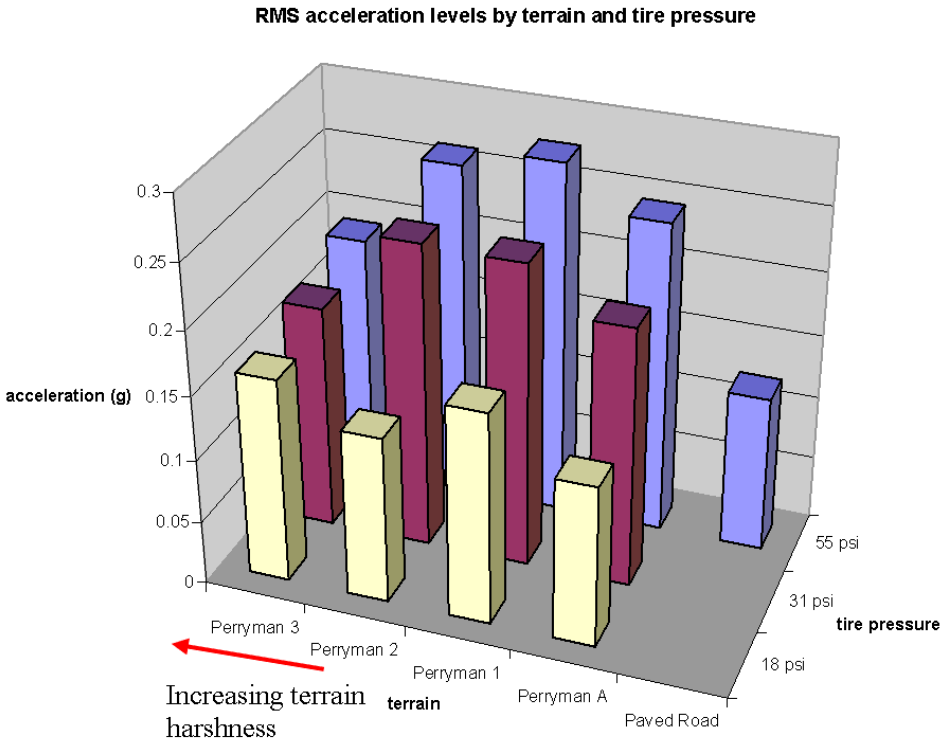

Figure 74. RMS acceleration vs. Terrain vs. Tire Pressure

Figure 73 and Figure 74 does not show a correlation between RMS strain (or RMS acceleration) and terrain. As expected, without speed information, RMS strain (or RMS acceleration) and terrain fails to show any correlation. On the other hand, RMS strain and RMS acceleration levels appear to consistently increase with tire pressure.

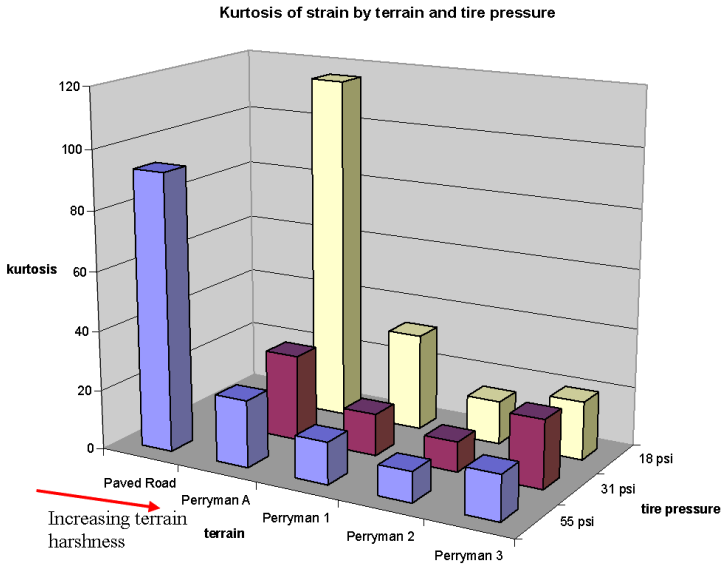

Figure 75. Kurtosis of Strain vs. Terrain vs. Tire Pressure

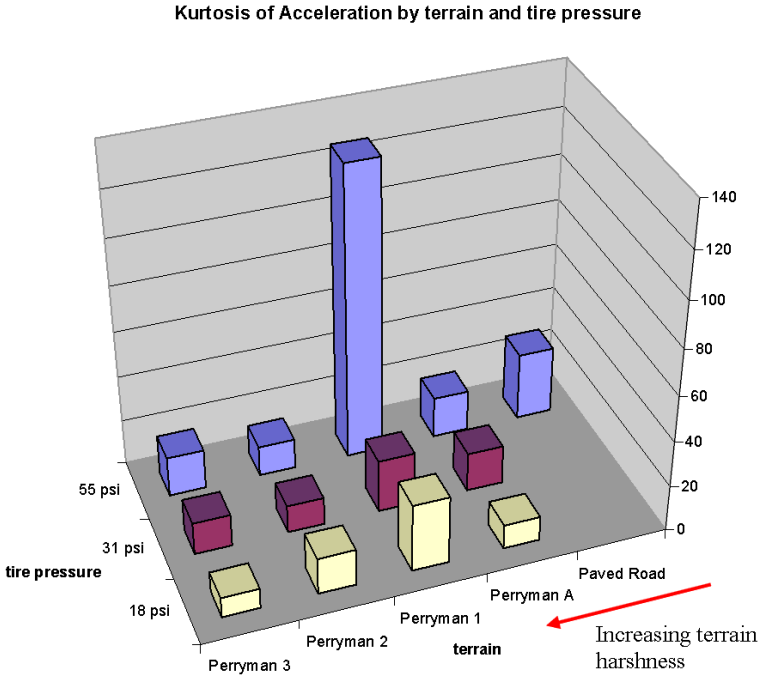

Figure 76. Kurtosis of Acceleration vs. Terrain vs. Tire Pressure

Figure 75 and Figure 76 show that kurtosis of strain/acceleration does not correlate well with terrain or tire pressure.

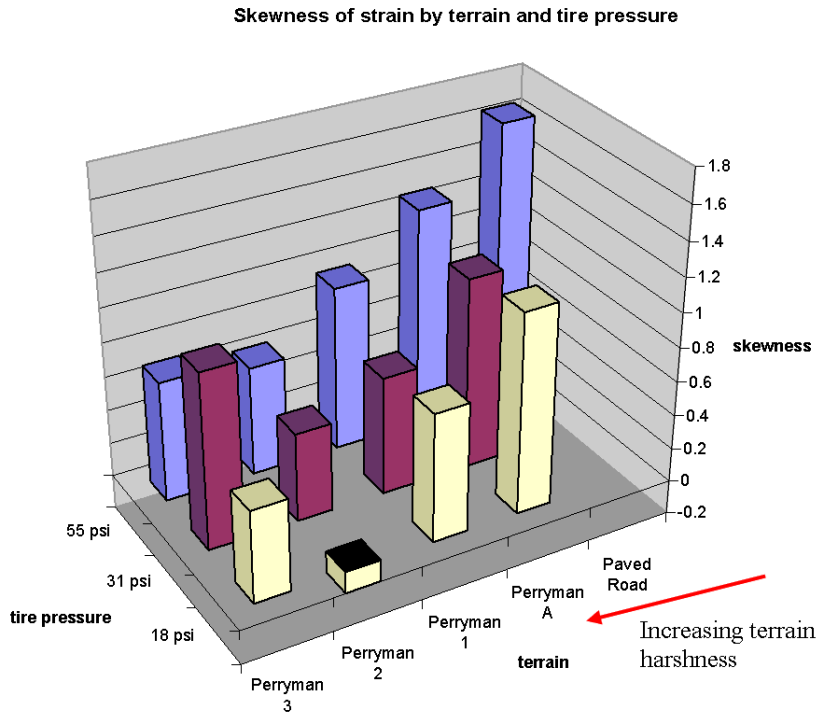

Figure 77. Skewness of Strain vs. Terrain vs. Tire Pressure

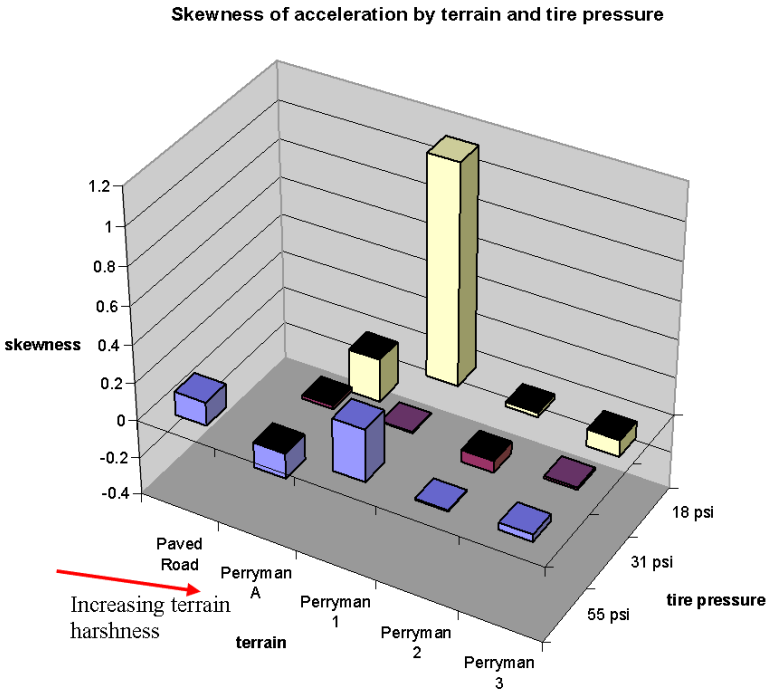

Figure 78. Skewness of Acceleration vs. Terrain vs. Tire Pressure

Figure 77 and Figure 78 show skewness of strain/acceleration not correlating well with terrain or tire pressure.

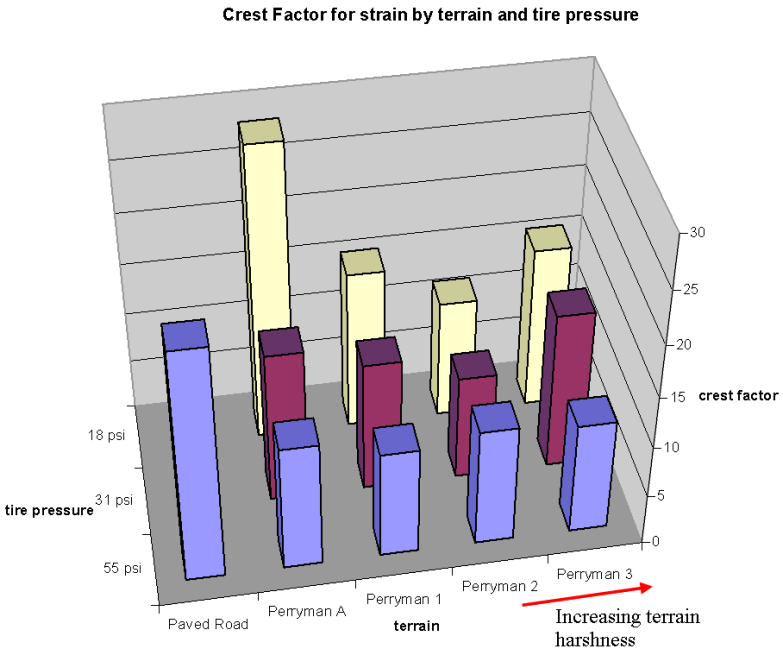

Figure 79. Crest Factor of Strain vs. Terrain vs. Tire Pressure

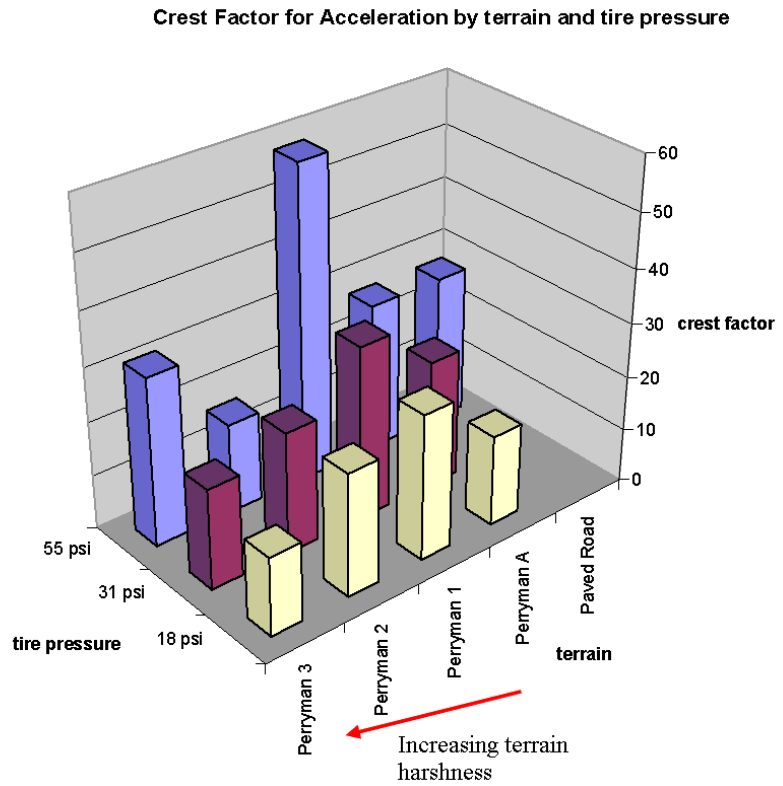

Figure 80. Crest Factor of Acceleration vs. Terrain vs. Tire Pressure

Crest Factor of strain/acceleration does not appear to correlated to terrain in Figure 79 and Figure 80. However, Crest Factor of strain/acceleration appears to increase with tire pressure with the exception of Crest Factor for Perryman 2 acceleration.

As demonstrated by Figure 73 to Figure 80, terrain information does not correlate well with any readily available statistic (RMS, kurtosis, skewness, Crest Factor) of acceleration and strain data. Without speed information, statistics of strain and acceleration broken up by terrain will not yield useful information. Tire pressure demonstrated a trend with RMS and Crest Factor statistics of acceleration and strain. Therefore, tire pressure is an important parameter to record due to its potential relationship with acceleration and strain levels.

Figure 81. Printed Circuit Board Construction Details [34]

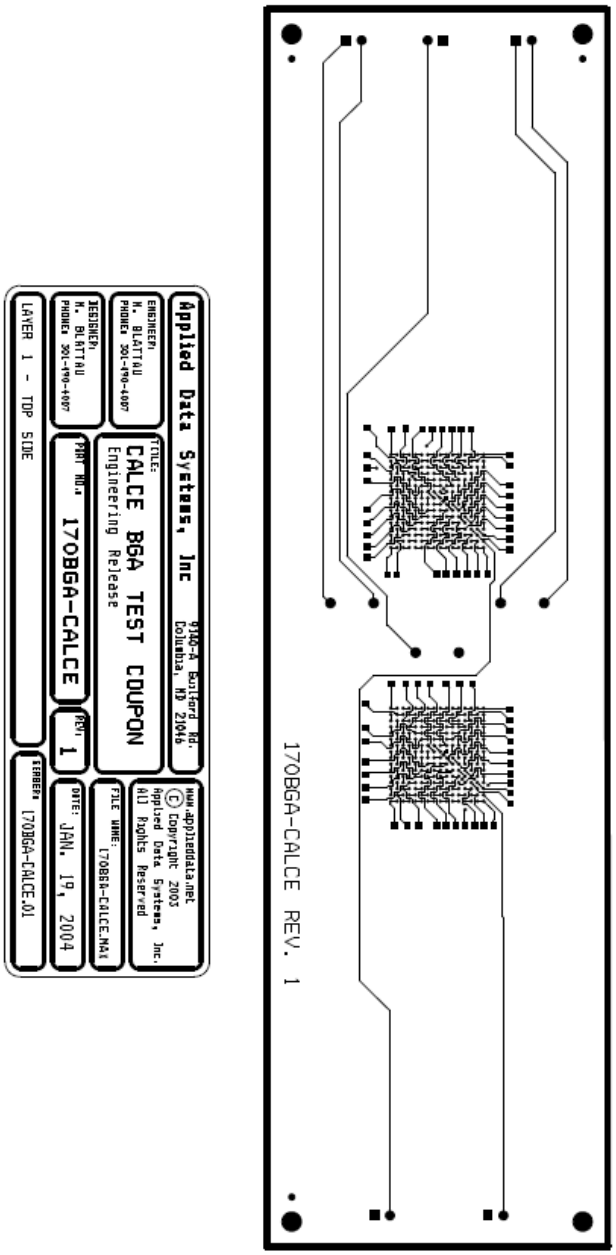

Figure 82. BGA Board Wiring Diagram [34]

TopLine™

TEL 1-714-898-3830
info@toplinedunnm y.com

BGA256T1.0-DC169A

BALLS	PITCH	SIZE	MATRIX	ROWS	CENTER	MAT'L
256	1.0mm	17mm SQ	16 x 16	full	full	BT

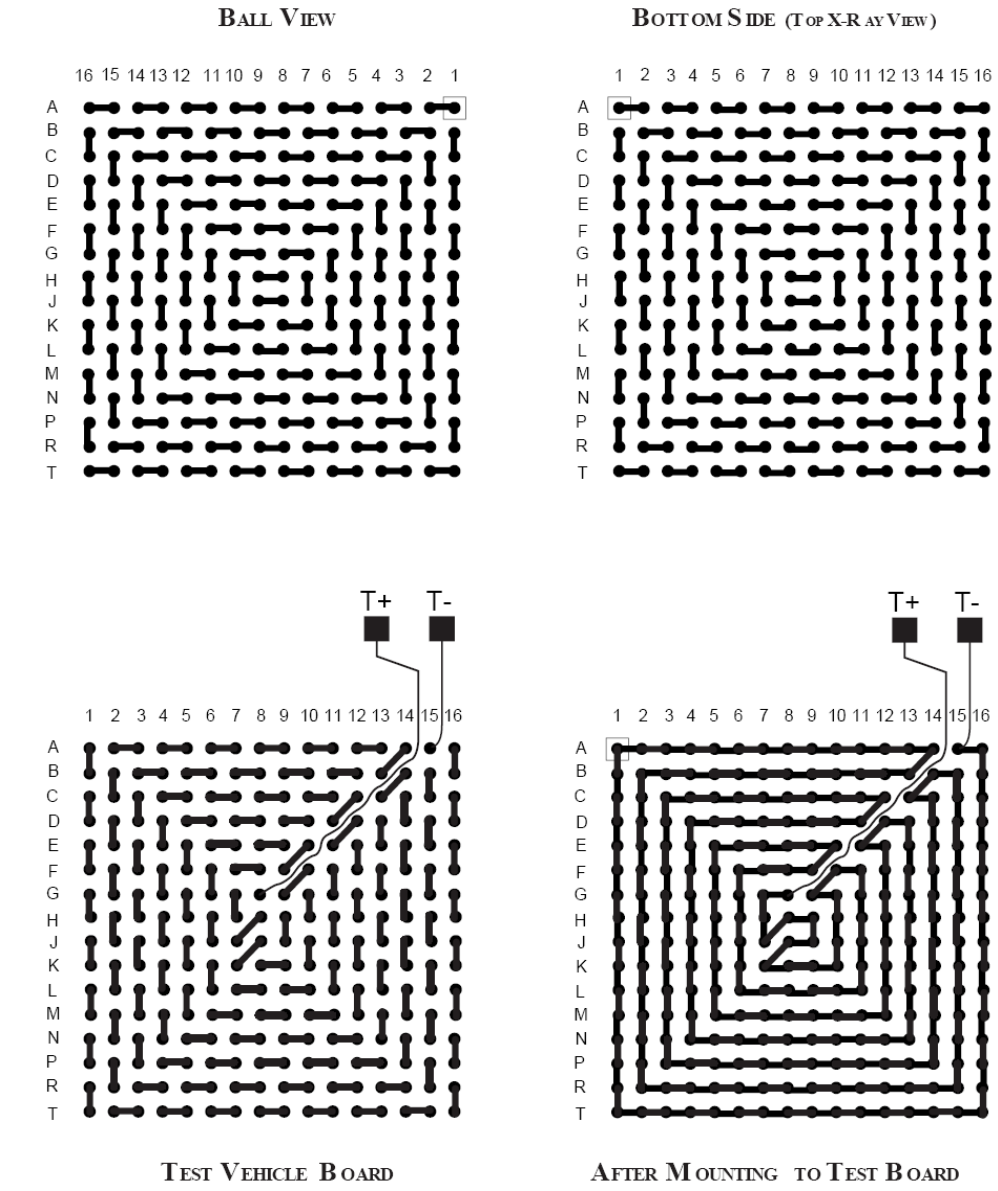

Figure 83. Topline 256 BGA Wiring [29]

BGA256T1.0-DC169A

BALLS	PITCH	SIZE	MATRIX	ROWS	CENTER	MAT'L
256	1.0mm	17mm SQ	16 x 16	full	full	BT

TopLine™
TEL 1-714-898-3830
info@toplinedumm y.com

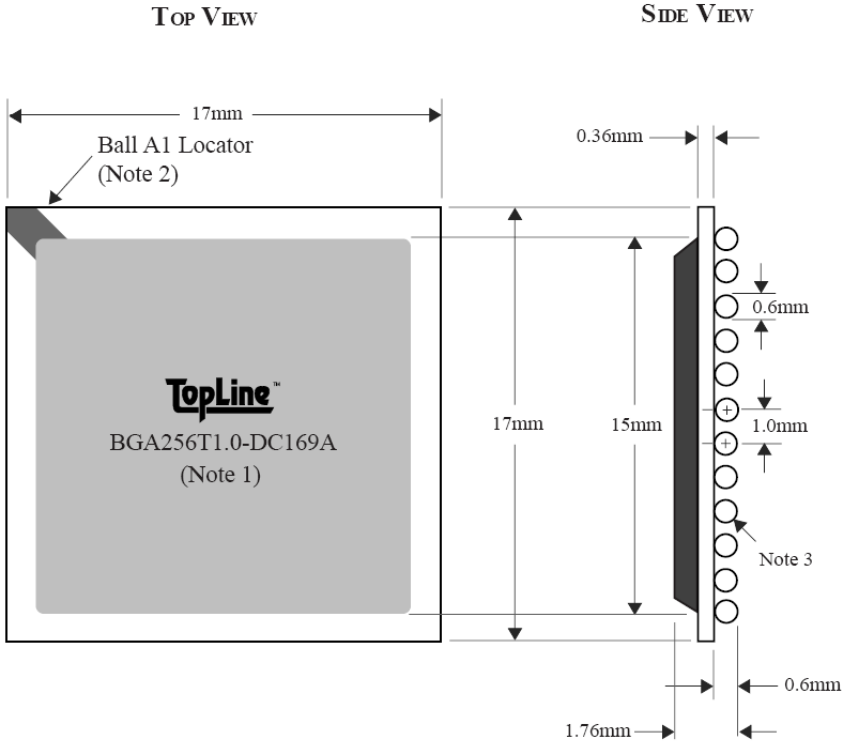

NOTES	
Note 1	Logo and part number centered White ink or laser marked
Note 2	Ball A1 locator mark positioned in corner
Note 3	Ball Material: 63/37 SnPb
Note 4	Substrate Material: BT laminate

REVISIONS		
Rev	Date	Changes

PACKAGING TRAYS

Tray BGATRAY17mm-6x15
Tray Quantity 90

Figure 84. Topline 256 BGA Dimensions [29]

Part # **SO8**
Leads **8** Pitch **1.27mm (0.05")**
Body Size **150mil (3.9mm)**

TopLine™
Tel 1-714-898-3830
info@topline.tv

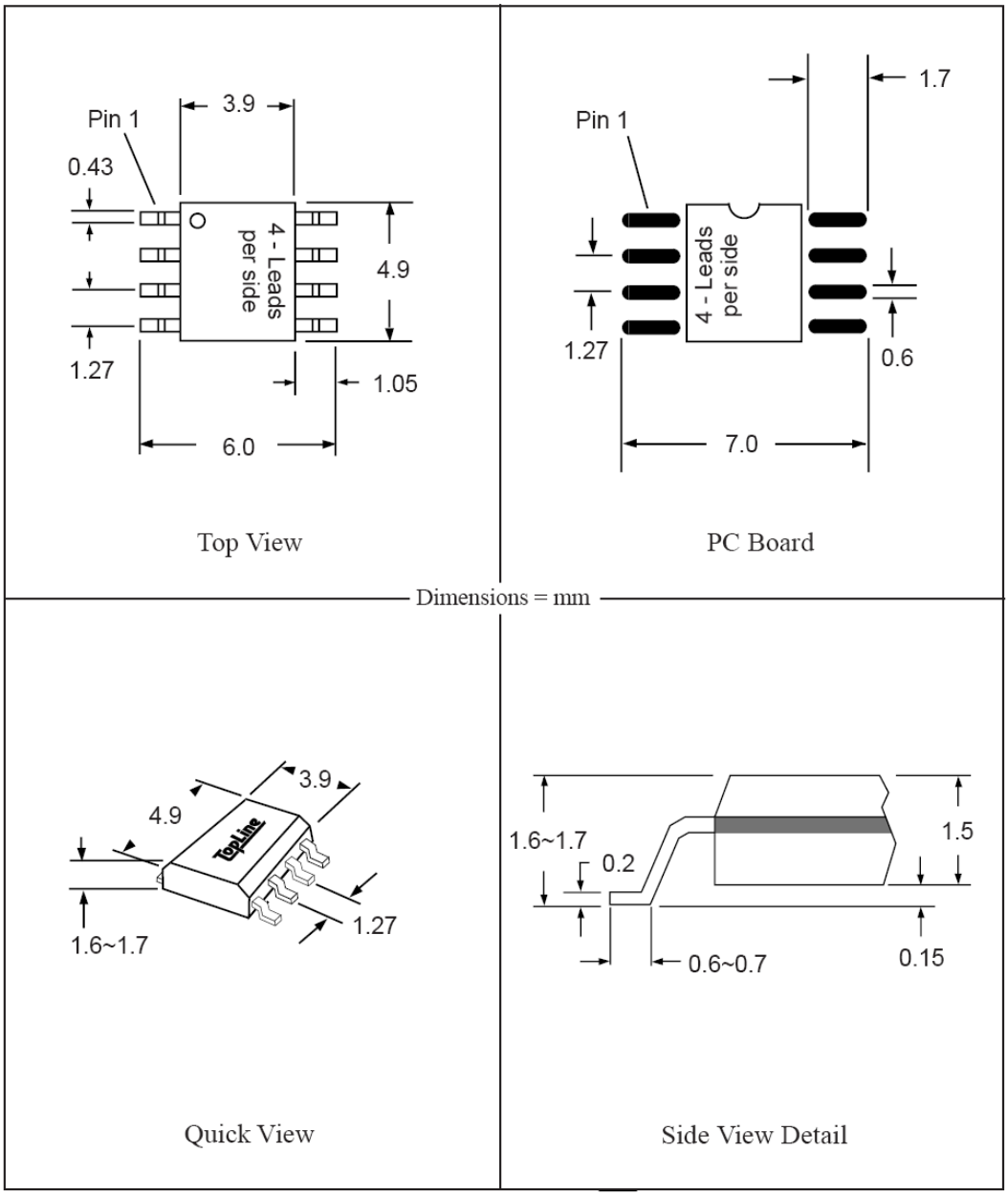

Figure 85. SOIC-8 Dimensions [30]

KEMET CHARGED.

CERAMIC CHIP CAPACITORS

FEATURES

- C0G (NP0), X7R, X5R, Z5U and Y5V Dielectrics
- 10, 16, 25, 50, 100 and 200 Volts
- Standard End Metalization: Tin-plate over nickel barrier
- Available Capacitance Tolerances: ±0.10 pF; ±0.25 pF; ±0.5 pF; ±1%; ±2%; ±5%; ±10%; ±20%; and +80%-20%
- Tape and reel packaging per EIA481-1. (See page 92 for specific tape and reel information.) Bulk Cassette packaging (0402, 0603, 0805 only) per IEC60286-6 and EIAJ 7201.
- RoHS Compliant

CAPACITOR OUTLINE DRAWINGS

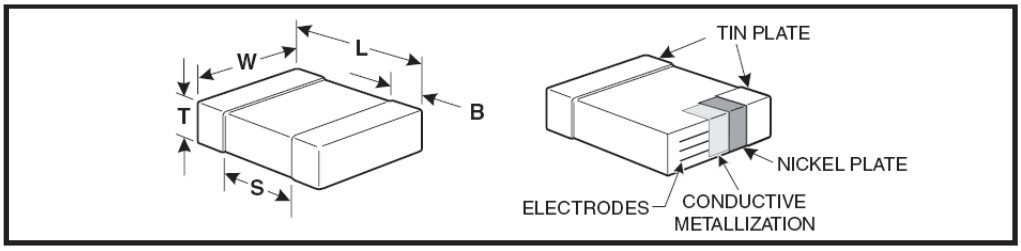

DIMENSIONS—MILLIMETERS AND (INCHES)

EIA SIZE CODE	METRIC SIZE CODE	L - LENGTH	W - WIDTH	T THICKNESS	B - BANDWIDTH	S SEPARATION minimum	MOUNTING TECHNIQUE
0201*	0603	0.6 (.024) ± .03 (.001)	0.3 ± (.012) ± .03 (.001)	See page 78 for thickness dimensions.	0.15 (.006) ± .05 (.002)	N/A	Solder Reflow
0402*	1005	1.0 (.04) ± .05 (.002)	0.5 (.02) ± .05 (.002)		0.20 (.008) - .40 (.016)	0.3 (.012)	
0603	1608	1.6 (.063) ± .15 (.006)	0.8 (.032) ± .15 (.006)		0.35 (.014) ± .15 (.006)	0.7 (.028)	Solder Wave + or Solder Reflow
0805*	2012	2.0 (.079) ± .20 (.008)	1.25 (.049) ± .20 (.008)		0.50 (.02) ± .25 (.010)	0.75 (.030)	
1206*	3216	3.2 (.126) ± .20 (.008)	1.6 (.063) ± .20 (.008)		0.50 (.02) ± .25 (.010)	N/A	
1210*	3225	3.2 (.126) ± .20 (.008)	2.5 (.098) ± .20 (.008)		0.50 (.02) ± .25 (.010)	N/A	
1812	4532	4.5 (.177) ± .30 (.012)	3.2 (.126) ± .30 (.012)		0.60 (.024) ± .35 (.014)	N/A	Solder Reflow
1825*	4564	4.5 (.177) ± .30 (.012)	6.4 (.252) ± .40 (.016)		0.60 (.024) ± .35 (.014)	N/A	
2220	5650	5.6 (.220) ± .40 (.016)	5.0 (.197) ± .40 (.016)		0.60 (.024) ± .35 (.014)	N/A	
2225	5664	5.6 (.220) ± .40 (.016)	6.3 (.248) ± .40 (.016)		0.60 (.024) ± .35 (.014)	N/A	

* Note: Indicates EIA Preferred Case Sizes (Tightened tolerances apply for 0402, 0603, and 0805 packaged in bulk bassette, see page 96.)
+ For extended value 1210 case size - solder reflow only.

CAPACITOR ORDERING INFORMATION (Standard Chips - For Military see page 87)

C 0805 C 103 K 5 R A C*

CERAMIC

SIZE CODE

SPECIFICATION
C - Standard

CAPACITANCE CODE
Expressed in Picofarads (pF)
First two digits represent significant figures.
Third digit specifies number of zeros. (Use 9 for 1.0 through 9.9pF. Use 8 for 0.5 through 0.99pF)
(Example: 2.2pF = 229 or 0.50 pF = 508)

CAPACITANCE TOLERANCE
B – ±0.10pF J – ±5%
C – ±0.25pF K – ±10%
D – ±0.5pF M – ±20%
F – ±1% P – (GMV) – special order only
G – ±2% Z – +80%, -20%

VOLTAGE
1 - 100V 3 - 25V
2 - 200V 4 - 16V
5 - 50V 8 - 10V
7 - 4V 9 - 6.3V

TEMPERATURE CHARACTERISTIC
Designated by Capacitance Change Over Temperature Range
G – C0G (NP0) (±30 PPM/°C)
R – X7R (±15%) (-55°C + 125°C)
P – X5R (±15%) (-55°C + 85°C)
U – Z5U (+22%, -56%) (+10°C + 85°C)
V – Y5V (+22%, -82%) (-30°C + 85°C)

FAILURE RATE LEVEL
A- Not Applicable

END METALLIZATION
C-Standard (Tin-plated nickel barrier)

* Part Number Example: C0805C103K5RAC (14 digits - no spaces)

Figure 86. Kemet 1206 Capacitor Specifications [31]

Part # **SOT23E7A**
Leads 3

TopLine™
Tel 1-714-898-3830
info@toplinedummy.com

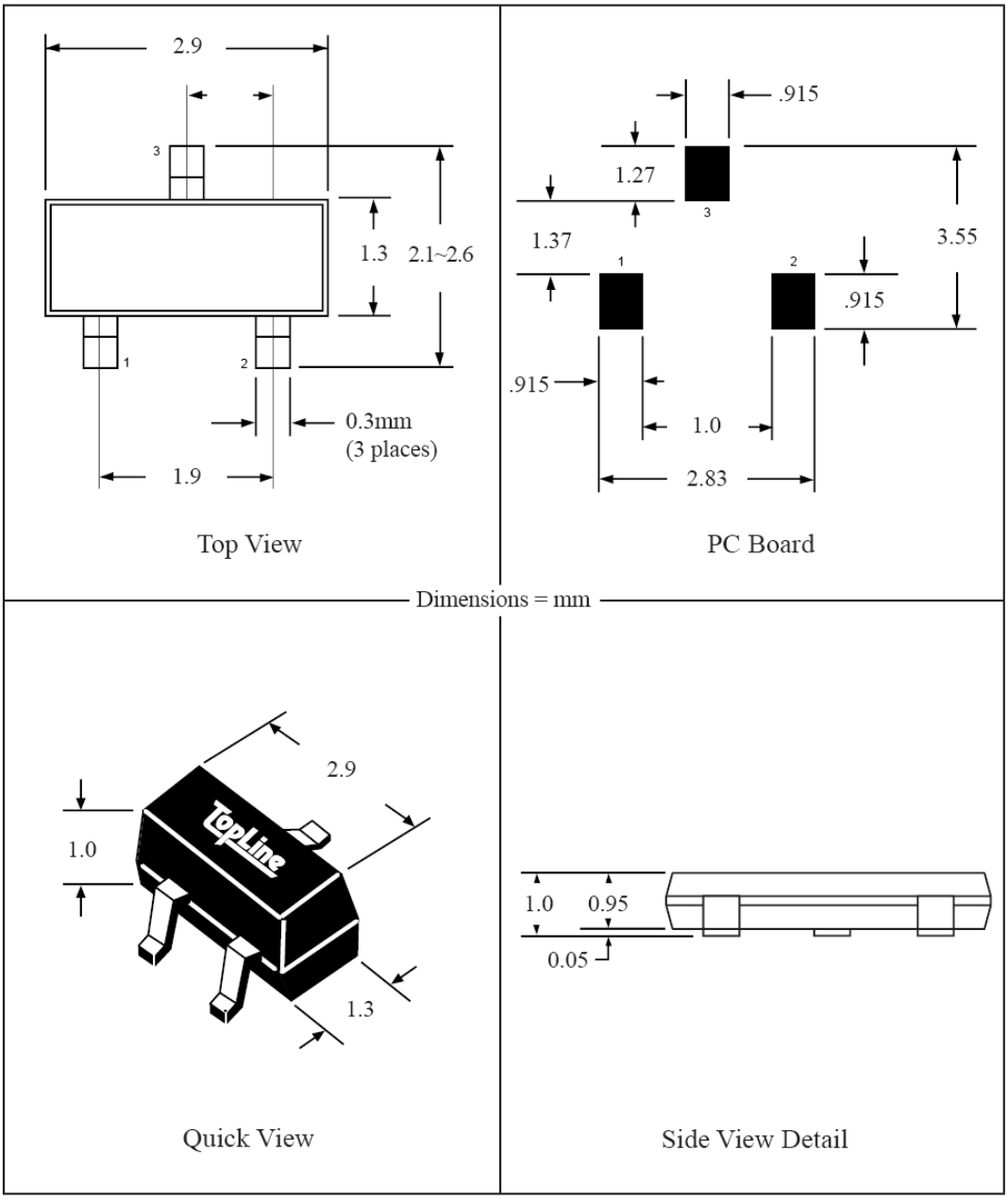

Figure 87. SOT-23 Dimensions [32]

TopLine™
Tel 1-714-898-3830
info@topline.tv

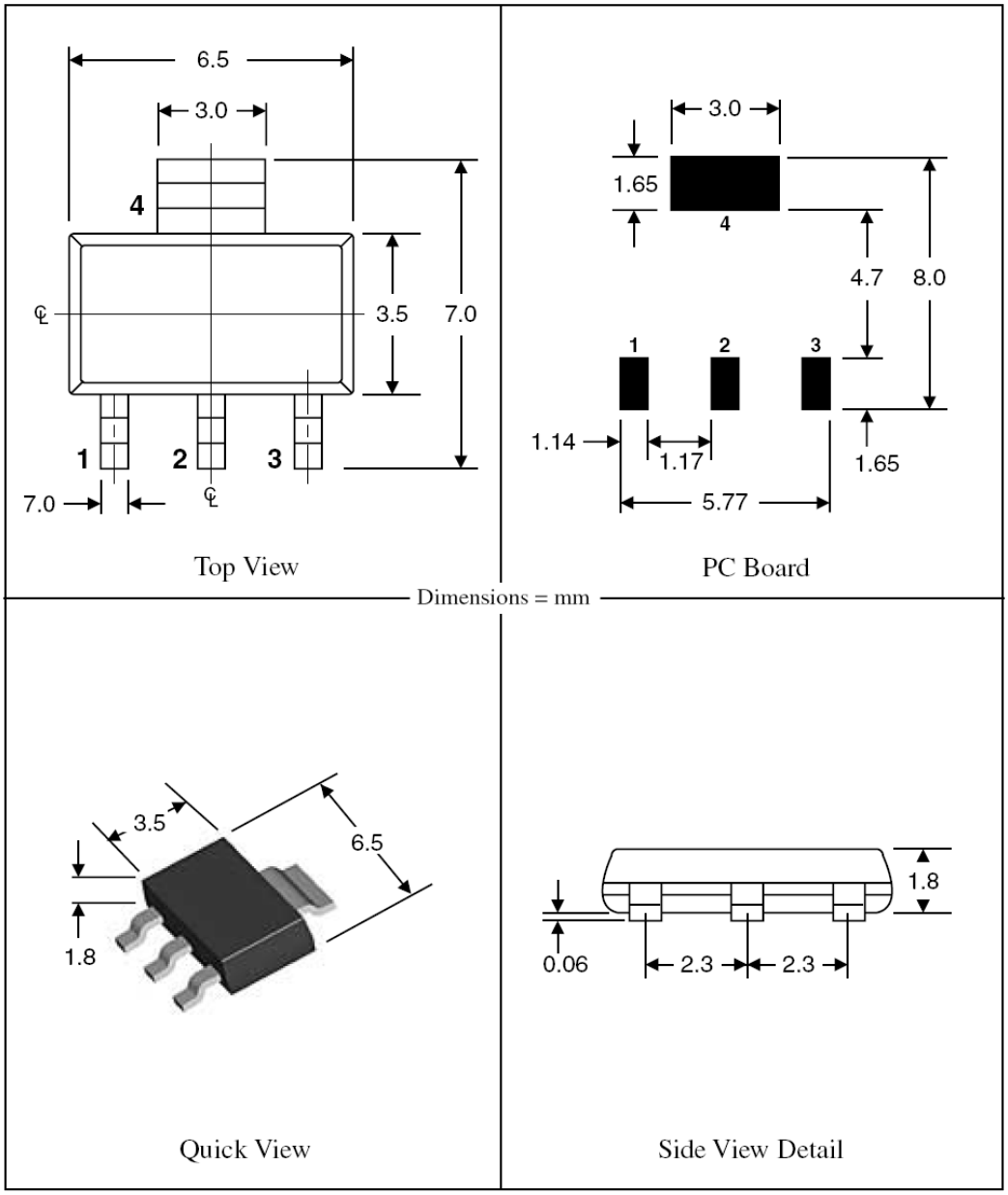

Figure 88. SOT 223 Dimensions [33]

Bibliography

1. Ramakrishnan, A., and M. Pecht, "A Life Consumption Monitoring Methodology for Electronic Systems," *IEEE Transactions on Components and Packaging Technologies*, Vol. 26, No. 3, September 2003, pp. 625-634.
2. Mishra, S., Pecht, M., et al., "Remaining Life Prediction of Electronic Products Using Life Consumption Monitoring Approach," *European Microelectronics Packaging and Interconnection Symposium*, June 16-18, 2002, pp. 136-142.
3. IEEE Reliability Society, "IEEE Std 1413" *IEEE Standard Methodology for Reliability Prediction and Assessment for Electronic Systems and Equipment*, New York, January 1999
4. Vichare, N., Rodgers, P., Eveloy, V., and M. Pecht, "Environment and Usage Monitoring of Electronic Products for Health Assessment and Product Design," *International Journal of Quality Technology and Quantitative Management*, Vol. 4, No. 2, 2007, pp. 235-250.
5. P. Sandborn, Course Notes on Manufacturing and Life Cycle Cost Analysis of Electronic Systems, CALCE EPSC Press, 2005.
6. Vichare, N., and M. Pecht, "Prognostics and Health Management of Electronics," *IEEE Transactions on Components and Packaging Technologies*, Vol. 29, No. 1, March 2006, pp. 222-229.
7. Gu, J., Barker, D., and M. Pecht, "Prognostics Implementation Under Vibration Loading." *Accepted for Publication in Microelectronics Reliability Journal*.
8. Halfpenny, A., "Methods for Accelerating Dynamic Durability Tests," nCode International, Accessed 14 June 2007, < http://www.ncode.com/page.asp?section=000100010001000200130007&page code=00010001000100002001300070004>
9. Pecht, M., Tuchband, B., and N. Vichare, "Prognostics Research Update," CALCE PHM Research Consortium, Accessed 14 June 2007, < http://www.prognostics.umd.edu/calcepapers.htm>.
10. Heine R., Barker D., "Simplified terrain identification and component fatigue damage estimation model for use in a health and usage monitoring system," *Microelectronics Reliability*, doi:10.1016/j.microrel.2007.02.017
11. "Somat eDAQ-lite," nCode International, Accessed 18 August 2007, <http://www.ncode.com/page.asp?section=000100010001000100002>.
12. "Random Vibration," Wikipedia, Accessed 18 August 2007, <http://en.wikipedia.org/wiki/Random_vibration>.
13. Haag, Michael, "Introduction to Random Signals and Processes," Connexions, Accessed 18 August 2007, <http://cnx.org/content/m10649/latest/>.
14. Wirsching, P., Paez, T., Ortiz, K. Random Vibrations, Theory and Practice, New York: Wiley, 1995.
15. "Root Mean Square," Wikipedia, Accessed 18 August 2007, <http://en.wikipedia.org/wiki/Root_mean_square>.
16. J.Collins. Failure of Materials in Mechanical Design, New York: Wiley, 1993.

17. D. Steinberg, Vibration Analysis for Electronic Equipment, New York: Wiley, 2000.
18. Malatkar, P., Wong, S., Pringle, T., and W. Loh, "Pitfalls An Engineer Needs To Be Aware Of During Vibration Testing," *2006 Electronic Components and Technology Conference*.
19. "Understanding FFT Windows," LDS Group, Accessed 21 June 2007, <http://www.lds-group.com/docs/site_documents/AN014%20Understanding%20FFT%20Windows.pdf>
20. Gregory, P., Barker, D., and M. Osterman, "C06-05 Effect of Load Sequencing on Pb-free solder durability," CALCE Internal Presentation.
21. Shetty, S., Lehtinen, V., et al., "Fatigue of Chip Scale Package Interconnects Due to Cyclic Bending," *Journal of Electronic Packaging*, Vol. 123, Issue 3, September 2001, pp. 302-308.
22. H. O. Fuchs, D. V. Nelson, M. A. Burke, and T. L. Toomay, "Shortcuts in cumulative damage analysis," Fatigue Under Complex Loading: Analyses and Experiments, R. M. Wetzel, Ed. Warrendale, PA: SAE, 1977.
23. Steinberg, D.E., Vibration Analysis for Electronic Equipment, New York: Wiley, 2000.
24. D. Barker, "C07-15 Shock– *calcePWA* Shock Model Improvements (continuation of C05-15)," CALCE Internal Presentation.
25. Simmons, Ryan, "FEMCI Book– Calculating Grms," NASA Goddard, Accessed 13 August 2007, <http://femci.gsfc.nasa.gov/random/randomgrms.html>.
26. "Kurtosis," Wikipedia, Accessed 28 August 2007, <http://en.wikipedia.org/wiki/Kurtosis>.
27. "Skewness," Wikipedia, Accessed 28 August 2007, <http://en.wikipedia.org/wiki/Skewness>.
28. "Crest Factor," Wikipedia, Accessed 28 August 2007, <http://en.wikipedia.org/wiki/Crest_factor>.
29. "BGA256T1.0-DC169A.pdf," Topline, Accessed 4 September 2007, <http://www.topline.tv/drawings/pdf/BGA%201,0mm%20pitch/BGA256T1.0-DC169A.pdf>.
30. "SO8.pdf," Topline, Accessed 4 September 2007, <http://www.topline.tv/drawings/pdf/SO/SO8.pdf>.
31. "F3102_X7R.pdf," Kemet, Accessed 4 September 2007, <http://www.kemet.com/kemet/web/homepage/kechome.nsf/file/Commercial%20Ceramic%20Chips%20X7R%20Dielectric/$file/F3102_X7R.pdf>.
32. "SOT23E7A.pdf," Topline, Accessed 4 September 2007, <http://www.topline.tv/drawings/pdf/sot/SOT23E7A.pdf>.
33. "SOT223E13A," Topline, Accessed 4 September 2007, <http://www.topline.tv/drawings/pdf/sot/SOT223E13A.pdf>.
34. Blattau, M., "Printed Wiring Board CALCE BGA TEST COUPON," CALCE internal document, 19 January 2004.